Physical-layer Network Coding for Cooperative Wireless Networks

Dong Fang

Doctor of Philosophy

University of York

Electronics

March 2014

Abstract

As a newly-emerged paradigm in the networking techniques, physical-layer network coding (PNC) [1, 5] takes advantage of the superimposition of the electromagnetic waves, and embraces the interference which was typically deemed as harmful, by performing exclusive-or mapping. Therefore, the spectral efficiency is utilized, which in turn boosts the network throughput. In the classical 2-way relay channel (2-WRC), PNC only spends two channel uses for the bi-directional data exchange. However, one challenge for such a paradigm is that the singular fading states in the uplink of 2-WRC, might result in ambiguity for decoding the network coded symbol. One major focus of this thesis is to address the fading issue for PNC in the 2-WRC. Another fundamental challenge for PNC is to extend the PNC from the 2-WRC to a multi-user network such as the multi-way relay channel (M-WRC) or the hierarchical wireless network (HWN). To tackle these two fundamental challenges of PNC, several solutions are proposed in this thesis, which are summarized as follows: First, we introduce two efficient fading correction strategies, i.e., the rotationally-invariant coded modulation and the soft-bit correction. Second, a novel multilevel coded linear PNC scheme with extended mapping for the Rayleigh fading 2-WRC is proposed. Third, we design a new type of linear PNC for the Rayleigh fading 2-WRC, based on rings. We refer to such design as linear PNC over the hybrid finite ring. Fourth, we redesign PNC for the HWN, which facilitates the multi-user data exchange. To combat the co-channel interference introduced by multi-user data exchange, two efficient interference exploitation strategies based on network coding are proposed: 1) PNC with joint decoding; and 2) analogue network coding with interference-aware maximum likelihood detection. Finally, we propose a multilevel coded LPNC for the data exchange in the M-WRC.

Contents

List of Figures

List of Tables

Acknowledgements

First of all, I would like to express my sincere gratitude to my supervisor, Prof. Alister G. Burr, for his enthusiastic support, excellent guidance and continuous encouragement throughout my Ph.D. study at the University of York.

I am grateful to all colleagues and staffs in Communications Research Group for their help and support.

This thesis is dedicated to my parents and my girlfriend. Their endless love and unconditional support have always been my source strength to go through difficulties and my motivation to achieve success.

Declaration

All work presented in this thesis as original is so, to the best knowledge of the author. References and acknowledgements to other researchers have been given as appropriate.

Elements of the research presented in this thesis have resulted in some publications. A list of these publications can be found below.

Journal Papers

1. Dong Fang, Alister G. Burr, and Jinhong Yuan, "Linear Physical-layer Network Coding in Hybrid Finite Ring for Rayleigh fading Two-way Relay Channels", *Accepted, IEEE Trans. on Comms.*

2. Dong Fang, Alister G. Burr, and Jinhong Yuan, "Network coding based Interference Exploitation Strategies for Hierarchical Wireless Network", *submitted to IEEE Trans. on Comms. (Under Review)*

3. Dong Fang and Alister G. Burr, "Hybrid Physical-layer and Analog Network coding for Multi-user Hierarchical Wireless Network", *in preparation for IEEE Trans. on Comms.*

4. Dong Fang and Alister G. Burr, "Linear Physical-layer Network Coding in Galois Field for Multi-user Multi-way Relay Channels", *in preparation for IEEE Trans. on Comms.*

5. Dong Fang and Alister G. Burr, "Linear Physical-layer Network Coding enhanced Multiple Access Channels", *in preparation for IEEE Trans. on Wireless Comms.*

6. Dong Fang, Alister G. Burr, and Maged Elkashlan, "Vector Quantization based in Two-Way Relay Channels", *in preparation for IEEE Communications Letters*

Conference Papers

1. Dong Fang and Alister G. Burr, "Rotationally Invariant Coded Modulation for Physical Layer Network Coding in Two-Way Relay Fading Channel", *European Wireless Conference (EW), Poznan, Poland, Apr., 2012, pp.1-6* (***Best Paper Award***)

2. Alister G. Burr and Dong Fang, "Linear Physical Layer Network Coding for Multihop Wireless Networks", *European Signal Processing Conference (EUSIPCO) 2014*, Lisbon, Portugal, Sept., 2014, pp.1-6,

3. Dong Fang and Alister G. Burr, "Eisenstein Integer based Multi-dimensional Coded Modulation for Physical-layer Network Coding over $\mathbb{F}_4$ in the Two-way Relay Channels", *European Conference on Networks and Communications (EuCNC) 2014*, Bologna, Italy, June, 2014, pp.1-5

4. Alister G. Burr, Dong Fang, and Mehdi M. Molu, "Linear Wireless Physical-layer Network Coding based on binary matrices for Multilayer Relay Networks", *IEEE International Symposium on Wireless Communication Systems (ISWCS) 2014*, Barcelona, Spain, Aug., 2014, pp.1-5

5. Dong Fang and Alister G. Burr, "Equivocation Performance of Linear Wireless Physical Layer Network Coding", *URSI General Assembly and Scientific Symposium (URSI-GASS) 2014*, Beijing, China, Aug., 2014, pp.1-5

6. Alister G. Burr and Dong Fang, "Linear Block Physical-layer Network Coding for Multiple-User Multiple-Relay Wireless Networks", *URSI General Assembly and Scientific Symposium (URSI-GASS) 2014*, Beijing, China, Aug., 2014, pp.1-5

7. Dong Fang and Alister G. Burr, "Diversity Performance of Physical Layer Network Coding based on Reed-Solomon Codes", *European Wireless Conference (EW) 2014*, Barcelona, Spain, May, 2014, pp.1-5

8. Alister G. Burr and Dong Fang, "Performance of Adaptive Linear Physical Layer Network Coding", *European Wireless Conference (EW) 2014*, Barcelona, Spain, May, 2014, pp.1-5

9. Alister G. Burr and Dong Fang, "Linear Physical Layer Network Coding Based on Rings", *IEEE Wireless Communications and Networking Conference (WCNC)*, Istanbul, Turkey, Apr. 2014, pp.370-375.

10. Alister G. Burr and Dong Fang, "Linear mapping functions in Wireless Network Coding", *COST IC1004 TD(13) 08038, WG2 Radio Signalling*, Ghent, Belgium, Sept., 2013

11. Dong Fang and Alister G. Burr, "Multilevel Linear Network Coded Modulation for the Wireless Cloud", *IEEE International Symposium on Wireless Communication Systems (ISWCS)*, Ilmenau, Germany, Aug. 2013, pp.597-601

12. Dong Fang and Alister G. Burr, "Multilevel Coded Linear Physical-layer Network Coding With Extended Mapping in Galois Field for Rayleigh fading Two-Way Relay Channels", *IEEE International Symposium on Personal, Indoor and Mobile Radio Communications (PIMRC)*, London, UK, Sept. 2013, pp.95-99

13. Dong Fang and Alister G. Burr, "Quantization based Rotationally Invariant Coded Modulation for Physical Layer Network Coding in Two-Way Relay Fading Channel", *COST IC1004 TD(12)05065, WG2 Radio Signalling*, Bristol, UK, Sept, 2012

14. Dong Fang, Peng Li, Alister G. Burr and Rodrigo C. de Lamare, "Physical-layer Network Coding based Interference Utilization Scheme for Multi-user in Hierarchical Wireless Network", *European Wireless Conference (EW)*, Poznan, Poland, April, 2012, pp.1-6

15. Dong Fang and Alister G. Burr, "Soft-bit Correction with Robust Quantize-and-Forward for Physical Layer Network coding in Two-Way Relay Fading Channel", *IEEE International Conference on Communications (ICC)*, Ottawa, Canada, June. 2012, pp.1-5

16. Dong Fang and Alister G. Burr, "Quantize and forward relaying for coded physical layer network coding", *COST IC1004 TD(11)01053, WG2 Radio Signalling*, Lund, Sweden, June, 2011

17. Dong Fang and Alister G. Burr, "Soft Bits based fading Correction for Coded Physical Layer Network Coding", *IEEE International Symposium on Wireless Communication Systems (ISWCS)*, Aachen, Germany, Nov. 2011, pp.357-361

18. Dong Fang and Alister G. Burr, “Quantization based Estimate-and-Forward with Unequal Error Protection for Turbo coded Physical Layer Network Coding on the TWRC”, *IEEE International Symposium on Wireless Communication Systems (ISWCS)*, Aachen, Germany, Nov. 2011, pp.859-863

19. Dong Fang and Alister G. Burr, “Performance Degradation of Turbo Coded Physical Layer Network Coding on the Two-Way Relay Channel”, *IEEE International Symposium on Personal, Indoor and Mobile Radio Communications (PIMRC)*, Toronto, Canada, Sept. 2011, pp.1748-1752

Chapter 1

Introduction

1.1 Background and Motivation

In recent years, the application of physical-layer network coding (PNC) [1] has attracted significant attention. Compared with the conventional network coding which consumes three time slots and time scheduling scheme which consumes four time slots, PNC provides a substantial throughput enhancement in two-way relay channels (2-WRC) as it requires only two transmission time slots. For the PNC enabled bi-directional relaying in 2-WRC, we refer to the uplink in the first time slot as the multiple access (MAC) phase and the downlink in the second time slot as the broadcast (BC) phase. However, the authors in [7, 8] pointed out that some singular fading states in the MAC phase inevitably reduce the minimum distance between different network coded symbols (NCS). This significantly degrades the performance of PNC. As such, one fundamental challenge for PNC is how to deal with the fading in the 2-WRC.

We note that the 2-WRC only supports two users' data exchange. As a natural and enriched extension, redesigning the PNC to accommodate the multi-user network (more than two users) is seen as an attractive topic. However, the PNC should be able to deal with interference which increases proportionally with the increase of the number of users. Moreover, the PNC should ensure that the NCS can be unambiguously decoded at each user such that the desired symbol from the other users can be extracted. One possible

solution is to transmit the NCSs with larger code space. However, this sacrifices the spectral efficiency. In summary, the the challenge of PNC in multi-user network is that the redesigned PNC should transmit fewer symbols but support more users.

1.2 Contributions

The aims of this thesis are to tackle the aforementioned challenges of combating fading in 2-WRC and redesigning PNC in multi-user network. The major research outputs are concluded in the following contributions:

1) We propose a coded modulation strategy, named rotationally-invariant coded modulation (RICM), for PNC in 2-WRC. To fully exploit the nature of phase shift which is introduced by the relative fading of 2-WRC, the RICM provides a solution for ambiguous decoding caused by the phase shift using independent decoding for each bit level. Using an adaptive soft demodulator and independent decoding levels, the RICM can eliminate the effect of fading on the 2-WRC. Furthermore, we introduce a low-complexity approach for RICM such that only two fixed demodulators are required. Simulations confirm the performance enhancements by the proposed RICM strategies over the traditional hierarchical decode-and-forward strategy using XOR mapping.

2) We propose a novel PNC based bi-directional data exchange protocol in 2-WRC, in which the fading correction is implemented at the user side. We call it the soft-bit correction (SBC). In such a strategy, the relay maps the received superimposed signal into the network coded soft-bit rather than decoding them. Then the network coded soft-bit is quantized and forwarded to users. The fading effect is then removed at the soft-bit level at each user. The SBC provides the advantages in terms of system complexity and error performance over the the traditional hierarchical decode-and-forward strategy using XOR mapping.

3) We propose a novel linear physical-layer network coding scheme with extended mapping (LPNC-EM) for Rayleigh fading 2-WRC. The LPNC-EM scheme forms two or three independent coding levels which facilitate the use of multilevel coding. This enables the hierarchical decode-and-forward strategy. The numerical results show that uncoded

LPNC-EM outperforms the original PNC using bit-wise eXclusive-OR (XOR) mapping and can achieve a error performance as good as the 5QAM denoise-and-forward (5QAM-DNF) in [8]. Furthermore, the multilevel coded LPNC-EM also provides coding gain over 5QAM-DNF and the coded original PNC.

4) We propose a new type of PNC for 2-WRC by extending the size of alphabet of NCS. We refer to such design as linear physical-layer network coding over hybrid finite ring (HFR-LPNC). In HFR-LPNC, the relay maps the superimposed signal of the two users to a linear network coded combination (LNCC) over the hybrid finite ring, rather than using the simple bit-wise XOR mapping [1]. The optimal linear coefficients are selected to generate the LNCC, aiming to: 1) maximize the sum-rate in the MAC phase; and 2) ensure unambiguous decoding. To avoid the performance degradation caused by high-order irregular mappings, properly designed source coding is used for compressing the LNCC alphabet over the hybrid finite ring into the unifying 4-ary alphabet. We derive the constellation constrained sum-rates for HFR-LPNC in comparison with 5QAM denoise-and-forward (5QAM-DNF) [8], which we use as a reference scheme. Furthermore, we explicitly characterize the rate difference between HFR-LPNC and 5QAM-DNF. Our analysis and simulation show that: 1) HFR-LPNC has a superior ability to mitigate the singular fading compared with 5QAM-DNF; and 2) HFR-LPNC is superior to 5QAM-DNF over a wide range of SNRs.

5) We extend the PNC from the 2-WRC to the hierarchical wireless network (HWN). We redesign the PNC such that network coded symbols of the useful signal and interference signal are jointly decoded. The proposed PNC transforms the naturally occurring co-channel interferences (CCI) into useful signal instead of suppressing them. By fully utilizing the network infrastructure, the proposed strategies provide extra diversity. In addition, we design a new analogue network coding (ANC) for HWN which adopts the interference-aware maximum likelihood detection to mitigate the interference. A straightforward design, the TDMA based PNC (TDMA-PNC), is also introduced as the benchmark. We further derive and compare the constellation constrained sum-rate for each scheme, which clearly demonstrates the substantial performance enhancement provided by the proposed strategies over the TDMA-PNC in HWN.

6) A novel multi-way data exchange enhanced by the coded LPNC is proposed. In

such a design, the relay maps the superimposed signal into the LNCC by multiplying the user data vector by a properly selected generator matrix. A sum-rate based mapping selection scheme is also introduced for generating the optimal LNCC. The unambiguous decoding and minimum cardinality of the proposed LPNC mapping are investigated. The proposed LPNC facilitates the multilevel coding structure using the parallel independent coding levels in which each level is a linear function of user data. This enables the hierarchical decode-and-forward paradigm as in [7]. The simulation results show that: 1) the un-encoded LPNC achieves equal error performance compared with the latin cube based PNC [12]. 2) the un-encoded LPNC provides a superior sum-rate over the opportunistic scheduling based PNC. and 3) MLC-LPNC shows the coding gain over the two benchmarks.

1.3 Thesis Outline

The rest of thesis is organized as follows:

In Chapter 2, the fundamentals of PNC are presented. Firstly, the concept of 2-WRC and PNC are described. Secondly, the challenges of PNC in 2-WRC are discussed. Lastly, the detailed challenge of PNC in multi-user networks is investigated.

In Chapter 3, two fading-resistant strategies for PNC are introduced. The whole chapter is divided into 2 sub-chapters for the RICM and SBC, respectively. The first sub-chapter describes the RICM for PNC in 2-WRC, in which the fully adaptive design and the low-complexity design are introduced. The second sub-chapter describes the SBC for PNC in 2-WRC, in which the fading correction at soft-bit level and robust quantization design are introduced.

In Chapter 4, a novel multilevel coded linear PNC scheme with extended mapping (LPNC-EM) for Rayleigh fading 2-WRC is proposed. We design a mapping selection criterion for LPNC-EM which ensures unambiguous decoding and maximizes the individual rate of each user. The LPNC-EM scheme forms two or three independent coding levels which facilitate the use of multilevel coding. Lastly, we compare the end-to-end sum-rate and frame error rate for LPNC-EM, original PNC and 5QAM-DNF.

In Chapter 5, a new LPNC over the hybrid finite ring is proposed. The analysis of sum-rate in MAC phase for LPNC over different rings are presented. Based the analyzed results of sum-rate, we provide a simplified design for LPNC. A rate based 5QAM-DNF is also introduced as the benchmark. Lastly, we compare the end-to-end sum-rate for each strategy.

In Chapter 6, we redesign the PNC and ANC for HWN. The TDMA based PNC is also introduced as the benchmark. The constellation constraint sum-rate for each strategy are derived. The rate analysis for each strategy is also given. Lastly, we discuss the resulting diversity performance of each strategy, based on the outage probability analysis.

In Chapter 7, a coded LPNC for M-WRC is proposed. We firstly present the detailed design of its mapping strategy. Then the unambiguous decoding and sum-rate of proposed are discussed. Lastly, we compare the proposed LPNC with several strategies in the literature.

In Chapter 8, conclusions and a discussion on possibilities for future work are presented.

1.4 Notation

In this thesis, we use upper case characters to denote random variables, and lower case characters to denote the numerical values of a random variable. We use capital and small bold fonts to denote matrices and vectors. $\mathbb{E}\{\cdot\}$ denotes the statistical expectation operator.

Chapter 2

The Fundamentals of Physical-layer Network Coding

2.1 The 2-way Relay Channels

Wireless relaying is identified as a promising technique to offer spatial diversity and to extend the coverage of wireless networks. In a wireless relay network, the relay acts as the 'intermediary' for data exchange among different users. The 2-way relay channel is regarded as a classical representative of wireless relay network and has been investigated extensively in recent years. The origin of 2-WRC can be traced to Shannnon's pioneering work in [9], where the rudiment of 2-WRC, i.e., the 2-way channel (2-WC) without relay was investigated. Later on, some pioneer work was led and done by Van der Meulen [10], Cover and El Gamal [11].

The 2-WRC can be treated as a combination of 2-WC and relay network. As seen in Fig. 2.1, the 2-WRC is a three-node linear network in which two users A and B want to exchange their data via a relay node R. The uplink of 2-WRC, i.e., the links from the two users to the relay, can be seen as a multiple access channel (MAC) while the downlink, i.e., the links from the relay to the two users, can be seen as a broadcast channel (BC). All nodes operate in half-duplex mode and a direct link between the two users is unavailable. Similar to other types of relay network, the traditional amplify-and-forward (AF) and

decode-and-forward (DF) strategies can be implemented in the 2-WRC [5].

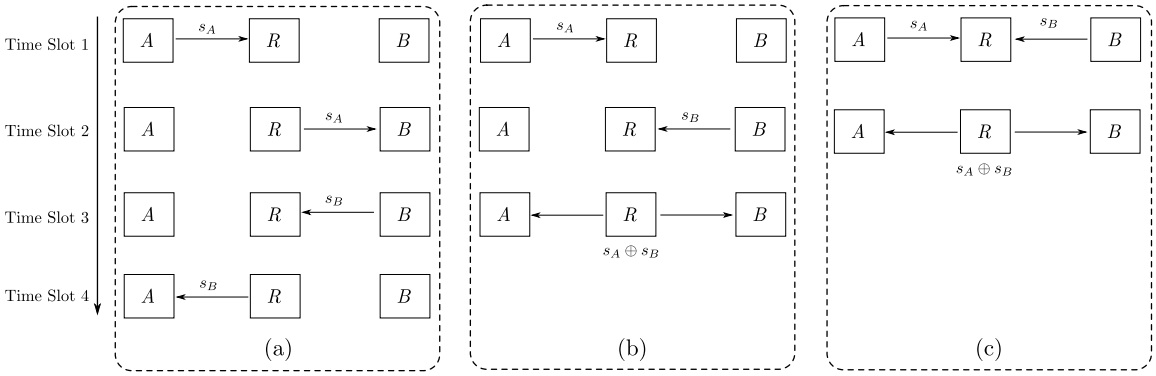

Figure 2.1: (a) Conventional TDMA (b) Standard NC (c) PNC

A conventional bi-directional data exchange protocol is TDMA, as shown in Fig. 2.1(a). In such a protocol, each user alternately transmits their signal to the relay which avoids the co-channel interference. However, this consumes four orthogonal time slots and hence sacrifices spectral efficiency. As an alternative approach, standard network coding, as shown in Fig. 2.1(b), allows the relay to generate the XOR combination (regarded as the network coded data) of the data from the two users and forward to them. Two users then extract the desired data by using the XOR operation on the received network coded data and their side-information. However, the standard NC still requires three transmission phases as each user transmits data to the relay using different time-slots.

By fully exploiting the superposition nature of electromagnetic waves, PNC in [1, 5] allows two users simultaneously to transmit their signals to the relay in the MAC phase, as shown in Fig. 2.1(c). The relay directly maps the superimposed signal into the XOR combination of data from the two users, which is referred to as the network coded symbol. Then in the BC phase, the resulting network coded symbol is forwarded to the users. PNC provides a substantial improvement in terms of the spectral efficiency over the TDMA and standard NC protocol as it only consumes two transmission time slots. The concept of PNC is detailed in the next section.

2.2 The Multi-way Relay Channels

The natural extension of the 2-WRC is the multi-way relay channel (M-WRC), as shown in Fig. 2.2. The M-WRC consists of M users ($U_i, i \in \{1, 2, 3, ..., M\}$) and a shared relay ($R$). All users operate in half-duplex mode and there is no direct link among users. The multi-way data exchange takes place among the users with the help of the relay. Each user expects to decode the data from all other users based on exploiting the signal received from the relay and its own side information.

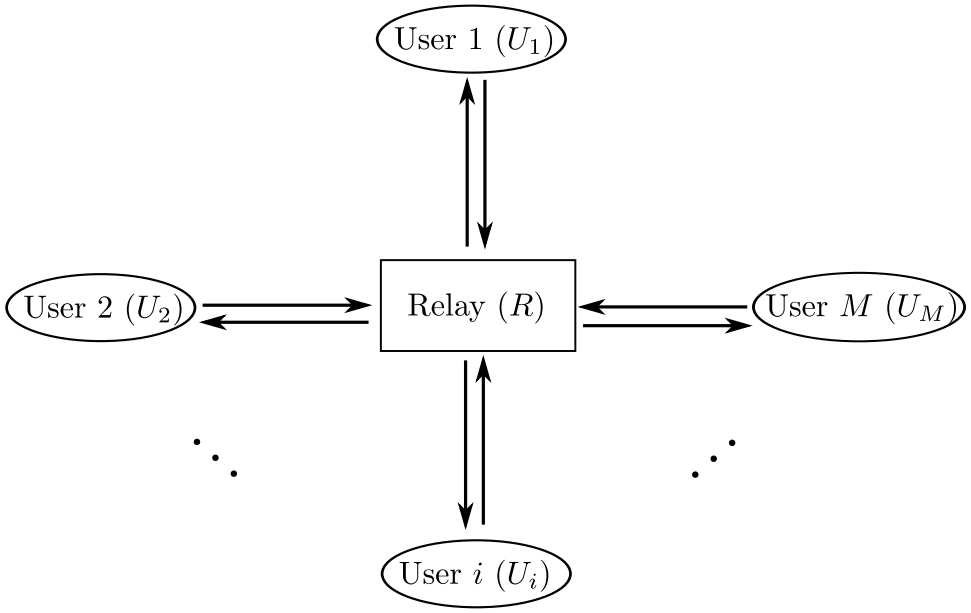

Figure 2.2: The model of M-WRC

The conventional data exchange protocol is the user scheduling [14], in which the users alternately transmit their signal to avoid co-channel interference. However, this results in a low spectral efficiency. In contrast to the scheduling approach, PNC allows the users to simultaneously transmit the signals in the same channel. The spectral efficiency is thus much improved. However, due to the co-channel interference in the MAC phase, the question of how the users recover their desired signal with the minimum cost is the major concern for PNC design in M-WRC.

2.3 Physical-layer Network Coding

In this section, we provide the fundamental concept of PNC.

2.3.1 PNC using XOR mapping

Here, we show the simplest case of PNC in the 2-WRC, where two users adopt BPSK modulation. Let $\mathscr{A}_2 = \{-1, +1\}$ denote the Gray coded BPSK alphabet. The mapping from user symbol to modulated symbol is denoted as $\mathcal{M}_{\mathrm{B}} : \mathrm{GF}(2) \rightarrow \mathscr{A}_2$. The BPSK symbols transmitted by user i, $i \in \{A,B\}$ denoted as x_i, is then given by $x_i = \mathcal{M}_{\mathrm{B}}(s_i) = 1 - 2s_i$. The channel gain from user i to *R* is denoted as h_i. In the MAC phase, *A* and *B* simultaneously transmit their signal to *R*. Due to the superimposition nature of EM waves, the relay *R* receives

$$y_R = h_A x_A + h_B x_B + n_R, \tag{2.1}$$

where n_R is the additive white Gaussian noise (AWGN) with the variance σ^2. Without loss of generality, we assume that $|h_A| \geq |h_B|$. The noiseless superimposed constellation at the relay is illustrated in Fig. 2.3, where the PNC mapping proposed in [1] is implemented. We observe that the superimposed signal is in fact mapped as the XOR combination of data from the two users, given by $s_R = s_A \oplus s_B$, where s_R denotes the network coded symbol (NCS) and $\oplus$ denotes the bit-wise XOR operation (the module-2 sum in the binary field). Let $x_{AB} \triangleq h_A x_A + h_B x_B$ denote the superimposed signal. Based on Fig. 2.3, the mapping from the superimposed signal into the NCS is given by

$$\begin{aligned} & x_{AB} \rightarrow s_R \\ & \text{s.t. } s_R = s_A \oplus s_B. \end{aligned} \tag{2.2}$$

Let $\mathcal{S}_R$ denote the alphabet of NCS. Clearly, the above mapping function results in a compression on data from the two users since the cardinality of $\mathcal{S}_R$ is equal to that of the user alphabet. As such, BPSK can be adopted to transmit the NCS. The BPSK modulated NCS, denoted as x_R, is given by $x_R = \mathcal{M}_{\mathrm{B}}(s_R)$. After receiving the NCS, each user can decode their desired symbol by using XOR operation, i.e., $\tilde{s}_B = s_A \oplus s_R$ and $\tilde{s}_A = s_B \oplus s_R$, where $\tilde{s}_i$ denotes the recovered symbol.

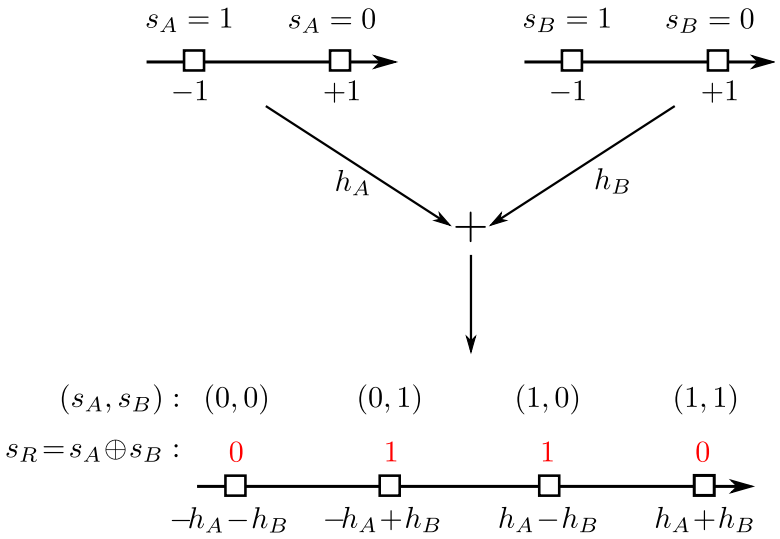

Figure 2.3: Superimposed Constellation of PNC when using BPSK

2.3.2 Rate Region of PNC

The authors in [5, 7] pointed out that in PNC, the individual rate of each user in the MAC is bounded by the mutual information between the received signal and the NCS, ,denoted by $I(Y_R; S_R)$, where Y_R and S_R are the random variable of y_R and s_R, respectively. The mutual information $I(Y_R; S_R)$ can be expanded as

$$R_A = R_B \leq I(Y_R; S_R), \tag{2.3}$$

where R_i denotes the achievable rate of user i.

The mutual information $I(Y_R; S_R)$ is expanded as

$$I(Y_R; S_R) = H(Y_R) - H(Y_R|S_R). \tag{2.4}$$

The entropy of the received signal is given by

$$H(Y_R) = -\int_{y_R \in \mathbb{C}} p(y_R) \log_2 \left(p(y_R)\right) dy_R, \tag{2.5}$$

where the PDF of the received signal is calculated as

$$p(y_R) = \sum_{x_A, x_B \in \mathscr{A}_2} P(x_A) P(x_B) p(y_R|x_A, x_B). \tag{2.6}$$

The conditional entropy $H(Y_R|S_R)$ in (12) can be calculated as

$$\begin{aligned} H(Y_R|S_R) &= -\sum_{s_R\in\mathscr{A}_2}\int_{y_R\in\mathbb{C}} p\left(y_R, s_R\right)\log_2\left(p\left(y_R|s_R\right)\right)dy_R \\ &= -\sum_{s_R\in\mathscr{A}_2} P(s_R)\int_{y_R\in\mathbb{C}} p\left(y_R|s_R\right)\log_2\left(p\left(y_R|s_R\right)\right)dy_R. \end{aligned} \tag{2.7}$$

Note that neither $H(Y_R)$ in (2.5) nor $H(Y_R|S_R)$ in (2.7) can be written in closed form. Hence, we use Monte-Carlo integration instead. The mutual information in (2.4) thus can be computed as

$$I(Y_R; S_R) = \mathbb{E}\left[\log_2\left(p(Y_R)\right)\right] - \mathbb{E}\left[\log_2\left(p\left(Y_R|S_R\right)\right)\right], \tag{2.8}$$

where $\mathbb{E}[\cdot]$ means the the empirical mean.

2.3.3 Fading issue of PNC in 2-WRC

The well-known challenge for PNC in 2-WRC is the fading in the MAC phase. We can see that when two channels in MAC phase experience different fading, there will be a relative phase rotation and amplitude variation. So the fading issue can be treated as a combination of phase synchronization and amplitude variation [8]. In the following, we describe the fading issue of PNC in detail.

Consider a 2-WRC where the users adopt QPSK modulation. Let $\mathscr{A}_4 = \{+1, +j, -1, -j\}$ denote the Gray coded QPSK alphabet with unit energy constraint. The mapping from user symbol to complex symbol is denoted as $\mathcal{M}_{\mathrm{Q}} : \mathrm{GF}\left(2^2\right) \rightarrow \mathscr{A}_4$. The QPSK symbols transmitted by user i, $i \in \{A,B\}$ denoted as x_i, is then given by $x_i = \mathcal{M}_{\mathrm{Q}}(s_i)$. The superimposed signal is given in (2.1). Let $h_{re} \triangleq h_B/h_A = re^{j\phi}$ denote the relative fading factor, where r is the channel amplitude ratio and ϕ is phase shift. We refer to

$$x_{AB} \triangleq h_A x_A + h_B x_B \tag{2.9}$$

as the noiseless *superimposed signal (SS)*.

Based on the original PNC design using XOR mapping, we have the following maxi-

mum likelihood (ML) detection

$$\hat{s}_R = \arg\max_{s_R \in \mathscr{A}_4} p(y_R|s_R) = \arg\max_{s_R \in \mathscr{A}_4} \sum_{x_A, x_B : s_R = s_A \oplus s_B} P(x_A)P(x_B)p(y_R|x_A, x_B), \quad (2.10)$$

where the conditional probability density function (PDF) $p(y_R|x_{AB})$ is given by

$$p(y_R|x_A, x_B) = \frac{1}{2\pi\sigma_w^2} \exp\left(-\frac{|y_R - x_{AB}|^2}{2\sigma_w^2}\right). \quad (2.11)$$

We define the set of x_{AB} associated with the same s_R as $\mathcal{X}_{AB}(s_R)$ while we define $\bar{\mathcal{X}}_{AB}(s_R) \triangleq \bigcup_{s_R \neq s'_R} \mathcal{X}_{AB}(s'_R)$ as its complementary set. The minimum squared Euclidean distance (MSED) between different x_{AB} associated with different s_R is computed as

$$d^2_{\min}(s_R) = \min_{\substack{x_{AB} \in \mathcal{X}_{AB}(s_R) \\ x'_{AB} \in \bar{\mathcal{X}}_{AB}(s'_R)}} |x_{AB} - x'_{AB}|^2. \quad (2.12)$$

The authors in [8] pointed out that the original PNC using XOR mapping has a significant performance degradation when h_{re} occurs on: $h_{re} = \pm j$, $h_{re} = \pm\frac{1}{2}(1 \pm j)$, $h_{re} = \pm 1 \pm j$ and $h_{re} \approx 0$, which are referred to as *singular fading*. This can be reflected on the MSED plot over the complex plane of h_{re}, as shown in Fig. 2.4. We can clearly observe that the MSED around the singular fade states approaches zero. As such, around these singular points, the XOR mapping cannot distinguish the nearest neighbouring x_{AB} associated with different s_R. As a result, the mutual information $I(Y_R; S_R)$ is degraded, as shown in Fig. 2.5. From Fig. 2.5, we clearly observe that different singular fading has different the degradation effect on $I(Y_R; S_R)$. The most severe degradation is caused by $h_{re} \approx 0$. In such circumstances, one of the links from users is completely faded such that the NCS can not be generated from (2.10).

2.3.4 Denoise-and-forward in 2-WRC

In the previous section, we discussed the challenge of PNC in 2-WRC, i.e., the singular fading in the MAC phase. To address this issue, several fading correction strategies for PNC are proposed [8, 12, 15]. Of all these strategies, DNF in [8] is a remarkable one which investigates the issue of singular fading for PNC and proposes a solution for it. In the following, we describe the basic idea of DNF.

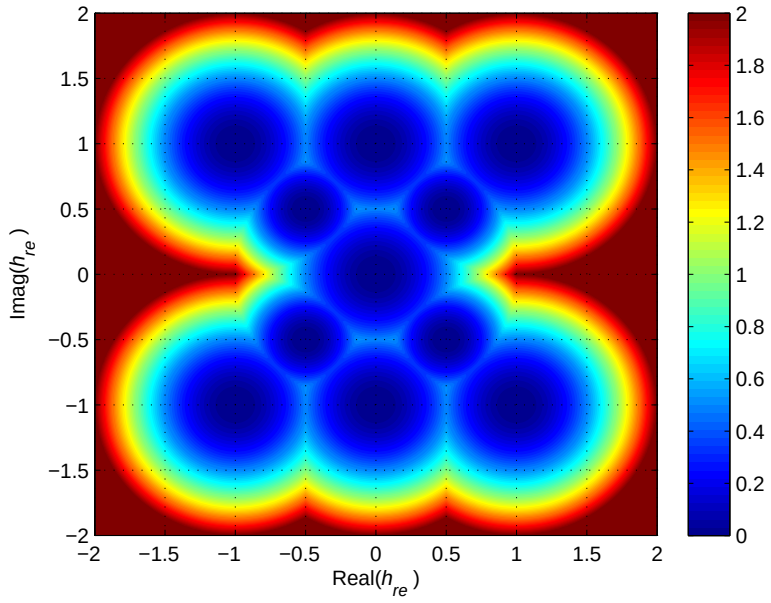

Figure 2.4: d^2_{min} v.s. h_{re} for PNC using XOR mapping [1]

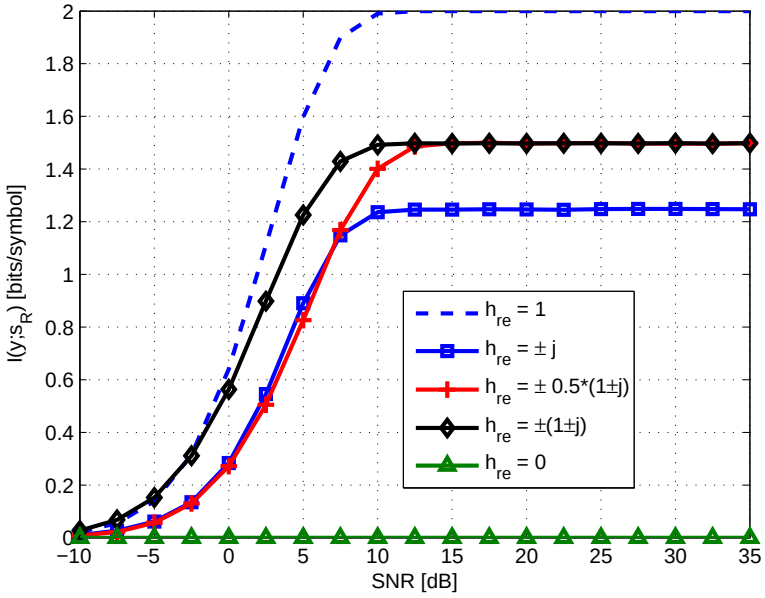

Figure 2.5: $I(Y_R; S_R)$ v.s. SNR

Consider a QPSK based 2-WRC. The authors in [8] propose a non-linear mapping for PNC, i.e., the 4-ary user data are adaptively mapped into the 4- or 5-ary NCS, defined as

$$\mathcal{C} : x_{AB} \rightarrow s_R, \quad s_R \in \mathbb{Z}_4 \ \text{ or } \ \mathbb{Z}_5, \tag{2.13}$$

where $\mathbb{Z}_q = \{0, 1, 2, ..., q-1\}$.

For successful decoding, the non-linear mapping $\mathcal{C}$ must meet the following requirement

$$\begin{aligned} \mathcal{C}(s_A, \ \ s_B) &\neq \mathcal{C}(s'_A, \ \ s_B), \ \forall s_A \neq s'_A, \\ \mathcal{C}(s_A, \ \ s_B) &\neq \mathcal{C}(s_A, \ \ s'_B), \ \forall s_B \neq s'_B, \end{aligned} \tag{2.14}$$

which is referred to as the *exclusive law*.

The authors in [8] also proposed the so-called closest-neighbour clustering algorithms, taking the exclusive law into consideration, as shown in Algorithm 1 of [8]. The resulting mapping $\mathcal{C}$ is provided in Table 1 of [8]. This algorithm provides an optimal code which has the largest MSED profile for a given channel condition. Fig. 2.6 shows the MSED d^2_{min} of DNF against the relative fading factor h_{re}. Based on Fig. 2.6, we observe that the DNF mitigates the singular fading around $h_{re} = \pm j$, $h_{re} = \pm\frac{1}{2}(1 \pm j)$ and $h_{re} = \pm 1 \pm j$ except $h_{re} \approx 0$.

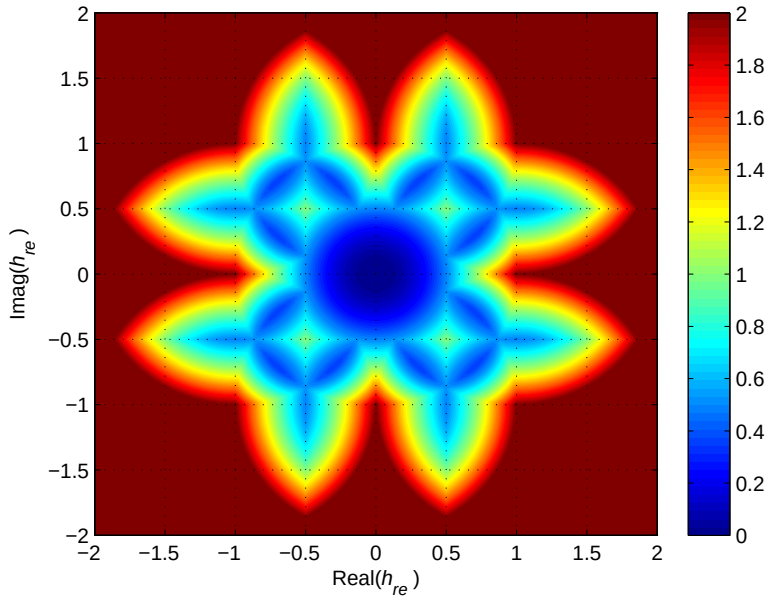

Figure 2.6: d^2_{min} v.s. h_{re} for DNF [8].

DNF extends the cardinality of NCS alphabet from 4-ary to 5-ary. As such, the BC

phase might require the irregular modulation. Greedy sphere packing is used to generate the 5QAM for 5-ary mapping [8]. The 5QAM modulation brings out the irregularity in the modem communication systems. In Chapter 4, we propose a novel linear physical-layer network coding which avoids the irregular modulation and has a superior capability to mitigate the singular fading.

2.3.5 The challenge of PNC in M-WRC

In this subsection, we discuss the challenges of PNC in the M-WRC. The design criteria of PNC in the M-WRC mainly focus on: 1) ensuring the multi-user exclusive law; and 2) following the minimum cardinality constraints as in [8].

We extend the 2-WRC to the M-WRC. We assume that there are M users which employ the same constellation mapper $\mathcal{M}_U(\cdot)$. The superimposed signal at the relay ***R*** is given by

$$y_R = \sum_{i=1}^{M} h_i x_i + n_R, \tag{2.15}$$

where $x_i = \mathcal{M}_U(s_i)$, $i \in \{1, 2, ..., M\}$ is the modulated symbol of the i-th user and s_i is the user data.

We refer to

$$x_{ss} \triangleq \sum_{i=1}^{M} h_i x_i \tag{2.16}$$

as the noiseless superimposed signal (SS) at R.

The PNC mapping for the M-WRC is defined as

$$\mathcal{M} : x_{ss} \rightarrow s_R \tag{2.17}$$

such that

$$\begin{aligned}
&\mathcal{M}(s_1, s_2, s_3, \cdots, s_M) \neq \mathcal{M}(s_1, s'_2, s_3, \cdots, s'_M), \ \forall (s_2, s_3, \cdots, s_M) \neq (s'_2, s'_3, \cdots, s'_M) \\
&\mathcal{M}(s_1, s_2, s_3, \cdots, s_M) \neq \mathcal{M}(s'_1, s_2, s'_3, \cdots, s'_M), \ \forall (s_1, s_3, \cdots, s_M) \neq (s'_1, s'_3, \cdots, s'_M) \\
&\mathcal{M}(s_1, s_2, s_3, \cdots, s_M) \neq \mathcal{M}(s'_1, s'_2, s_3, \cdots, s'_M), \ \forall (s_1, s_2, \cdots, s_M) \neq (s'_1, s'_2, s'_4 \cdots, s'_M) \\
&\qquad\qquad \vdots \\
&\mathcal{M}(s_1, s_2, s_3, \cdots, s_M) \neq \mathcal{M}(s'_1, s'_2, s'_3, \cdots, s_M), \ \forall (s_1, s_2, \cdots, s_{M-1}) \neq (s'_1, s'_2, \cdots, s'_{M-1})
\end{aligned} \tag{2.18}$$

is satisfied. We refer to (2.18) as the multiuser exclusive law which extends (2.14) from the 2-WRC to the M-WRC.

We define the alphabet of NCS as $\mathcal{S}_R$. The cardinality of $\mathcal{S}_R$ is defined as $|\mathcal{S}_R|$. Given that (2.18) is satisfied, $|\mathcal{S}_R|$ should be as small as possible. This is referred to as the minimum cardinality constraint. Clearly, the minimum cardinality guarantees the superiority of PNC in BC transmission.

In summary, the multiuser exclusive law and the minimum cardinality constraint should be jointly taken into account. This poses a challenge for PNC in the M-WRC.

2.3.6 Latin Hyper-Cube PNC in the M-WRC

The authors in [12] proposed an adaptive PNC for the M-WRC, which adopts the Latin hypercube to generate the network coded mapping at the relay. The elements in such a Latin cube are the value of NCS for which the superimposed signal is mapped into.

Consider a 3-WRC, the received signal is given in (2.15). The mapping function at the relay is denoted as (2.17), which is generated from a 3-fold Latin cube as shown in Fig. 2.7. The definition of the Latin cube is given by

Definition 1 [12, 57]: A 3-fold Latin cube L of side N on the symbols from the set $\mathbb{Z}_t = \{0,\ 1,\ 2,\ ...,\ t-1\}$, where $t = M^2$, is an $N \times N \times N$ array, in which each cell contains one symbol and each symbol occurs at most once in each row, column and file.

The cell of such a Latin cube, namely, the NCS is generated from Algorithm 1 of [57].

It is worth noting that if any side of the Latin cube and resulting NCS are determined, then the values of the other two sides are uniquely determined. This in fact indicates that the multiuser exclusive law (2.18) is satisfied. The Algorithm 1 in [57] generates the NCS using row-wise or column-wise permutation such that the singular fade states in the MAC phase are mitigated. For a given channel state, the Algorithm 1 of [57] always outputs the NCS with the largest MSED profile. However, this results in an enlarged cardinality of NCS alphabets and requires a 3-dimensional exhaustive search. The Latin cube based mapping design is in fact a type of non-linear mapping. As such, linear codes cannot be adopted.

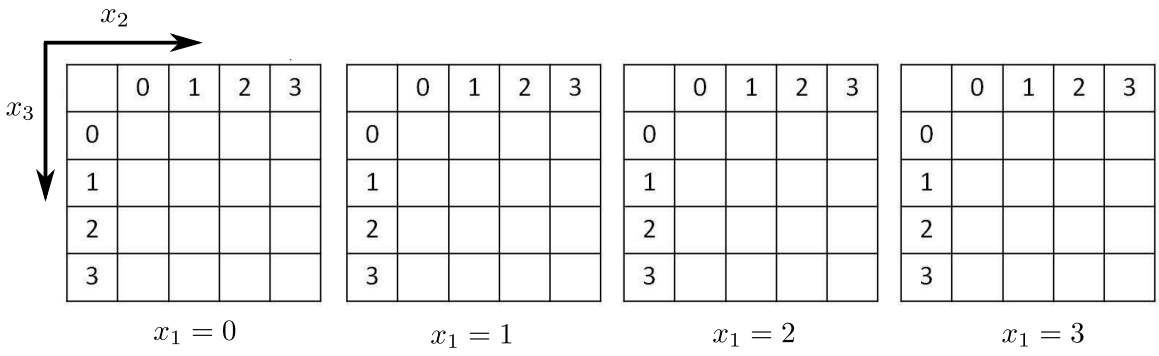

Figure 2.7: A 3-fold Latin Cube for 3-WRC.

2.3.7 Hierarchical Decode-and-forward

The hierarchical decode-and-forward (HDF) paradigm for PNC was originally proposed in [7]. In essence, such a scheme aims to exploit the PNC mapping in order to use the linear codes, that is, the mapped NCS sequence is a valid code sequence which can be directly fed into the channel decoder. In this subsection, we will describe the HDF scheme in detail.

Suppose that both users in the 2-WRC employ a rate k/n linear code $\mathcal{C} : \{0,1\}^k \mapsto \{0,1\}^n$ such that the uncoded data sequence $\boldsymbol{d}_i$, $i \in \{A, B\}$ is mapped into the coded sequence $\boldsymbol{s}_i$, i.e., $\mathcal{C}(\boldsymbol{d}_i) = \boldsymbol{s}_i$. Then the two users adopt the same modulation scheme $\mathcal{M}_S(.)$ to transmit simultaneously in the MAC phase. The electromagnetic signals are superimposed and received by the relay, given by

$$\boldsymbol{y}_R = h_A \boldsymbol{x}_A + h_B \boldsymbol{x}_B + \boldsymbol{n}_R, \tag{2.19}$$

where $\boldsymbol{x}_i = \mathcal{M}_S(\boldsymbol{x}_i), i \in \{A, B\}$ is the modulated symbol.

Let $\boldsymbol{x}_{ss} \triangleq h_A\boldsymbol{x}_A + h_B\boldsymbol{x}_B$ denote the superimposed sequence. In [7], the authors state that the HDF paradigm enables the PNC mapping: $\mathcal{M}_{\mathcal{R}} : x_{ss}[t] \mapsto s_R[t]$, where s_R denotes the resulting NCS and t is the symbol index, such that the NCS sequence $\boldsymbol{s}_R$ is a valid codeword belonging to $\mathcal{C}$, i.e., $\boldsymbol{s}_R \subset \mathcal{C}$. Therefore $\boldsymbol{s}_R$ can be directly fed into the channel decoder $\mathcal{C}^{-1} : \{0,1\}^n \mapsto \{0,1\}^k$. The output of the channel decoder, denoted by $\boldsymbol{d}_R$ is also a network coded combination of the original data sequences of the two users, given by $\boldsymbol{d}_R = \mathcal{C}^{-1}(\boldsymbol{s}_R)$. The diagram of HDF is shown in Fig. 2.8.

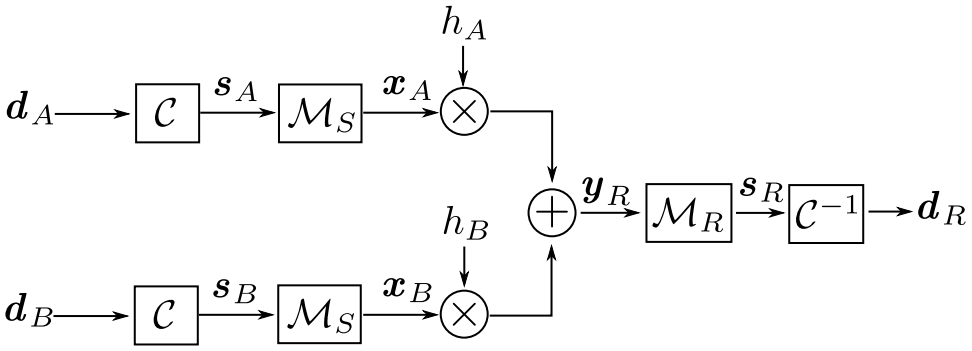

Figure 2.8: System Diagram of HDF.

Clearly, the HDF for PNC should also satisfy the exclusive law, given by

$$\begin{aligned} \mathcal{C}\left(\mathcal{M}_R\left(\boldsymbol{d}_A, \boldsymbol{d}_B\right)\right) &\neq \mathcal{C}\left(\mathcal{M}_R\left(\boldsymbol{d'}_A, \boldsymbol{d}_B\right)\right), \boldsymbol{d}_A \neq \boldsymbol{d'}_A, \\ \mathcal{C}\left(\mathcal{M}_R\left(\boldsymbol{d}_A, \boldsymbol{d}_B\right)\right) &\neq \mathcal{C}\left(\mathcal{M}_R\left(\boldsymbol{d}_A, \boldsymbol{d'}_B\right)\right), \boldsymbol{d}_B \neq \boldsymbol{d'}_B. \end{aligned} \tag{2.20}$$

where we note that the linearity of codes should be guaranteed by the PNC mapping $\mathcal{M}_R$. This implies that to facilitate the HDF scheme, constructing linear PNC (LPNC) mapping is necessary. Some examples of HDF are provided in Chapters 3, 4 and 5.

Chapter 3

Fading Correction for Physical-layer Network Coding in the 2-way Relay Channels

Contents

3.1 Overview

In this chapter, we propose two schemes for PNC to combat fading in 2-WRC: 1) rotationally invariant coded modulation (RICM) for PNC; and 2) soft-bit correction with robust quantize-and-forward (SBC-QF) for PNC. These two schemes provides different approaches to combat fading, i.e., RICM mitigates the fading of MAC phase at relay while SBC eliminates the effect of fading at destination.

3.2 Scheme 1: Rotationally Invariant Coded Modulation for Physical-layer Network Coding

3.2.1 Overview

In this section, we propose a novel coded modulation scheme for PNC in the fading 2-WRC. Using an adaptive soft demodulator and several parallel decoders, the proposed scheme can eliminate the effect of fading on the 2-WRC. To reduce system complexity at the relay, we also give a low-complexity two-demodulator scheme. Based on maximizing the mutual information between received signal at the relay and network coded symbol, the optimal one of two PNC mappers is then selected. The proposed simplified scheme exhibits advantages in terms of flexibility, complexity and performance.

3.2.2 Introduction

For the PNC protocol, it has been proven [2, 3] that fading in MAC phase can introduce phase shifts which lead to exclusive law failure for some points in the superimposed constellation, which significantly degrades the performance. Thus, to combat fading in the 2-WRC is an important issue for PNC. The achievement in [3] provides a novel denoise-and-forward (DNF) scheme to mitigate the effect of fading on the 2-WRC. A 5-ary irregular constellation mapping is involved in the design of the adaptive network coding for different channel parameters. But their proposed 5-ary mapping is too irregular to be employed in common wireless systems. Moreover, the adaptive receivers at the relay need to use the closest-neighbor clustering algorithm to select the proper mapping, which would require exhaustive search. In [4], the authors combine DNF with trellis coded modulation (TCM). The drawback of their scheme is that the coding structure for TCM is changed and the relay needs to adapt two different relaying protocols. Another novel scheme was introduced in [15], the authors introduced a kind of Pseudo XOR (PXOR) algorithm to optimize the LDPC Coded PNC in a fading 2-WRC. In order to compensate the channel fading, the PXOR algorithm optimizes the Euclidean distance by dynamically adjusting the symbol distance. Their scheme is limited to the LDPC code, and is not flexible for an

arbitrary channel code. In addition, we should notice that a common shortcoming of the above mentioned schemes is the high system complexity.

In this section, we aim to eliminate the effect of fading in the 2-WRC. We propose the RICM scheme which is robust for any phase shifts and flexible for any channel code. The proposed scheme can achieve a proper balance between the complexity and performance.

3.2.3 Simple Model of PNC in 2-WRC

The 2-WRC consists of two users (*A* and *B*) and one relay (*R*). PNC allows two users using the same modulation scheme $\mathcal{M}_S(.)$ to transmit simultaneously in the MAC phase. The electromagnetic signals are superimposed and received by the relay, given by

$$\boldsymbol{y}_R = h_A \boldsymbol{s}_A + h_B \boldsymbol{s}_B + \boldsymbol{n}_w, \tag{3.1}$$

where $\boldsymbol{s}_i = \mathcal{M}_S(\boldsymbol{x}_i), i \in \{A, B\}$ is the modulated symbol for each user, especially, we assume that both users employ Gray mapped QPSK whose constellation has unity energy (thus, $s_i \in \mathcal{Q}_4,\ i \in \{A, B\}, \forall s_i \in \boldsymbol{s}_i$, where $\mathcal{Q}_4$ is the QPSK alphabet whose cardinality is 4). The codeword $\boldsymbol{x}_i$ is obtained by encoding the data word $\boldsymbol{d}_i, i \in \{A, B\}$. For QPSK, each symbol in the codeword sequence can be represented as a *2-bit binary tuple*, i.e. $x_i \in \mathcal{Z}_4,\ i \in \{A, B\}$, (where $\mathcal{Z}_q = \{0, 1, ...q-1\}$). We refer to the result of the bit-wise eXclusive-OR (XOR) operation on x_A and x_B as the network coded symbol $x_\oplus$, i.e. $x_\oplus = x_A \oplus x_B$, which also takes the form of a 2-bit binary tuple. Here, we suppose that both users are memoryless uniform sources and they employ an identical codebook $\mathcal{C}$. h_A and h_B are the channel gains from *A* and *B* to *C*, respectively. $\boldsymbol{n}_w$ is the complex Additive Gaussian White Noise (AWGN) with the variance σ_w^2 per complex dimension. We substitute the *superimposed signal* $\boldsymbol{s}_\oplus = h_A \boldsymbol{s}_A + h_B \boldsymbol{s}_B$ into (3.1) and obtain $\boldsymbol{y}_R = \boldsymbol{s}_\oplus + \boldsymbol{n}_w$. The relay processes the received signal based on the network coding paradigm and forwards network coded data stream $\boldsymbol{x}_\oplus$ or its variations (compressed version, etc.) with modulation scheme $\mathcal{M}_R(.)$ for the BC phase.

3.2.4 RICM with Fully Adaptive Demodulator

Normally, it is assumed that the channel status information (CSI) is known to the receiver side only, that is, to the relay only for the MAC phase and to the destination users only for the BC phase [2, 3]. We pay particular attention to the fading in the MAC phase since the fading in the BC phase can be well compensated at the destination users. Based on (3.1), we denote the relative fading factor as $h = h_B/h_A = re^{j\varphi}$ which is the ratio of two channel gains (r is the channel amplitude ratio and φ is the phase shift). So after a scaling by $1/h_A$, the superimposed signal can be equivalently expressed as $\boldsymbol{s}_\oplus = \boldsymbol{s}_A + h\boldsymbol{s}_B$. As in [2-5], we also assume that two channel links in MAC phase have same average power: $E[|h_A|^2] = E[|h_B|^2]$ ($E[.]$ is the expectation function) to respect the symmetry of the rates from A and B.

Adaptive Soft Demodulator with Network Coded Symbol based Clustering

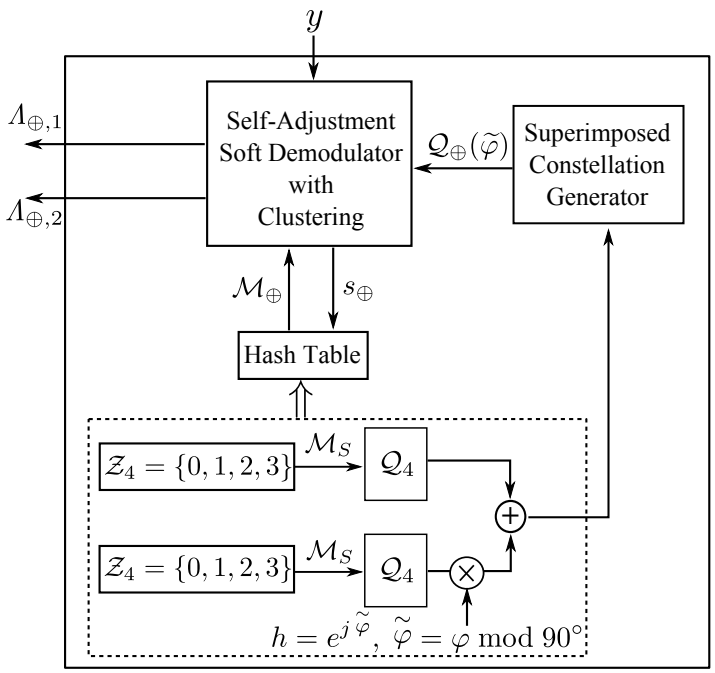

Figure 3.1: Structure of Adaptive Soft Demodulator.

Clearly, an appropriate mapping scheme $\mathcal{M}(x_A, x_B)$ will determine the performance of PNC. In [3], the authors state the requirement of successful decoding with an arbitrary

mapping: the *exclusive law*, which is

$$\begin{aligned}\mathcal{M}(x_A, x_B) \neq \mathcal{M}(x_A^{'}, x_B) \forall\, x_A \neq x_A^{'} \in \mathcal{Z}_4 \text{ and } x_B \in \mathcal{Z}_4,\\ \mathcal{M}(x_A, x_B) \neq \mathcal{M}(x_A, x_B^{'}) \forall\, x_B \neq x_B^{'} \in \mathcal{Z}_4 \text{ and } x_A \in \mathcal{Z}_4.\end{aligned} \tag{3.2}$$

Note that DNF is an uncoded scheme. In order to effectively eliminate the distortion, DNF must avoid the reduction of Euclidean distance between neighboring points in the superimposed constellation. Under some specific singular fade states, the irregular 5-ary mapping is involved. In order to avoid using such an irregular network coding and fully utilize the capability of the channel codes, we propose a network coded symbol based clustering algorithm to design the adaptive soft demodulator. The detailed structure is shown in Fig. 3.1.

At the relay, we build a virtual scenario in which two sources are used to simulate *A* and *B*. Each virtual user generates the integer set $\mathcal{Z}_4$ and then maps its elements to the QPSK symbols. Also, a phase shift $\widetilde{\varphi}$ and signal superimposition are introduced to simulate the PNC paradigm in the MAC phase. Here, note that the phase shift is taken modulo-90°, i.e. $\widetilde{\varphi} = \varphi \bmod 90^\circ$ (the reason for this is explained below). In this virtual scenario, both source symbols and the corresponding superimposed signals with fading information will be stored in a Hash table. At the same time, the constellation generator provides a superimposed constellation $\mathcal{Q}_{\oplus}(\widetilde{\varphi})$ to the self-adjustment soft demodulator based on the virtual code superimposition. At the final stage, the demodulator queries the Hash Table to check all possible original code pairs $(x_A, x_B) \in \mathcal{Z}_4 \times \mathcal{Z}_4$ for each superimposed signal $s_{\oplus} \in \mathcal{Q}_{\oplus}(\widetilde{\varphi})$.

Fig. 3.2 shows an example of store-and-query procedure for our designed Hash table. The superimposed codes are all stored in a super-table and all possible signal superimposition actions are stored in the sub-tables. The soft demodulator will check whether the closest neighbor superimposed codes $s_{\oplus} \in \mathcal{Q}_{\oplus}(\widetilde{\varphi})$ can be clustered and mapped to a same network coded symbol $x_{\oplus}$. It successively queries the superimposed code $s_{\oplus}$ in the Hash Table. The super-table is firstly traversed and the matched ones are picked, then the corresponding sub-table gives all superimposition actions. By demapping function $\mathcal{M}_S^{-1}(.)$, the original code pairs (x_A, x_B) will be given. Then the network coded symbols $x_{\oplus}$ are obtained by eXclusive-OR operation and the satisfaction of clustering and mapping to a same network coded symbol for the closest points can be easily checked. Obviously, the

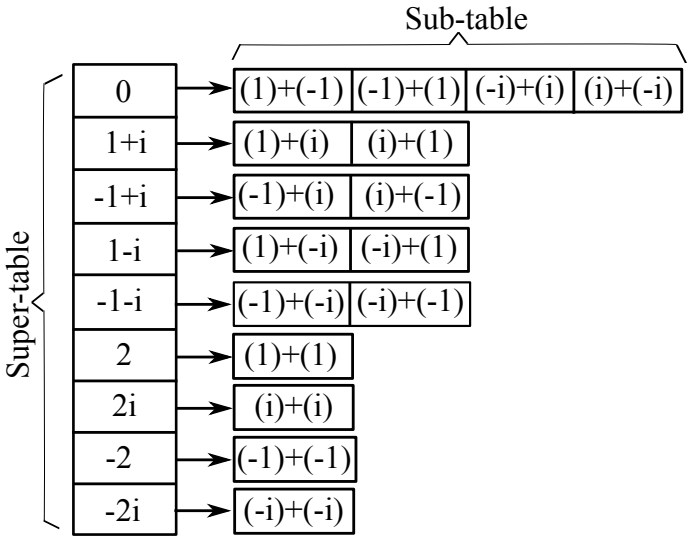

Figure 3.2: Store-and-query procedure of Hash Table ($\varphi = 0°$).

network coded symbol based clustering always guarantees the eXclusive-OR mapping: $\mathcal{M}_{\oplus}(x_A, x_B) = x_A \oplus x_B$ (see Fig. 3.1), which satisfies the principle (3.2).

Detecting the network coded symbols is based on the MAP (Maximum A Posteriori) principle. We denote $x_{\oplus,n}(s_{\oplus})$ as the n-th ($n \in \{1, 2\}$) network coded bit corresponding to a superimposed signal $s_{\oplus}$. The n-th network coded LLR (log-likelihood ratio) $\Lambda_{\oplus,n}$ can be computed as

$$\Lambda_{\oplus,n} = \ln\left(\frac{p(x_{\oplus,n}(s_{\oplus}) = 0|y_R)}{p(x_{\oplus,n}(s_{\oplus}) = 1|y_R)}\right),\ n \in \{1, 2\}, \tag{3.3}$$

where for each network coded bit $x_{\oplus,n}(s_{\oplus})$, the alphabet of the superimposed signal, $\mathcal{Q}_{\oplus}(\widetilde{\varphi})$, can be split into two parts: $S_n^{(0)}$ and $S_n^{(1)}$, which correspond to $x_{\oplus,n}(s_{\oplus}) = 0$ and $x_{\oplus,n}(s_{\oplus}) = 1$, giving: $S_n^{(0)} = \{s_{\oplus}|x_{\oplus,n}(s_{\oplus}) = 0,\ s_{\oplus} \in \mathcal{Q}_{\oplus}(\widetilde{\varphi})\}$ and $S_n^{(1)} = \{s_{\oplus}|x_{\oplus,n}(s_{\oplus}) = 1,\ s_{\oplus} \in \mathcal{Q}_{\oplus}(\widetilde{\varphi})\}$. Then (3.3) can be rewritten as

$$\Lambda_{\oplus,n} = \ln\left(\frac{\sum\limits_{s_{\oplus} \in S_n^{(0)}} p(y_R|s_{\oplus})P(s_{\oplus})}{\sum\limits_{s_{\oplus} \in S_n^{(1)}} p(y_R|s_{\oplus})P(s_{\oplus})}\right),\ n \in \{1, 2\}, \tag{3.4}$$

where $p(y_R|s_{\oplus})$ is the conditional probability density function (PDF) of the received signal and $P(s_{\oplus})$ is the prior probability, both depend on the specific superimposed constellation design in virtual PNC scenario. With the store-and-query procedure, it is easy to calculate them. The calculated network coded LLRs are directly used by channel decoder to implement the *Hierarchical Decode-and-forward* (HDF) scheme [2].

Phase shifts over $[0°, 360°)$

We find that with the modulo-$90°$ operation for the phase shift: $\widetilde{\varphi} = \varphi \bmod 90°$, the generated superimposed constellations are relevant to the range $[0°, 90°)$. Thus, we need to extend this to all phase shifts in the range $[0°, 360°)$. For a point-to-point Gray Mapped QPSK system, the effect of $90°$ phase shift can be illustrated as in Fig. 3.3. The 2-bit binary tuple (x_1, x_2) for QPSK is transformed to $(x_2, \overline{x}_1)$ (where $\overline{(.)}$ is the inverse operation for binary bit) after passing through a $90°$ phase shift channel.

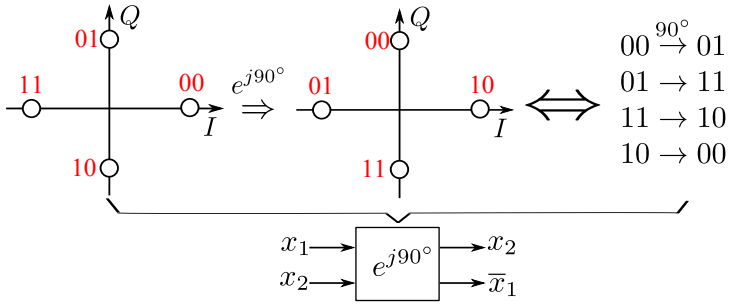

Figure 3.3: The effect of $90°$ phase shift for point-to-point QPSK system.

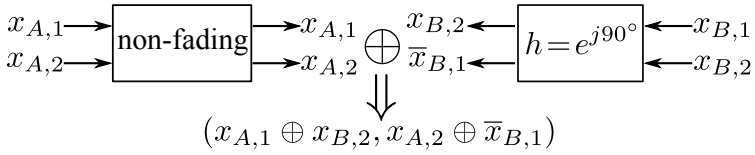

Figure 3.4: The effect of $90°$ phase shift relative fading for PNC-QPSK system.

Obviously, if both codewords $\boldsymbol{x}_A$ and $\boldsymbol{x}_B$ experience non-fading channel link, the PNC paradigm generates each network coded symbol in the form: $(x_{A,1} \oplus x_{B,1},\ x_{A,2} \oplus x_{B,2})$ (2-bit binary tuple of $x_{\oplus}$). This makes the network coded sequence $\boldsymbol{x}_{\oplus}$ still a valid code sequence in the codebook $\mathcal{C}$, which is $\boldsymbol{x}_{\oplus} \subset \mathcal{C}$. That is a prerequisite for HDF [2]. However, Fig. 3.4 shows that with $90°$ phase shift relative fading, the 2-bit binary tuple of network coded symbol is obtained in the form: $(x_{A,1} \oplus x_{B,2},\ x_{A,2} \oplus \overline{x}_{B,1})$, which makes $\boldsymbol{x}_{\oplus}$ an invalid code sequence: $\boldsymbol{x}_{\oplus} \not\subset \mathcal{C}$. HDF thus completely fails. Intuitively, a simple way is that an inverse operation on the 2nd bit of network coded symbol could correct it to the normal eXclusive-OR combination, that is: $\overline{x_{A,2} \oplus \overline{x}_{B,1}} = x_{A,2} \oplus x_{B,1}$. And if $\boldsymbol{x}_{i,1}$ and $\boldsymbol{x}_{i,2}$ $(i \in \{A, B\})$ are obtained by separately encoding at users and separately decoding for $\boldsymbol{x}_{\oplus,1}$ and $\boldsymbol{x}_{\oplus,2}$ are applied at the relay, the correct operation of the HDF scheme can be

guaranteed. The simple illustration is as shown in Fig. 3.5.

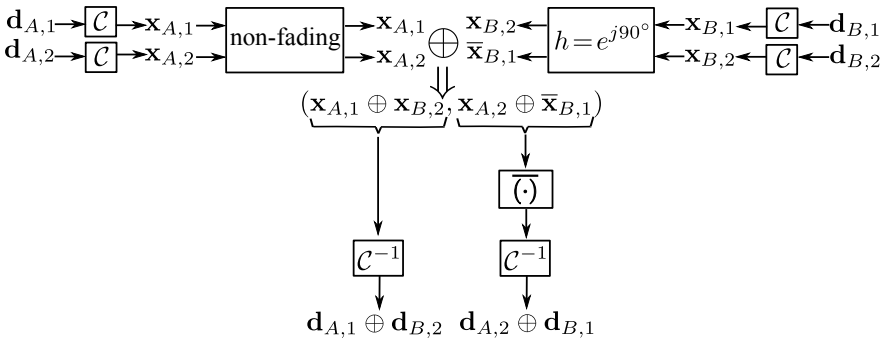

Figure 3.5: The illustration of independent encoding and decoding for 90° phase shift in PNC system.

The independent encoding and decoding scheme can thus ensure correct operation of HDF when $\varphi = 90^\circ$. For $\varphi = 180^\circ$ or $\varphi = 270^\circ$, we only need to change the correction pattern. With the appropriate correction pattern, the Adaptive Soft Demodulator with independent decoding is robust for any phase shift in the range $[0^\circ, 360^\circ)$. This scheme is thus named Rotationally Invariant Coded Modulation (RICM). The detailed structure of the decoder for RICM is shown in Fig. 3.6. The Switch Array controls the correction patterns for different phase shifts. From top to bottom, the switches can be changed to a specific correction pattern according to Table 3.1.

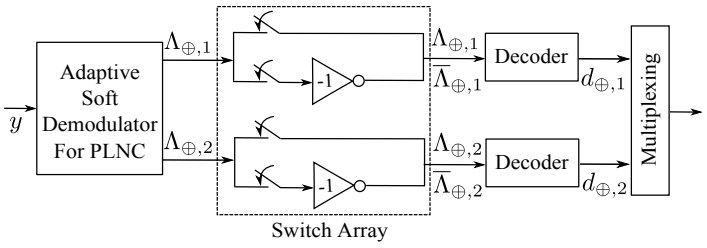

Figure 3.6: Detailed structure of decoder for RICM system.

Table 3.1: Selection Principle of Correction Pattern

Order No.	**Switch Array Action**	**Available Range** (φ)
Correction Pattern I	{On, Off, On, Off}	Range I:$[0^\circ, 90^\circ)$
Correction Pattern II	{On, Off, Off, On}	Range II:$[90^\circ, 180^\circ)$
Correction Pattern III	{Off, On, Off, On}	Range III:$[180^\circ, 270^\circ)$
Correction Pattern IV	{Off, On, On, Off}	Range IV:$[270^\circ, 360^\circ)$

Here, we give an example to illustrate the capability of RICM dealing with all phase shifts. For a specific phase shift $\varphi = 200^\circ$ in the Range III. A superimposed constellation for $\widetilde{\varphi} = 200^\circ \bmod 90^\circ = 20^\circ$ is first generated, i.e. $\mathcal{Q}_\oplus(20^\circ)$ (clearly, the relative positions of superimposed signals in $\mathcal{Q}_\oplus(20^\circ)$ are the same as in $\mathcal{Q}_\oplus(200^\circ)$). Based on this constellation, the network coded LLRs are computed by the adaptive soft demodulator. The switch array chooses the correction pattern III for $\mathbf{\Lambda}_{\oplus,n},\ n \in \{1,2\}$. Then corrected network coded LLRs: $\overline{\mathbf{\Lambda}}_{\oplus,1}$ and $\overline{\mathbf{\Lambda}}_{\oplus,2}$ are separately fed into two channel decoders for independent decoding.

3.2.5 Simplified Low-Complexity Scheme

In the previous subsection, we have provided the detailed design of RICM with fully adaptive demodulator for PNC. Although compared with the schemes in [3, 4, 15], it is a flexible and simple design for the fading 2-WRC, nevertheless we still want to further reduce its complexity. Fig. 3.7(a) shows the comparison between the superimposed constellations $\mathcal{Q}_\oplus(22^\circ)$ and $\mathcal{Q}_\oplus(0^\circ)$. The blue squares represent points on $\mathcal{Q}_\oplus(22^\circ)$. Points which can be clustered and mapped by the principle provided in section III are encircled by a black solid line. It is clear that there are some mismatches between the points of $\mathcal{Q}_\oplus(0^\circ)$ and the clustered points for $\mathcal{Q}_\oplus(22^\circ)$. However the basic shapes of these two superimposed constellations are almost the same. Similarly, Fig. 3.7(b) shows that the superimposed constellations for $\varphi = 58^\circ$ and $\varphi = 45^\circ$ again are very similar.

Inspired by this observation, we simplify the adaptive soft demodulator by using only two soft demodulators, designed for $\varphi = 0^\circ$ and $\varphi = 45^\circ$. The fundamental idea of this simplification is to apply an approximate constellation $\mathcal{Q}_\oplus(0^\circ)$ or $\mathcal{Q}_\oplus(45^\circ)$ to approach a constellation whose phase shift is near 0° or 45° respectively. This approximation is a form of simplified network coded symbol based clustering. Fig. 3.8 illustrates the structure of the decoder for our simplified scheme.

We need to determine how to *adaptively select* these two demodulators according to phase shifts and how to optimize this *adaptive selection*. It has been proven that for HDF, when each user employs the same mapping scheme and codebook, the achievable rates in

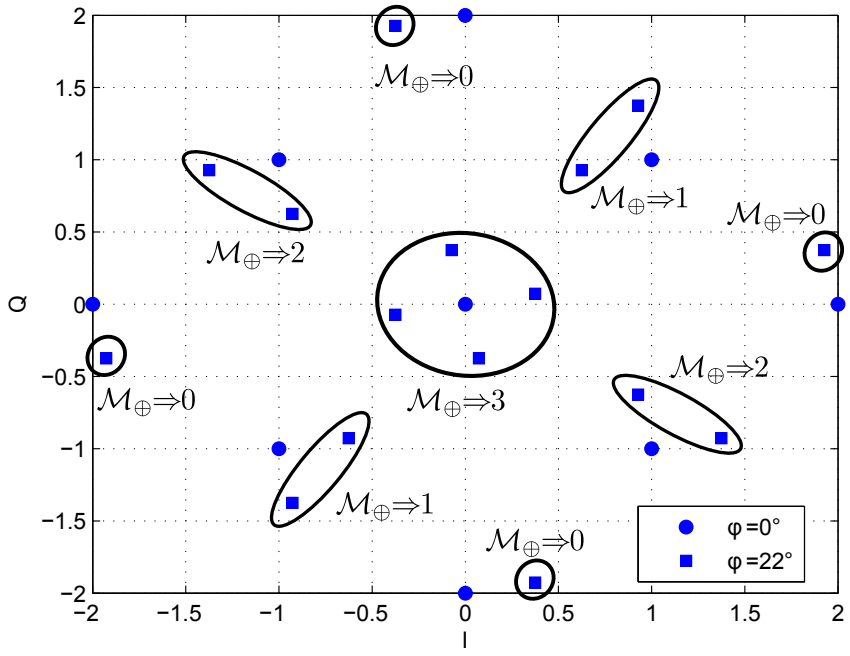

(a)

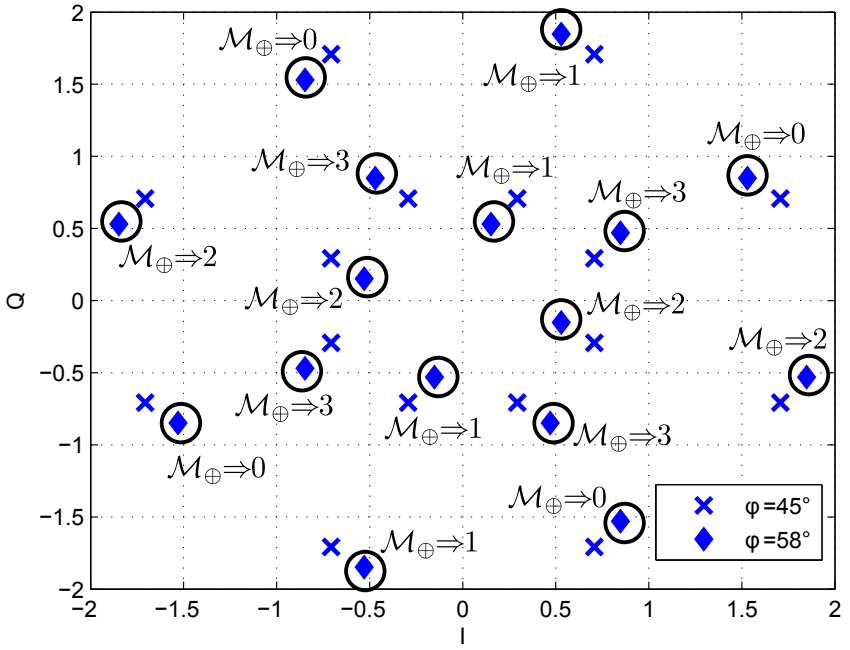

(b)

Figure 3.7: Comparison of Superimposed Constellations.

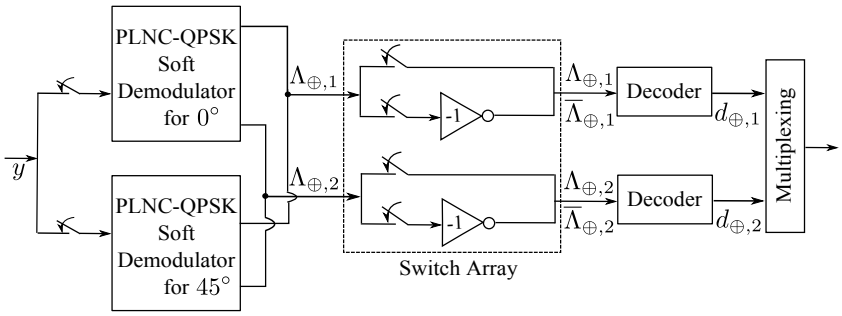

Figure 3.8: Structure of decoder for the simplified low-complexity scheme.

the MAC phase should obey

$$R_A = R_B = R_{x_\oplus} \leq I(Y_R; X_\oplus), \tag{3.5}$$

where $R_{i,}i \in \{A, B\}$ is the achievable rate for *A* or *B*. $R_{x_\oplus}$ is the virtual achievable rate for network coded symbol $x_\oplus$ and $I(Y_R; X_\oplus)$ is the mutual information between received signal and network coded symbol. So it is clear that maximizing $I(Y_R; X_\oplus)$ thus maximizes all achievable rates for HDF in MAC phase. So we aim to maximize $I(Y_R; X_\oplus)$ to optimize the adaptive selection. $I(Y_R; X_\oplus)$ can be given as

$$I(Y_R; X_\oplus) = H(Y_R) - H(Y_R|X_\oplus), \tag{3.6}$$

where $H(Y_R)$ is the received signal's Entropy

$$H(Y_R) = -\int\limits_{y_R \in \mathbb{C}} p(y_R) \log_2(p(y_R)) dy_R, \tag{3.7}$$

where the PDF of received signal $p_Y(Y)$ is

$$p(y_R) = \frac{1}{M_C^2} \sum_{s_\oplus} \frac{1}{2\pi\sigma_w^2} \exp(-\frac{|y_R - s_\oplus|^2}{2\sigma_w^2}), \tag{3.8}$$

where M_C is the cardinality of symbol alphabet for specific modulation scheme, and here it is 4 for QPSK (Note that all coincident points on the superimposed constellation need to be separately counted). $s_\oplus$ is dependent on specific constellation ($\mathcal{Q}_\oplus(0°)$ or $\mathcal{Q}_\oplus(45°)$).

The conditional entropy $H(Y_R|X_\oplus)$ can be computed as

$$H\left(Y_R|X_\oplus\right) = -\sum_{x_\oplus \in \mathscr{A}_4} \int\limits_{y_R \in \mathbb{C}} P(x_\oplus) p\left(y_R|x_\oplus\right) \log_2\left(p\left(y_R|x_\oplus\right)\right) dy_R, \tag{3.9}$$

where $P(x_\oplus) = \frac{1}{M_C}$ and the conditional PDF $p\left(y_R|x_\oplus\right)$ can be expressed as

$$p\left(y_R|x_\oplus\right) = \frac{1}{M_C} \sum_{S_\oplus:\forall S_\oplus \to X_\oplus} \frac{1}{2\pi\sigma_w^2} \exp(-\frac{|y_R - s_\oplus|^2}{2\sigma_w^2}), \tag{3.10}$$

where the summation is operated over all possible superimposed signals $s_\oplus$ which can be mapped to a specific $x_\oplus$.

By using the *Monte-Carlo Evaluation* on (3.7) and (3.9), we can separately compute $I(Y_R; X_\oplus)$ as the function of φ when employing the demodulator for $0°$ or $45°$, denoted as $I(Y_R; X_\oplus)_{0°}(\varphi)$ and $I(Y_R; X_\oplus)_{45°}(\varphi)$, which are shown in Fig. 3.9.

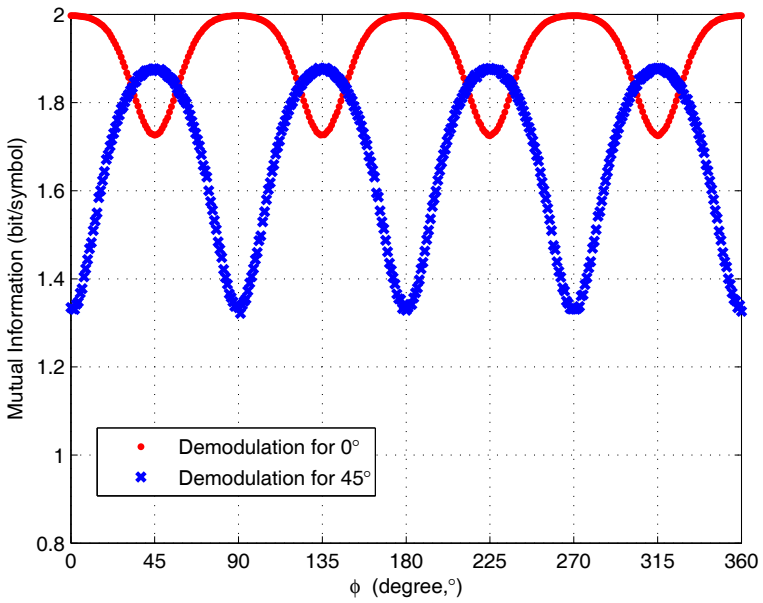

Figure 3.9: Simulated $I(Y_R; X_\oplus)_{0°}(\varphi)$ and $I(Y_R; X_\oplus)_{45°}(\varphi)$ when SNR=15dB.

Clearly, for a specific SNR, in some range of φ, $I(Y_R; X_\oplus)_{0°}$ is better than $I(Y_R; X_\oplus)_{45°}$; and *vice versa* in its complement. The critical angles are defined as the boundaries of the optimized adaptive selection for $0°$ and $45°$ demodulation, such that $I(Y_R; X_\oplus)_{0°} = I(Y_R; X_\oplus)_{45°}$. We give the details of an algorithm to find critical angles as follows. The pair of critical angles in in the first quadrant is denoted as $(\theta_{(1)}, \theta_{(2)}) \in \Phi_E$. Due to the symmetry, the critical angles in the other three quadrants should be $(\theta_{(1)} + 90°, \theta_{(2)} + 90°)$, $(\theta_{(1)} + 180°, \theta_{(2)} + 180°)$ and $(\theta_{(1)} + 270°, \theta_{(2)} + 270°)$, as illustrated in Fig. 3.10.

The Switch Array action for each correction pattern is same with that in Table 3.1. The

The Algorithm to find the critical angles:

1. Make a Cell Array Φ in which each cell is initialized as

   a null set to store the critical angles:

   $\Phi[i]=\emptyset,\ i=1,2...length(SNRs)$

2. **for** all $SNRs$ **do**

   for all phase shifts $\varphi \in [0°, 90°)$ **do**

   Compute $I(Y_R; X_\oplus)_{0°}(\varphi, SNR[i])$

   Compute $I(Y_R; X_\oplus)_{45°}(\varphi, SNR[i])$

   if $I(Y_R; X_\oplus)_{0°}(\varphi, SNR[i]) = I(Y_R; X_\oplus)_{45°}(\varphi, SNR[i])$, **then**

   Update current phase shift in angle set:$\Phi[i] \leftarrow \Phi[i] \cup \varphi$

   end if

   end for

   end for

3. Average Φ over all $SNRs$ to obtain a new set:$\Phi_E = \mathrm{E}(\Phi)$

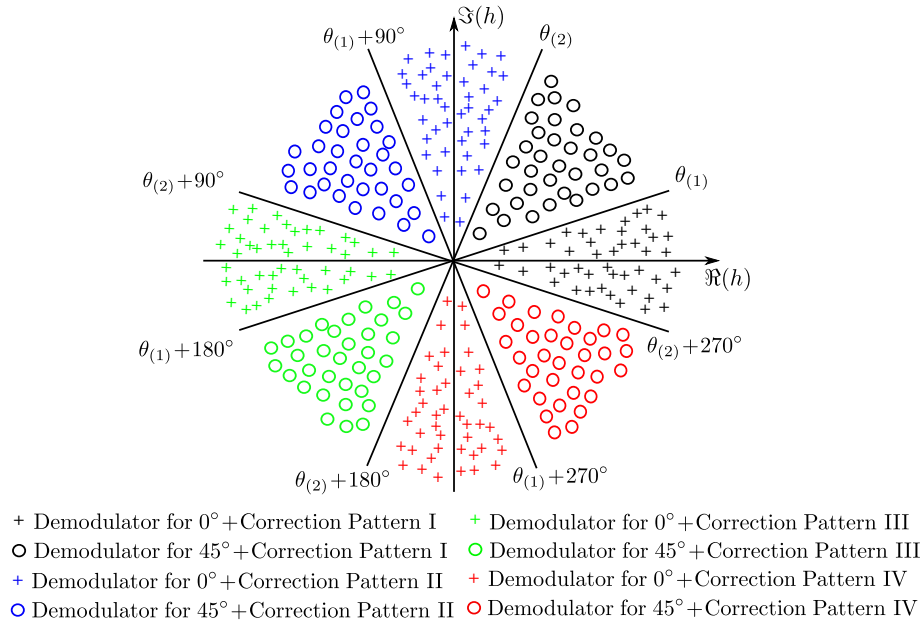

Figure 3.10: Adaptive Selection for two demodulators and correction patterns.

resulting mutual information $I(Y_R; X_\oplus)$ can be maximized as

$$I(Y_R; X_\oplus)_{\max} = \max_{\theta_{(1)},\theta_{(2)} \in \Phi_E} \{I(Y_R; X_\oplus)_{0^\circ},\ I(Y_R; X_\oplus)_{45^\circ}\}. \tag{3.11}$$

The corresponding simulation result is given in Fig. 3.11. Here, we denote the average SNR as $E[|h_A|^2 + |h_B|^2]/2\sigma_w^2$ and an extreme scenario for relative fading factor is also considered, where the phase shift obeys: $\varphi \sim U(0^\circ, 360^\circ)$.

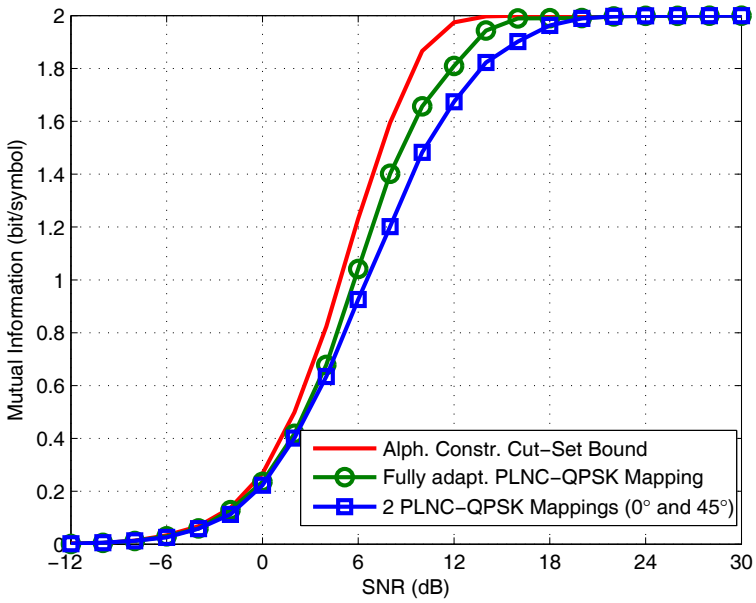

Figure 3.11: Comparison of Mutual Information $I(Y_R; X_\oplus)$ for proposed schemes.

From Fig. 3.11, we see that for both the fully adaptive demodulator scheme of section III and the two-demodulator scheme, the mutual information is very close to the QPSK alphabet constrained cut-set bound of the PNC system. The constellation approximation results in a small performance degradation for the two-demodulator scheme compared with the fully adaptive scheme.

3.2.6 Performance Evaluation

In this section, we evaluate the end-to-end throughput efficiency for our proposed RICM schemes.The end-to-end throughput efficiency is defined as the ratio of successful packets received by users. In our simulation, 10^5 trials are implemented, where one trial means a

whole transmission from one user to the other user. Both h_A and h_B are assumed to be frequency-flat, quasi-static Rician fading channels with a certain K factor. The Rician K factor is the ratio between the power in the direct path and the power in the scattered paths. Here we consider $K = 10dB$ and $K = 0dB$. The length of the original data packet is 512 bits. A rate 1/3 convolutional code with generator polynomials $\boldsymbol{G} = (133, 171, 145)_8$ is applied.

In order to give a clear comparison, we choose the traditional HDF scheme [2] as the benchmark in which a fixed XOR demodulator is employed to obtain the network coded/hierachical LLRs which are then directly fed into the channel decoder. Fig. 3.12 and Fig. 3.13 show the corresponding simulations when $K = 10dB$ and $K = 0dB$, respectively.

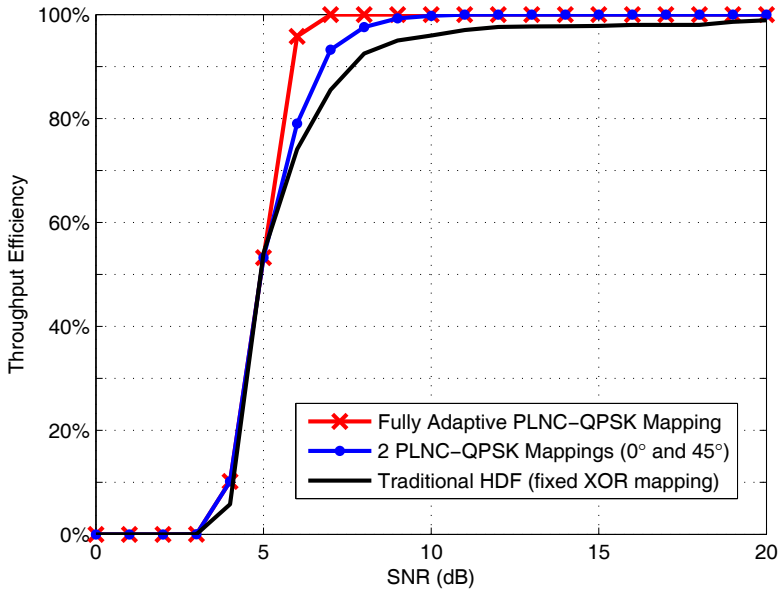

Figure 3.12: Performance evaluation on the end-to-end throughput efficiency for Rician fading channels when $K = 10dB$.

Based on Fig. 3.12 and Fig. 3.13, it is clear the traditional HDF scheme (the benchmark) can not achieve the full (100%) throughput efficiency at high SNR even though the channel fading condition ($K = 10dB$) is not too bad. However, the performance of the benchmark when $K = 0dB$ is severely degraded, compared with that when $K = 10dB$. This is because the fixed XOR mapping can not deal with all phase shifts of the relative fading which causes the failure of the exclusive law which further leads to a mismatch

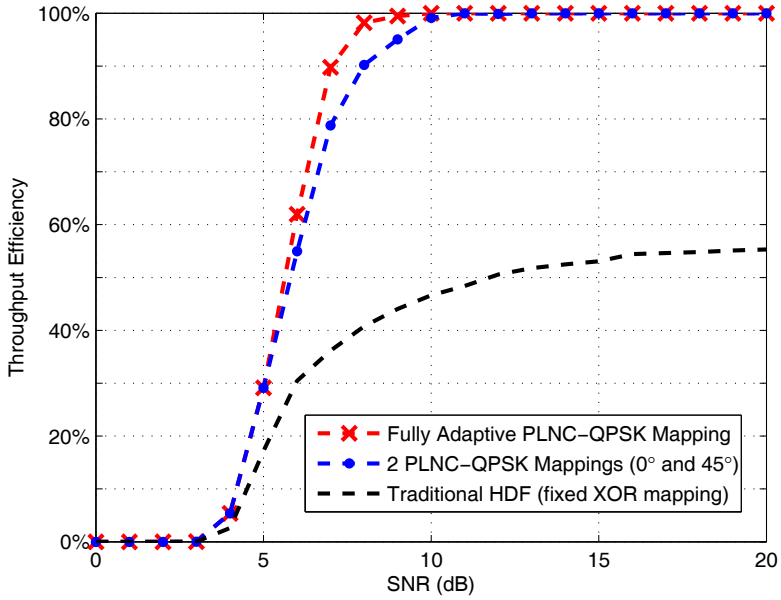

Figure 3.13: Performance evaluation on the end-to-end throughput efficiency for Rician fading channels when $K = 0dB$.

between data bits and parity bits. And we can see that our proposed schemes (both fully adaptive mapping scheme and the low complexity two-demodulator scheme) can rapidly reach full throughput efficiency in both fading cases. The proposed schemes can fully utilize the error correction capability of channel code. So compared with the 5QAM DNF (see Figs. 5 and 6 in [3]), the proposed schemes can achieve 100% throughput faster for Rician fading both with $K = 10dB$ and $K = 0dB$.

In addition, compared with the DNF scheme [2], the proposed two-demodulator scheme avoids both the irregular 5QAM modulation and the exhaustive search required for the closest-neighbor clustering algorithm, which significantly mitigates the burden on the relay and hence results in a low system complexity.

3.3 Scheme 2: Soft-bit Correction for Physical-layer Network Coding

3.3.1 Overview

In this section, we propose a novel fading correction and relaying scheme for PNC in a fading 2-WRC. The fading correction on the soft-bit level at users can eliminate the effect of fading in the 2-WRC. In order to broadcast the soft-bit in an optimal way, we design a quantize-and-forward scheme which is robust for the fading 2-WRC. In addition, an optimized mapping is used to implement unequal error protection (UEP) for bits with different significance in the quantization index. The soft-bit correction and the robust quantize-and-forward scheme are fully compatible with one another. The relay is thus effectively transparent: it can be entirely agnostic to the coding scheme employed at users, and the relay itself does not need to have decoding ability. It provides an appropriate approach to balancing system complexity and performance.

3.3.2 Detailed Structure of Proposed Scheme

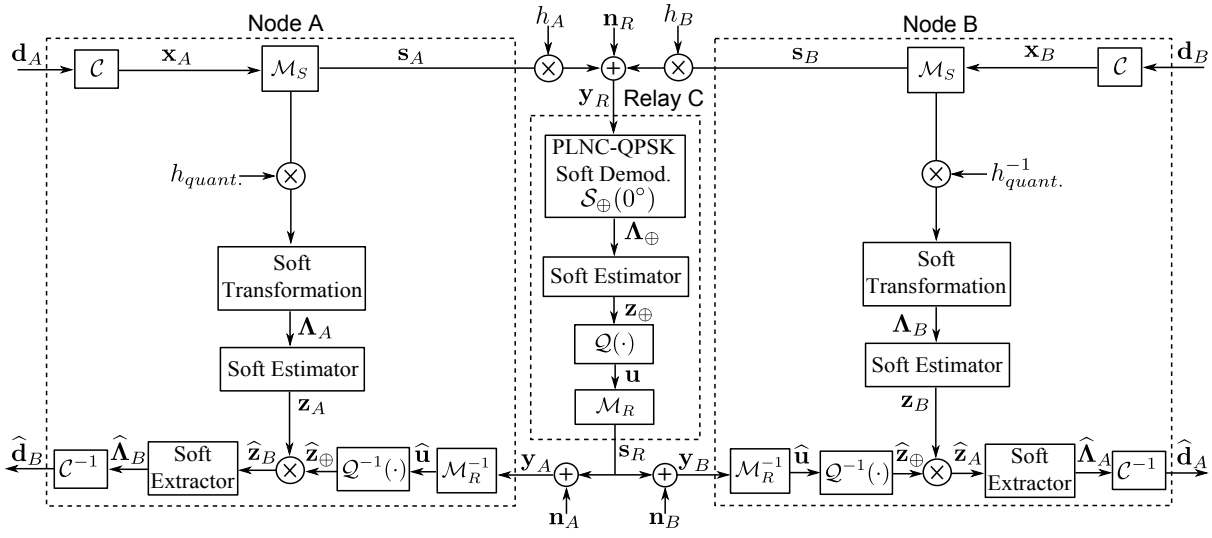

Figure 3.14: System Diagram of Proposed Soft-bit Correction.

The block diagram of the proposed scheme is shown in Fig. 3.14. We separately de-

scribe the detailed design of each functions and components in Fig. 3.14 in the following subsections.

3.3.3 Generating network coded soft-bit

The reliability of the superimposed code is obtained by the designed PNC-QPSK soft demodulator. Detecting the network coded symbol is based on the maximum a posteriori (MAP) principle. We use $x_{\oplus,n}(s_\oplus)$ to denote the n-th ($n \in \{1,2\}$) bit in the network coded symbol corresponding to the superimposed signal $s_\oplus$. The bit-wise network coded LLR (log-likelihood ratio) can be computed as

$$\Lambda_{\oplus,n} = \ln\left(\frac{p(x_{\oplus,n}(s_\oplus)=0|y_R)}{p(x_{\oplus,n}(s_\oplus)=1|y_R)}\right),\ n \in \{1,2\}, \tag{3.12}$$

where for each network coded bit $x_{\oplus,n}(s_\oplus)$, the alphabet of the superimposed signal, $\mathcal{S}_\oplus$, can be split into two parts: $S_n^{(0)}$ and $S_n^{(1)}$, which correspond to $x_{\oplus,n}(s_\oplus) = 0$ and $x_{\oplus,n}(s_\oplus) = 1$, giving as: $S_n^{(0)} = \{s_\oplus | x_{\oplus,n}(s_\oplus) = 0,\ s_\oplus \in \mathcal{S}_\oplus\}$ and $S_n^{(1)} = \{s_\oplus | x_{\oplus,n}(s_\oplus) = 1,\ s_\oplus \in \mathcal{S}_\oplus\}$. As such, (3.12) can thus be rewritten as

$$\Lambda_{\oplus,n} = \ln\left(\frac{\sum\limits_{s_\oplus \in S_n^{(0)}} p(y_R|s_\oplus)P(s_\oplus)}{\sum\limits_{s_\oplus \in S_n^{(1)}} p(y_R|s_\oplus)P(s_\oplus)}\right),\ n \in \{1,2\}, \tag{3.13}$$

where $p(y_R|s_\oplus)$ is the conditional probability density function (PDF) of the received signal and $P(s_\oplus)$ is the prior probability. Both depend on the mapping strategy of the soft demodulator. Fig. 3.15 illustrates the PNC's superimposed constellation with 0° phase shift, i.e., $\mathcal{S}_\oplus(0^\circ)$ ($\mathcal{M}_\oplus \Rightarrow m,\ m \in \mathbb{Z}_4$ represents the bit-wise XOR mapping). Then $p(Y_R|S_\oplus)$ can be calculated as

$$p(y_R|s_\oplus) = \frac{1}{2\pi\sigma_w^2}\exp(-\frac{|y_R - s_\oplus|^2}{2\pi\sigma_w^2}),\ s_\oplus \in \mathcal{S}_\oplus(0^\circ)\,. \tag{3.14}$$

Unlike [4, 15], there is no adaptive-selection in our proposed scheme. Regardless of the channel parameters, the relay employs only one PNC-QPSK soft demodulator, that corresponding to the superimposed constellation $\mathcal{S}_\oplus(0^\circ)$ with $\varphi = 0^\circ$ and $r = 1$. The network coded soft-bit can be calculated as

$$\boldsymbol{z}_\oplus = \tanh(\boldsymbol{\Lambda}_\oplus/2), \tag{3.15}$$

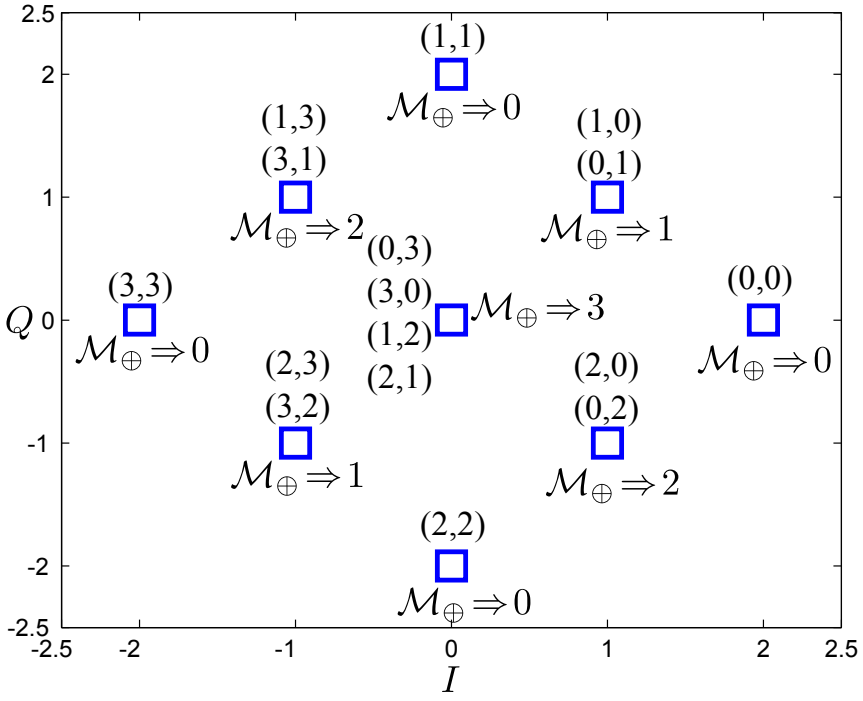

Figure 3.15: Superimposed constellation for $h = \frac{h_A}{h_B} = 1$.

where $\tanh(\cdot)$ is the bit-wise hyperbolic tangent function. The soft-bit has several advantages compared with LLR: 1) the hyperbolic tangent domain has a fixed range $[-1, +1]$ rather than $(-\infty, +\infty)$ for logarithm domain; 2) the eXclusive-OR operation in hyperbolic tangent domain is simpler than that in logarithm domain; and 3) the soft-bit is more effective than the LLR in power constrained scenarios.

Robust Quantize-and-Forward for fading 2-WRC

Note that directly transmitting analogue signal in digital communication systems is technically nontrivial. There are several quantize-and-forward strategies which have been proposed to overcome the weakness of broadcasting the analogue signal. In [16] and [17], an information bottleneck method (IBM) is involved to quantize the LLR in the 2-WRC. However, note that this scheme is designed for the AWGN channel and is not optimized for PNC. In addition, our soft-bit correction scheme is applied on the soft-bit rather than the LLR level.

Consider that the amplitude of the soft-bit lies only within the range $[-1, +1]$. A big

amplitude variation in the logarithm domain (for LLR) transforms to only a small change in the hyperbolic tangent domain (for soft-bit). Inspired by this, we suggest that the mean-square error (MSE) optimal quantization (Lloyd [18]-Max [19]) would be suitable for soft-bit. The MSE is mathematically defined as: $E\left[\left|x-\mathcal{Q}\left(x\right)\right|^2\right]$, where $\mathcal{Q}$ is the quantization function. The Lloyd-Max algorithm determines quantization levels based on minimizing the MSE for the input signal with a known distribution. So it is necessary to find out the statistical properties of the soft-bit to achieve the optimal quantization.

According to the Bayes' principle, the PDF of the received signal can be expressed as

$$p(y_R)=\sum_{s_\oplus\in\mathcal{S}_\oplus(0^\circ)} p(y_R|s_\oplus)P(s_\oplus). \tag{3.16}$$

The transformation for a function of a random variable [10] to calculate the PDF of network coded LLR can be expressed as

$$p_{\Lambda_\oplus}(\lambda)=p_{Y_R}(w(\lambda))\left|\frac{dw(\lambda)}{d\lambda}\right|, \tag{3.17}$$

where λ is the random variable for network coded LLR and $w(\lambda)$ is the inverse function of (3.15) for variable y_R. Based on (3.14), (3.16) and (3.17), the distribution of the network coded LLR can be calculated as

$$\begin{aligned} p_{\Lambda_\oplus}(\lambda)=&\frac{\exp\left(-\lambda-\cosh^{-1}(-\lambda+\frac{1}{\sigma_w^2})-\frac{1}{4}\sigma_w^2\cosh^{-1}(-\lambda+\frac{1}{\sigma_w^2})^2\right)}{4\sqrt{\pi\exp(-2\lambda+\frac{2}{\sigma_w^2})}}\\ &\times\left(1+\exp(2\cosh^{-1}(-\lambda+\frac{1}{\sigma_w^2}))+2\exp(\cosh^{-1}(-\lambda+\frac{1}{\sigma_w^2}))\right)\sigma_w. \end{aligned} \tag{3.18}$$

Due to the symmetry of the points on the superimposed constellation, both the 1st bit $\Lambda_{\oplus,1}$ and 2nd bit $\Lambda_{\oplus,2}$ obey the same distribution as (3.18). Similarly, the PDF of the soft bit can also be calculated by the transformation for a function of a random variable:

$$p_{Z_\oplus}(z)=p_{\Lambda_\oplus}(h(z))\left|\frac{dh(z)}{dz}\right|, \tag{3.19}$$

where z is the random variable for the soft-bit and $h(z)$ is the LLR extraction function, denoted as $h(z)=2\tanh^{-1}(z)$. The final PDF of soft-bit thus can be derived as

$$\begin{aligned} p_{Z_\oplus}(z)=&\frac{\exp\left(-2\tanh^{-1}(z)-\cosh^{-1}(-2\tanh^{-1}(z)+\frac{1}{\sigma_w^2})-\frac{1}{4}\sigma_w^2\cosh^{-1}(-2\tanh^{-1}(z)+\frac{1}{\sigma_w^2})^2\right)}{2(1-z^2)\sqrt{\pi\exp(-4\tanh^{-1}(z)+\frac{2}{\sigma_w^2})}}\\ &\times\left(1+\exp(2\cosh^{-1}(-2\tanh^{-1}(z)+\frac{1}{\sigma_w^2}))+2\exp(\cosh^{-1}(-2\tanh^{-1}(z)+\frac{1}{\sigma_w^2}))\right)\sigma_w. \end{aligned} \tag{3.20}$$

The theoretical analysis of the PDF (3.20) can be verified by *Monte-Carlo simulation*. Fig. 3.16 illustrates the comparison between the theoretical and simulated PDF of the soft-bit. The consistency between the theoretical and simulated results is clear, which implies that based on our derived theoretical PDF, the optimum MSE quantization in the non-fading MAC phase can be achieved.

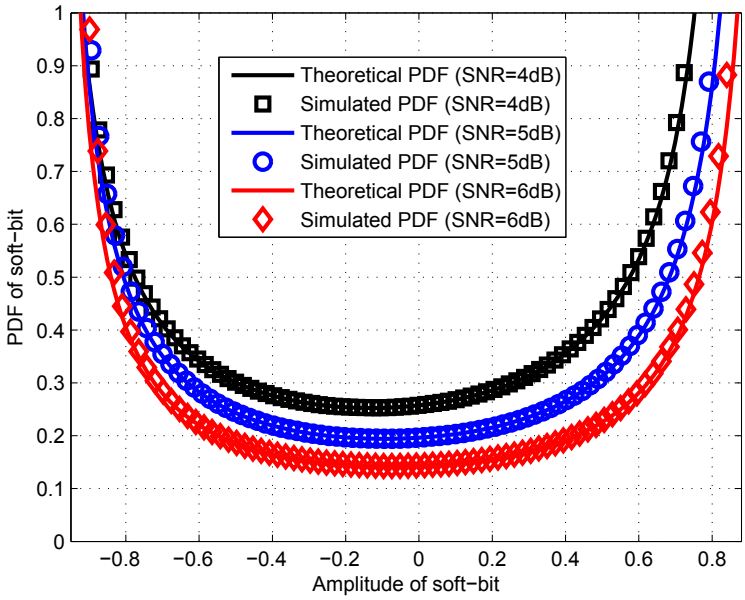

Figure 3.16: Comparison between theoretical and simulated PDF for soft-bit with different SNRs in non-fading MAC phase.

Next, we need to check the robustness of our design in approaching the quantization in fading MAC phase. As in [2, 4, 15], we also assume that two channel links in MAC phase have same power: $E[|h_A|^2] = E[|h_B|^2]$ (where, $E[\cdot]$ is the expectation function) to respect the symmetrical rates from A and B. We denote the average SNR in MAC phase as $E[|h_A|^2 + |h_B|^2]/2\sigma_w^2$. An extreme scenario for relative fading factor is also considered, where the phase shift obeys: $\varphi \sim U(0°, 360°)$. Fig. 3.17 shows the comparison between PDF for soft-bit in the non-fading and fading MAC phase .

Based on Fig. 3.17, it is clear that although the phase shift fading varies dramatically, the statistical properties of the soft-bit changes only slightly. This implies that our designed MSE quantization can be approximated in the fading MAC phase. But it is still not certain that this is a robust solution. So in the following parts of the chapter, we suc-

cessively measure the performance loss in terms of both MSE and mutual information (as shown in Fig. 3.18 and Fig. 3.19, respectively).

The designed MSE quantizer $\mathcal{Q}(\cdot)$ has 2^{R_Q} levels (R_Q is the number of quantization bits). If a soft-bit $z_\oplus$ is located within the quantization interval ℓ_u ($u \in \{0, 1, ..., 2^{R_Q} - 1\}$ is the quantization index), the quantizer maps it to the reconstruction value $\widehat{z}_\oplus$. This procedure can be described as

$$\mathcal{Q}(z_\oplus) = \widehat{z}_\oplus, \ if \ z_\oplus \in \ell_u, \tag{3.21}$$

where each quantization interval ℓ_u is iteratively calculated by the implementation of the Lloyd-Max algorithm [18, 19] .

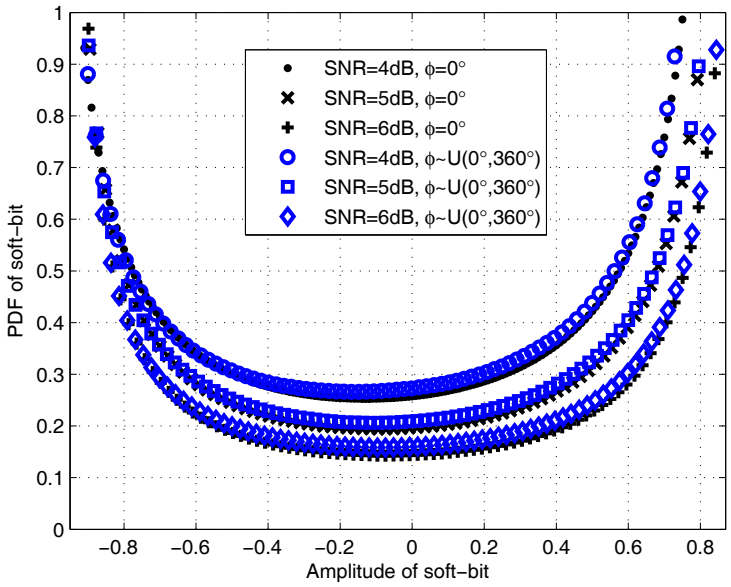

Figure 3.17: Comparison between simulated PDF for soft-bit in non-fading MAC phase and fading MAC phase with different SNRs.

In Fig. 3.18, we set SNR equal to 10dB, obviously, the more quantization bits involved, the higher quantization precision can be provided. We observe that if the number of quantization bits $R_Q \geq 3$, the MSE for the fading MAC can achieve almost the same level as that for the non-fading case.

The mutual information loss ΔI can be measured as the difference between the unquantized and the quantized mutual information: $\Delta I = I_{unquant.} - I_{quant.}$. Here, the unquantized mutual information is the bit-wise mutual information between network coded

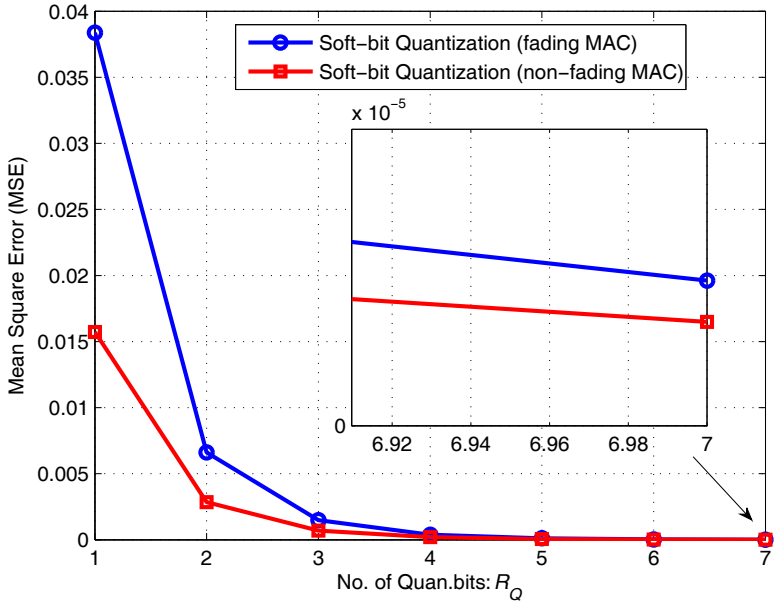

Figure 3.18: MSE vs. number of quantization bits when SNR=10dB.

bit and network coded LLR. In practice, this can be calculated by the ergodicity theorem [11]

$$I_{unquant.} = I(\widetilde{x}_{\oplus,k}; \Lambda_{\oplus,k}) \approx 1 - \frac{1}{K}\sum_{k=1}^{K} \log_2(1 + e^{-\widetilde{x}_{\oplus,k}\cdot\Lambda_{\oplus,k}}), \tag{3.22}$$

where $K = \text{length}(\boldsymbol{x}_{\oplus})$ and $k \in \{1, 2...K\}$. As the binary antipodal signal for the network coded bit, $\widetilde{x}_{\oplus,k}$ is defined in GF(2) with the elements $\{+1, -1\}$ (where $+1$ represents the 'null' element). Note that for (3.22), a long data sequence would guarantee the availability and precision of the measure of the mutual information even for a non-Gaussian or unknown distribution [21] (It is clear from (3.18) that the distribution of $\Lambda_{\oplus,k}$ is non-Gaussian). Moreover, by invoking the definition of fidelity in [21] and [22]: $E[z_{\oplus}] = \frac{1}{K}\sum_{k=1}^{K} \widetilde{x}_{\oplus,k} \cdot z_{\oplus,k}$, (3.23) can be rewritten as

$$I_{unquant.} \approx \frac{1}{K}\sum_{k=1}^{K} \log_2(1 + \widetilde{x}_{\oplus,k} \cdot z_{\oplus,k}) \tag{3.23}$$

Note that (3.23) is also not limited to the Gaussian distribution. Thus, the measure of the mutual information can be transformed to the soft-bit domain. Similarly, the quantized mutual information can be expressed as

$$I_{quant.} = I(\widetilde{x}_{\oplus,k}; \widehat{\Lambda}_{\oplus,k}) \approx \frac{1}{K}\sum_{k=1}^{K} \log_2(1 + \widetilde{x}_{\oplus,k} \cdot \widehat{z}_{\oplus,k}), \tag{3.24}$$

where $\widehat{\Lambda}_{\oplus,k}$ is the recovered bit-wise network coded LLR, which is $\widehat{\Lambda}_{\oplus,k} = 2\tanh^{-1}(\widehat{z}_{\oplus,k})$ and $\widehat{z}_{\oplus,k}$ is the reconstruction value of soft-bit: $\widehat{z}_{\oplus,k} = \mathcal{Q}^{-1}(u_k)$.

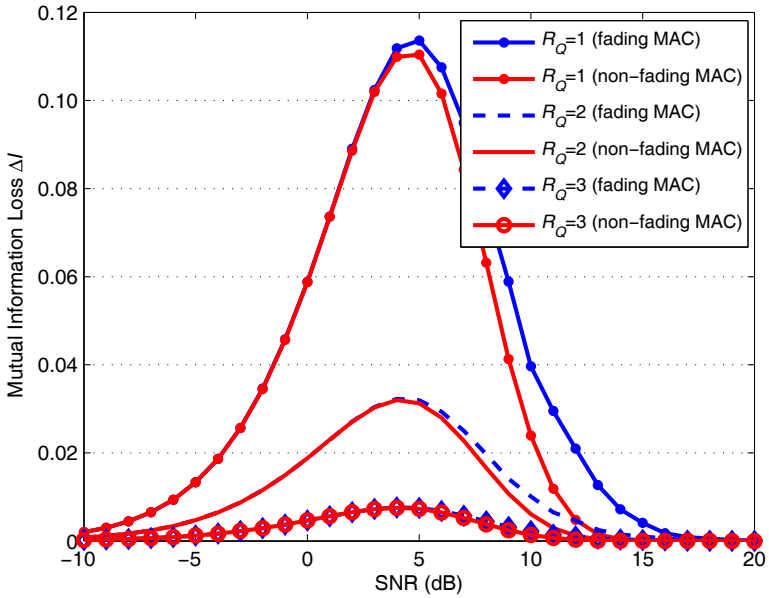

Figure 3.19: Comparison of bit-wise Mutual Information Loss ΔI.

Fig. 3.19 shows the comparison of the mutual information loss for quantization with different numbers of bits between the fading and non-fading MAC phase. Here, we choose 10^7 bits per frame and 10000 frames for *Monte-Carlo evaluation* of (3.23) and (3.24) to guarantee the precision. The simulation results imply that: 1. with $R_Q \geq 2$, the mutual information loss ΔI can decrease to an acceptable level ($< 4 \times 10^{-2}$) for the quantization in both fading and non-fading MAC phase; 2. the performance degradation caused by the designed approximated quantization for fading 2-WRC is small if the number of quantization bits $R_Q \geq 2$.

Soft-bit fading correction at each user

In this sub-section, we explore the soft-bit fading correction at each user, which is based on the following principles

$$\begin{aligned} \widehat{\boldsymbol{x}}_B &= [F(\boldsymbol{x}_A) \oplus \boldsymbol{x}_B] \oplus F(\boldsymbol{x}_A), \\ \widehat{\boldsymbol{x}}_A &= [\boldsymbol{x}_A \oplus F^{'}(\boldsymbol{x}_B)] \oplus F^{'}(\boldsymbol{x}_B), \end{aligned} \tag{3.25}$$

where $F(\cdot)$ represents the effect of the relative fading factor $h = \frac{h_A}{h_B}$ on the data stream from *A*, and $F^{'}(\cdot)$ represents the effect of the relative fading factor's reciprocal $h^{-1} = \frac{h_B}{h_A}$ on the data stream from *B*. From user *A*'s perspective, the data stream broadcasted by the relay affected by fading can be represented as $F(\boldsymbol{x}_A) \oplus \boldsymbol{x}_B$ and from *B*'s perspective, it is $\boldsymbol{x}_A \oplus F^{'}(\boldsymbol{x}_B)$. The corrected data at each user is denoted as $\widehat{\boldsymbol{x}}_i,\ i \in \{A, B\}$. Note that we apply this principle at the level of the soft-bit. Unlike hard bit, the soft-bit contains reliability information rather than simply '1' or '0'. The following equations show the equivalent relationship between hard bit and soft-bit for the eXclusive-OR operation

$$\boldsymbol{x}_{\oplus} = \boldsymbol{x}_A \oplus \boldsymbol{x}_B \quad \Leftrightarrow \quad \boldsymbol{z}_{\oplus} = \boldsymbol{z}_A . \times \boldsymbol{z}_B, \tag{3.26}$$

where both '$\oplus$' and '$.\times$' are *bit-wise* operations.

Besides the principle for fading correction of the soft-bit, the *correction factor* is also important. The correction factor for *A* then equals the relative fading factor $h = \frac{h_A}{h_B}$; for *B*, it is the reciprocal of the relative fading factor $h^{-1} = \frac{h_B}{h_A}$. Note that the destination users do not know the relative fading factor. Thus we need to quantize the relative fading factor. Since we assume symmetric channel power for both channel links in MAC phase, only the phase shift needs to be quantized uniformly over unit circle. Here, we apply 8-bit quantization to ensure sufficient accuracy for the phase shift. The quantized relative fading factor is inserted in the payload of each frame.

For *A* and *B*, the modulated signals will multiply the relative fading factor/its reciprocal, respectively. Next, the single user end-to-end QPSK soft demodulator is used to transform these faded signals into soft information $\boldsymbol{\Lambda}_A$ and $\boldsymbol{\Lambda}_B$. Then they are fed to the soft estimator to obtain their own soft-bit $\boldsymbol{z}_A$ and $\boldsymbol{z}_B$, which can be treated as the Complementary Side Information (C-SI) at each user. The C-SI contains the fading information which corresponds to that included in the network coded soft-bit. After recovering the network coded soft-bit $\widehat{\boldsymbol{z}}_{\oplus}$, the fading correction at the soft-bit level can be expressed using the following equations. This is equivalent to the correction principle

$$\widehat{\boldsymbol{z}}_B = \widehat{\boldsymbol{z}}_{\oplus} . \times \boldsymbol{z}_A \ \text{ and } \ \widehat{\boldsymbol{z}}_A = \widehat{\boldsymbol{z}}_{\oplus} . \times \boldsymbol{z}_B, \tag{3.27}$$

where $\widehat{\boldsymbol{z}}_i,\ i \in \{A, B\}$ represents the fading corrected soft-bit which can be extracted to obtain the corrected LLR ($\widehat{\boldsymbol{\Lambda}}_i = 2\mathrm{tanh}^{-1}(\widehat{\boldsymbol{z}}_i),\ i \in \{A, B\}$) for decoding. The mismatch caused by the fading between the data bits and parity bits can be removed by the soft-

bit correction. Thus, the system can utilize the error-correction capability of the channel code.

Optimized mapping for UEP based Broadcasting

Note that each network coded symbol carries two soft-bits, each soft-bit is quantized separately. So there are two quantization indices associated with one network coded symbol. If we apply 2-bit quantization, a group of quantization indices corresponding to a specific network coded symbol can be represented by their binary form: $(u_1^{(0)}, u_1^{(1)}; u_2^{(0)}, u_2^{(1)})$, where $u_n^{(0)}$ and $u_n^{(1)}$ ($n \in \{1, 2\}$) represent the MSB (Most Significant Bit) and the LSB (Least Significant Bit) in binary representation of the index which corresponds to the n-th bit of the network coded symbol. Similarly, if 3-bit quantization is applied, the binary form for quantization indices can be represented as $(u_1^{(0)}, u_1^{(1)}, u_1^{(2)}; u_2^{(0)}, u_2^{(1)}, u_2^{(2)})$. In order to conserve bandwidth efficiency and without reducing throughput, we should keep the transmission rate equal for the MAC and BC phases. Thus the 16QAM and 64QAM need to be employed for 2-bit and 3-bit quantization. It is obvious that different bits in the quantization index have different importance. Note that the MSB of the quantization index determines the sign of the quantized soft-bit. If the MSB is corrupted, a sign error will occur which could lead to a serious decision error. So the Gray mapping is not optimal. In [17], the authors use the *binary switching algorithm* (BSA) [13] to find an optimal mapping to achieve unequal error protection (UEP) for LLR quantization. We test the availability of BSA and find that *the natural mapping gives the same results as using BSA* (in [17], their designed optimized mapping is actually the natural mapping). In Fig. 3.20, the optimal/natural mapping for 64QAM is illustrated. We can clearly observe that UEP for the bits with different significance is achieved.

3.3.4 Simulation Results

In this section, we evaluate the BER (bit error rate) performance of the proposed scheme. Both h_A and h_B are assumed to be frequency-flat, quasi-static *Rayleigh* fading channels. The length of the original data packet on each user is 5000 bits. Then the data packet is encoded by a rate 1/3 turbo code with generator polynomials: $(G_r, G) = (37, 21)_8$ (where

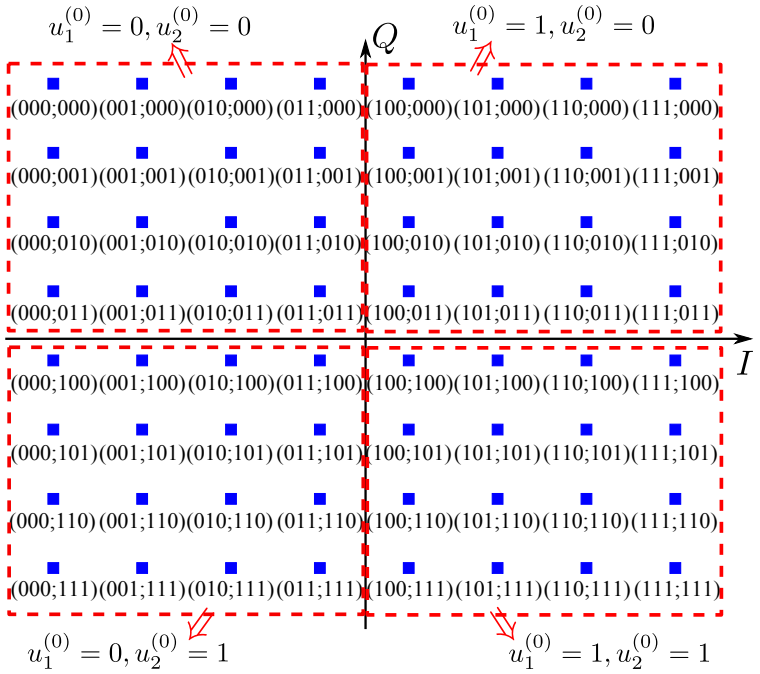

Figure 3.20: 64QAM Mapping with UEP for broadcasted quantization indices.

G_r stands for the recursive code polynomial). And the number of decoding iterations at the users is **18** for all simulations. The BER performance is measured at one of the users because of the symmetry of the 2-WRC. The simulation scenario includes channel links from user to relay (MAC phase) and relay to user (BC phase). So the average SNR in the MAC phase as defined above is unsuitable here. Considering the bit-wise property of the soft-bit, we choose E_b/N_0 (Bit Energy to Noise Power Spectral Density Ratio) as the simulation parameter. Note that due to the symmetry of the 2-WRC, the values of E_b/N_0 on MAC and BC phases are set to be equal. Fig. 3.21 shows the corresponding simulation.

In order to independently test the fade resistance capability of soft-bit correction, we introduce a perfect scenario in which the fading in MAC phase is set as described above but the BC phase is assumed to be undistorted (suppose that the soft-bits are unquantized and perfectly received by each user). From Fig. 3.21, we can see that, in such a scenario, the BER curve of the soft-bit correction scheme can rapidly converge to a low level compared with the scheme without soft-bit correction (in the case of without soft-bit correction, the relative fading causes the failure of the exclusive law and further leads to a mismatch between data bits and parity bits). It implies that the soft-bit correction could erase the fading effects on MAC phase and utilize the error-correction ability for channel

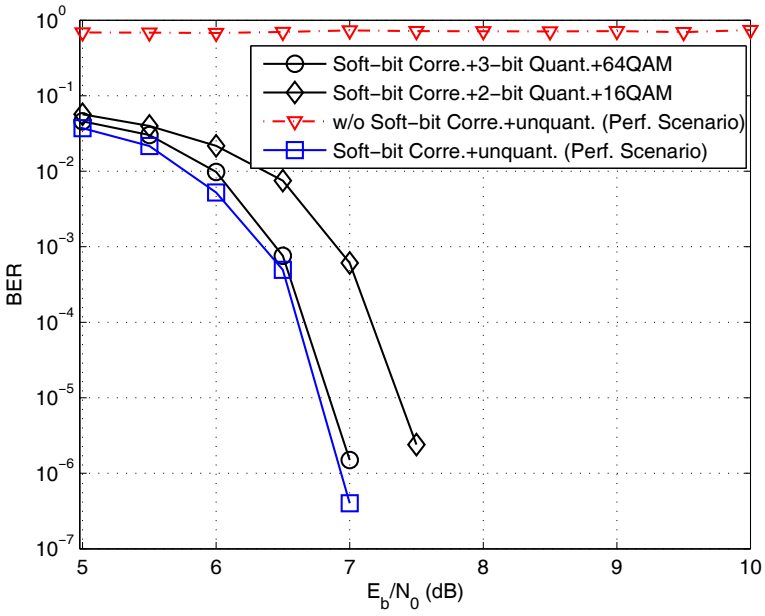

Figure 3.21: Comparison of BER performance.

codes.

To test the realistic performance, we separately choose 3-bit and 2-bit quantization for soft-bit correction (including the optimized mapping and a distorted BC phase). From Fig. 3.21, it is clear that the performance of 3-bit quantization with optimized 64QAM mapping can closely approach the limit for soft-bit correction in a perfect scenario. And we can conclude that in the BC phase, the quantization error will be the dominant factor affecting performance, rather than the noise.

In terms of system complexity at relay, the proposed scheme avoids the irregular 5QAM mapping [3], the exhaustive search required for the closest-neighbor clustering algorithm and adaptive-selection for mappings [3, 15]. The burden on the relay is significantly decreased since there is only one demodulator, one quantizer and one modulator at relay. The proposed scheme is a reliable approach to balancing the performance and system complexity.

3.4 Summary

In this section, we have proposed a two fading compensation strategies for PNC in 2-WRC: 1) rotationally invariant coded modulations (RICM) and soft-bit fading correction with robust quantize-and-forward (SBF-QF). These two schemes provided different approaches to combat fading, i.e., RICM mitigates the fading of MAC phase at relay while SBC-QF eliminates the effect of fading at destination.

The simulation results show that the RICM can effectively reduce the performance degradation which is caused by relative fading, hence improves performance. Since there is no need to employ the 5-ary irregular modulation scheme, the proposed scheme is more practical than the scheme in [3]. Moreover it is more flexible than the schemes in [4] and [15] as RICM does not change the coding structure and is suitable for arbitrary channel code.

The simulation result shows that the SBF-QF can eliminate the fading effect at destinations. With the robust quantize-and-forward, the soft-bit can be broadcasted over a noisy channel with less degradation. Since there is no need to employ the 5-ary irregular modulation scheme [3] or an exhaustive search for the optimum mapping [3, 15], the proposed scheme is more practical and flexible than the schemes in [3, 15]. In addition, the proposed scheme does not need the relay to decode the received signal. It exhibits significant advantages in terms of system complexity, flexibility and performance.

Chapter 4

Multilevel Coded Linear Physical-layer Network Coding over Fading 2-way Relay Channels

Contents

4.1 Overview

In this Chapter, we propose a novel multilevel coded LPNC scheme with extended mapping (LPNC-EM) for Rayleigh fading 2-WRC. The relay node adaptively selects the linear generator matrix and directly maps the superimposed signal of the two users into the linear network coded combination over the hybrid Galois Field ($\mathrm{GF}(2^2)$ or $\mathrm{GF}(2^3)$). The selection criterion ensures unambiguous decoding and maximizes the individual rate of each user. The LPNC-EM scheme forms two or three independent coding levels which facilitate the use of multilevel coding. This enables the HDF as in [7]. The numerical results show that uncoded LPNC-EM outperforms the original PNC in [1] and can achieve

a error performance as good as the 5QAM-DNF in [8]. Furthermore, the multilevel coded LPNC-EM also provides a superior error performance compared with the coded original PNC.

4.2 Introduction

Motivated by RICM for PNC in pervious chapter, in this chapter, we still discuss the HDF paradigm for PNC. We propose the LPNC-EM, using multilevel coding, aiming at: 1) maximizing the rate of each user in the MAC phase; and 2) making the strategy flexible for any channel code. We exploit the 'layered' approach to coded PNC introduced in [7], which allows any binary linear code to be used with a LPNC mapping. Unlike the prime q-ary mapping in [34], we focus on QPSK signalling. The relay directly maps the superimposed signal into the linear network coded combination by multiplying the user data by a properly selected generator matrix. The selection criterion ensures unambiguous decodablility and maximizes the individual achievable rate of each user in the MAC phase. The LPNC-EM over $\mathrm{GF}(2^2)$ or $\mathrm{GF}(2^3)$ facilitates the multilevel coded structure using either two or three independent coding levels in which each level is a linear function of two users' data bits. The numerical results, show that the multilevel coded LPNC-EM outperforms the original PNC and can achieve an average rate very close to 5QAM-DNF in [8], while providing a practical coding approach. In this Chapter, we focus on the MAC phase, assuming that the BC phase is lossless. We also focus on achievable rates rather than error rate performance.

4.3 System Model and Scheme Description

4.3.1 Multiple Access Phase

The 2-WRC consists of two users (A and B) and one relay (R). Two users A and B simultaneously transmit signals to relay R in the MAC phase. We assume that the two users employ the same constellation mapper $\mathcal{M}_S(\cdot)$. The electromagnetic signals are superim-

posed and received by *R*, given by

$$y_R = h_A x_A + h_B x_B + n_w, \tag{4.1}$$

where $x_i = \mathcal{M}_S(s_i)$, $i \in \{A, B\}$, is the modulated symbol for users *A* and *B* respectively. In particular, we assume that both users employ Gray mapped QPSK whose constellation has unit energy. The user data s_i is thus the 2-bit binary tuple. We define the channel gain from *A* or *B* to *R* as $h_i, i \in \{A, B\}$. We assume that all channels experience quasi-static i.i.d. frequency-flat Rayleigh fading with unit variance. We assume that the *channel state information* is perfectly known to the receiver side only as in [8]. The received signal is corrupted by complex Additive White Gaussian Noise (AWGN) n_w with variance σ_w^2 per complex dimension. We refer to

$$x_{AB} \triangleq h_A x_A + h_B x_B \tag{4.2}$$

as the noiseless superimposed signal.

Generating Linear Network Coded Combination

In the proposed LPNC-EM design, the relay *R* performs the linear mapping $\mathcal{L}$ in the hybrid Galois Field, given by

$$\mathcal{L} : x_{AB} \rightarrow \boldsymbol{s}_{\mathcal{L}}, \tag{4.3}$$

where the mathematical notation $\rightarrow$ indicates the mapping relationship. The quantity $\boldsymbol{s}_{\mathcal{L}}$ is referred to as the linear network coded combination (LNCC). The user data symbol s_i, $i \in \{A, B\}$, since it is drawn from a QPSK constellation, is treated as a member of a binary extension field $\mathrm{GF}(2^2)$. As such, the user data s_i can be re-expressed in a binary extension field form, given as $\boldsymbol{s}_i = \begin{bmatrix} s_{i,1} \\ s_{i,2} \end{bmatrix}, i \in \{A, B\}$. The linear mapping $\mathcal{L}$ is a linear function in either $\mathrm{GF}(2^2)$ or $\mathrm{GF}(2^3)$ of $\boldsymbol{s}_A$ and $\boldsymbol{s}_B$, given by

$$\boldsymbol{s}_{\mathcal{L}} = \boldsymbol{A} \otimes \boldsymbol{s}_A \oplus \boldsymbol{B} \otimes \boldsymbol{s}_B \tag{4.4}$$

where $\boldsymbol{A}$ and $\boldsymbol{B}$ are members of $\mathrm{GF}(2^2)$ or $\mathrm{GF}(2^3)$. These can be represented as 2×2 (or 3×2) binary matrices, and the field elements as length 2 (or 3) binary vectors. The resulting LNCC $\boldsymbol{s}_{\mathcal{L}}$ is the member of binary extension fields $\mathrm{GF}(2^2)$ or $\mathrm{GF}(2^3)$. It can be

expanded as $\boldsymbol{s}_{\mathcal{L}} = \begin{bmatrix} s_{\mathcal{L},1} \\ s_{\mathcal{L},2} \\ s_{\mathcal{L},3} \end{bmatrix}$, where $s_{\mathcal{L},n}$, $n \in \{1,2,3\}$, represents the *n*-th bit level of $\boldsymbol{s}_{\mathcal{L}}$. If $s_{\mathcal{L},1} = 0$, $\boldsymbol{s}_{\mathcal{L}}$ is a member of binary extension field $\mathrm{GF}(2^2)$; otherwise, $\boldsymbol{s}_{\mathcal{L}}$ is a member of binary extension field $\mathrm{GF}(2^3)$.

All matrix operations in the linear mapping function (4.3) obey modulo-2 arithmetic, i.e., $\boldsymbol{x} \otimes \boldsymbol{y} = \mathrm{mod}(\boldsymbol{x} \cdot \boldsymbol{y}, 2)$ and $\boldsymbol{x} \oplus \boldsymbol{y} = \mathrm{mod}(\boldsymbol{x} + \boldsymbol{y}, 2)$, which are closed within $\mathrm{GF}(2)$. We define the generator matrix as $\boldsymbol{G} \triangleq \begin{bmatrix} \boldsymbol{A} & \boldsymbol{B} \end{bmatrix}$ and the source symbol vector as $\boldsymbol{s}_{AB} \triangleq \begin{bmatrix} \boldsymbol{s}_A \\ \boldsymbol{s}_B \end{bmatrix}$. Hence, (4.4) can be rewritten as

$$\boldsymbol{s}_{\mathcal{L}} = \boldsymbol{G} \otimes s_{AB} = \boldsymbol{G} \otimes \begin{bmatrix} s_{A,1} \\ s_{A,2} \\ s_{B,1} \\ s_{B,2} \end{bmatrix} = \begin{bmatrix} s_{\mathcal{L},1} \\ s_{\mathcal{L},2} \\ s_{\mathcal{L},3} \end{bmatrix}. \tag{4.5}$$

The user data $\boldsymbol{s}_i, i \in \{A, B\}$ is treated as the *complementary side information* (C-SI). Based on this, the linear mapping function should guarantee the unambiguous decodability of the LNCC for users *A* and *B*, which is:

$$\begin{aligned} \mathcal{L}(\boldsymbol{s}_A, \boldsymbol{s}_B) &\neq \mathcal{L}(\boldsymbol{s'}_A, \boldsymbol{s}_B), \ \ \forall \boldsymbol{s}_A \neq \boldsymbol{s'}_A \\ \mathcal{L}(\boldsymbol{s}_A, \boldsymbol{s}_B) &\neq \mathcal{L}(\boldsymbol{s}_A, \boldsymbol{s'}_B), \ \ \forall \boldsymbol{s}_B \neq \boldsymbol{s'}_B. \end{aligned} \tag{4.6}$$

This is referred to as the *exclusive law* in [8].

Embedding the linear mapping function (4.3) into the maximum likelihood (ML) detection, we have

$$\begin{aligned} \boldsymbol{s}_{\mathcal{L}} &= \arg\max_{\boldsymbol{s}_{\mathcal{L}}} p(y_R|\boldsymbol{s}_{\mathcal{L}}) \\ &= \arg\max_{\boldsymbol{s}_{\mathcal{L}}} \sum_{\forall(x_A,x_B) \text{ s.t. } \mathcal{L}:x_{AB}\to\boldsymbol{S}_{\mathcal{L}}} P(x_A)P(x_B)p(y_R|x_{AB}), \end{aligned} \tag{4.7}$$

where we note that the summation includes all x_A and x_B such that $\mathcal{L} : x_{AB} \to \boldsymbol{s}_{\mathcal{L}}$. The conditional probability density function (PDF) $p(y_R|x_{AB})$ is the Gaussian distribution, given by

$$p(y_R|x_{AB}) = \frac{1}{2\pi\sigma_w^2} \exp\left(-\frac{|y_R - x_{AB}|^2}{2\sigma_w^2}\right). \tag{4.8}$$

The details of the selection criterion for the linear mapping functions are described in the next section.

4.3.2 Broadcast (BC) Phase

In the BC phase, *R* maps the LNCC into the modulated symbol, given as $x_R = \mathcal{M}_R(\boldsymbol{s}_{\mathcal{L}})$, where $\mathcal{M}_R(\cdot)$ is the relay constellation mapper. Then *R* broadcasts x_R to *A* and *B*. The received signal at each user is given by

$$y_i = x_R + n_i, \tag{4.9}$$

where n_i is the complex AWGN at user i, $i \in \{A, B\}$.

4.4 Adaptive Selection criterion For Linear Mapping

In this section, we provide the detailed design for the adaptive selection criterion of the linear mapping functions. As all channel states are known to *R*, the mapping functions are then selected according to these channel states, firstly to ensure unambiguous decodability, and secondly to maximize the individual achievable rate of each user.

4.4.1 Unambiguous Decodablity for Linear Mapping

At user *A*'s side, to successfully recover the desired symbol $\boldsymbol{s}_B$, the user *A* should exploit the generator matrix $\boldsymbol{G}$ to solve the linear equation (4.3) and similarly for user *B*. Hence fulfilling the unambiguous decoding criterion is equivalent to choosing the generator matrix $\boldsymbol{G}$ from those for which the linear function (4.3) is solvable. Given this, we provide the following Condition for unambiguous decoding.

Condition 1: Unambiguous decoding is possible if and only if both $\boldsymbol{A}$ and $\boldsymbol{B}$ have full column rank: that is, all columns are linearly independent. We note that when $\boldsymbol{A}$ and $\boldsymbol{B}$

have two columns each. This implies that the two columns are different and contain at least one '1'.

Proof. We note that the linear mapping in (4.3) in fact forms a set of linear Diophantine equations with four variables. Since each user has its own C-SI, (4.3) may be simplified to a set of linear equations with two variables for each user. These are soluble for $\boldsymbol{s}_A$ and $\boldsymbol{s}_B$ if and only if $\boldsymbol{A}$ and $\boldsymbol{B}$ are invertible, that is, have rank at least two. Since the row rank is equal to the column rank and there are two columns, $\boldsymbol{A}$ and $\boldsymbol{B}$ must have full column rank. Since there are only two columns, they are linearly independent if neither is zero and they are different. The proof of *Condition 1* is thus complete. □

We note that if we select the generator matrix as $\boldsymbol{G} = \begin{bmatrix} 0 & 0 & 0 & 0 \\ 1 & 0 & 1 & 0 \\ 0 & 1 & 0 & 1 \end{bmatrix}$, the value returned by the mapping function in 4.3 is in fact the original PNC, i.e., the bit-wise XOR mapping. Hence, the original PNC is a subset of the proposed LPNC-EM.

4.4.2 Rate based Adaptive Selection

In this subsection, we discuss the rate based adaptive selection in details. We denote the rate of each user in the MAC phase as $R_i^{(1)}$, $i \in \{A, B\}$ and the mutual information between y_R and $\boldsymbol{s}_{\mathcal{L}}$ as $I(Y_R; \boldsymbol{S}_{\mathcal{L}})$.

The mutual information $I(Y_R; \boldsymbol{S}_{\mathcal{L}})$ is calculated as

$$I(Y_R; \boldsymbol{S}_{\mathcal{L}}) = \log_2(M_{\boldsymbol{s}_{\mathcal{L}}}) + \sum_{\boldsymbol{s}_{\mathcal{L}}} P(\boldsymbol{s}_{\mathcal{L}}) \int_{y_R \in \mathbb{C}} p(y_R | \boldsymbol{s}_{\mathcal{L}}) \log_2 \left[\frac{p(y_R | \boldsymbol{s}_{\mathcal{L}}) P(\boldsymbol{s}\mathcal{L})}{\sum_{\boldsymbol{s'}_{\mathcal{L}}} P(\boldsymbol{s'}_{\mathcal{L}}) p(y_R | \boldsymbol{s'}_{\mathcal{L}})} \right] dy_R, \tag{4.10}$$

where $M_{\boldsymbol{s}_{\mathcal{L}}}$ is the cardinality of the LNCC.

We note that the rate region of LPNC-EM in the MAC phase is determined by the mapping function in (4.3). Here, we show the impact of the mapping function on the

individual achievable rate of each user. If the resulting LNCC is a member of $\mathrm{GF}(2^2)$, the rate region of LPNC-EM is given as

$$R_A^{(1)} = R_B^{(1)} \leq I(Y_R; \boldsymbol{S}_{\mathcal{L}}), \;\; \boldsymbol{s}_{\mathcal{L}} \in \mathrm{GF}(2^2). \tag{4.11}$$

However, when we select a $\boldsymbol{G}$ to generate a LNCC $\boldsymbol{s}_{\mathcal{L}}$ in $\mathrm{GF}(2^3)$, the rate of each user is proportional to $I(Y_R; \boldsymbol{S}_{\mathcal{L}})$. For example, given $\boldsymbol{G} = \begin{bmatrix} 1 & 0 & 0 & 1 \\ 1 & 0 & 1 & 0 \\ 0 & 1 & 0 & 1 \end{bmatrix}$, the resulting LNCC is calculated as $\boldsymbol{s}_{\mathcal{L}} = \begin{bmatrix} s_{A,1} \oplus s_{B,2} \\ s_{A,1} \oplus s_{B,1} \\ s_{A,2} \oplus s_{B,2} \end{bmatrix}$. We note that if the resulting LNCC $\boldsymbol{s}_{\mathcal{L}}$ is a member of $\mathrm{GF}(2^3)$, the following observations are obtained: 1) $\boldsymbol{s}_{\mathcal{L}}$ provides the redundancy for the binary bit $s_{i,j}, i \in \{A, B\}, j \in \{1, 2\}$; and 2) the maximum mutual information $I(Y_R; \boldsymbol{S}_{\mathcal{L}})$ can achieve 3bits/symbol when SNR is high. However, the effective achievable rate of user i, $i \in \{A, B\}$, is equal to the sum of the rates with respect to binary bits $s_{i,1}$ and $s_{i,2}$ in the $\boldsymbol{s}_{\mathcal{L}}$. Assuming an error-free BC phase, based on *Condition 1*, what each user needs to solve are the two and only two unknown variables $s_{i,1}$ and $s_{i,2}$ even though these two variables may appear more than once in the linear equations (4.5). As a result, we may expand the rates $R_A^{(1)}$ and $R_B^{(1)}$ as

$$\begin{aligned} R_A^{(1)} &\leq I(Y_R; S_{A,1}(\boldsymbol{S}_{\mathcal{L}})) + I(Y_R; S_{A,2}(\boldsymbol{S}_{\mathcal{L}})) \\ R_B^{(1)} &\leq I(Y_R; S_{B,1}(\boldsymbol{S}_{\mathcal{L}})) + I(Y_R; S_{B,2}(\boldsymbol{S}_{\mathcal{L}})), \end{aligned} \tag{4.12}$$

where $s_{i,j}(\boldsymbol{s}_{\mathcal{L}})$, $i \in \{A, B\}$, $j \in \{1, 2\}$, is the *j*-th data bit of user *i* carried by $\boldsymbol{s}_{\mathcal{L}}$ and $I(Y_R; S_{i,j}(\boldsymbol{s}_{\mathcal{L}}))$ denotes the mutual information between the received signal at relay and the user's binary bit carried by LNCC. Since the LNCC $\boldsymbol{s}_{\mathcal{L}}$ is uniformly distributed over either $\mathrm{GF}(2^2)$ or $\mathrm{GF}(2^3)$, each mapping level in (4.5) are equiprobable. Based on this, we have $I(Y_R; S_{i,j}(\boldsymbol{s}_{\mathcal{L}})) = \frac{1}{3} I(Y_R; \boldsymbol{S}_{\mathcal{L}})$. Hence, the rate region in (4.12) can be rewritten as $R_A^{(1)} = R_B^{(1)} \leq \frac{2}{3} I(Y_R; \boldsymbol{S}_{\mathcal{L}}), \;\; \boldsymbol{S}_{\mathcal{L}} \in \mathrm{GF}(2^3)$, where $\frac{2}{3} I(Y_R; \boldsymbol{S}_{\mathcal{L}})$ equals to the effective bits per symbol received by each user if the BC phase is error-free. Based on these observations, we have the following remark.

Remark 1: The individual achievable rate of each user in the MAC phase is proportional to the mutual information between the received signal and the LNCC, given by

$$R_A^{(1)} = R_B^{(1)} \leq \frac{H(\boldsymbol{S}_i)}{H(\boldsymbol{S}_{\mathcal{L}})} I(Y_R; \boldsymbol{S}_{\mathcal{L}}), i \in \{A, B\}, \tag{4.13}$$

where $H(\cdot)$ denotes the entropy function. The quantity $\frac{H(\boldsymbol{S}_i)}{H(\boldsymbol{S}_\mathcal{L})}$ is the proportion of user symbol $\boldsymbol{s}_i$ in $\boldsymbol{s}_\mathcal{L}$ and we have $H(\boldsymbol{S}_i) = 2$ due to the QPSK signaling and $H(\boldsymbol{S}_\mathcal{L}) = \log_2(q), q \in \{2^2, 2^3\}$ as $\boldsymbol{s}_\mathcal{L}$ is uniformly distributed over either $\mathrm{GF}(2^2)$ or $\mathrm{GF}(2^3)$.

Based on the *Remark 1*, we observe that *maximizing* $\frac{2}{\log_2(q)} I(Y_R; \boldsymbol{S}_\mathcal{L})$ *is equivalent to maximizing the individual achievable rate of each user in the MAC phase*. Since the mutual information $I(Y_R; \boldsymbol{S}_\mathcal{L})$ is strongly dependent on the generator matrix $\boldsymbol{G}$, we re-express $I(Y_R; \boldsymbol{S}_\mathcal{L})$ in terms of $\boldsymbol{G}$, given as $I^{\boldsymbol{G}}(Y_R; \boldsymbol{S}_\mathcal{L})$. The selection criterion of maximizing the individual achievable rate of each user returns the optimal $\boldsymbol{G}$, given by

$$\widetilde{\boldsymbol{G}} = \arg\max_{\boldsymbol{G}} \underbrace{\left[\frac{2}{\log_2(q)} I^{\boldsymbol{G}}(Y_R; \boldsymbol{S}_\mathcal{L})\right]}_{\Delta(\boldsymbol{G})}, \tag{4.14}$$

where $\widetilde{\boldsymbol{G}}$ is the generator matrix returned after exhaustive searching. The objective function for optimization is defined as $\Delta(\boldsymbol{G})$.

4.4.3 Rate Analysis for LPNC-EM

In this subsection, we explore the impact of fading on the effective individual achievable rate of each user. We note that after scaling by $1/h_A$, the SS in (4.2) can be re-expressed in terms of h_{re}, given as $x^*_{AB} \triangleq x_A + h_{re} x_B$. This indicates that the individual rate of each user in (4.13) is also a function of h_{re}. We plot this rate over the whole complex plane of h_{re} when SNR=10dB for LPNC-EM, 5QAM-DNF and the original PNC, as shown in Fig. 4.1. The authors in [2] pointed out that the original PNC has a significant performance degradation when h_{re} occurs on these places: $h_{re} = \pm j$, $h_{re} = \pm\frac{1}{2}(1 \pm j)$, $h_{re} = \pm 1 \pm j$ and $|h_{re}| \approx 0$, which are referred to as the *singular points*.

Based on Fig. 4.1, we have the following observations: 1) the original PNC cannot eliminate any of the singular points mentioned above; 2) the proposed LPNC-EM can eliminate the singular points around $h_{re} = \pm j$. It cannot eliminate the singular points around $h_{re} = \pm\frac{1}{2}(1 \pm j)$ and $h_{re} = \pm 1 \pm j$ but can mitigate them; 3) 5QAM-DNF can eliminate the singular points around $h_{re} = \pm j$, $h_{re} = \pm\frac{1}{2}(1 \pm j)$ and $h_{re} = \pm 1 \pm j$; and 4) The LPNC-EM has a superior capability of mitigating the singular points around $|h_{re}| \approx 0$ compared with 5QAM-DNF.

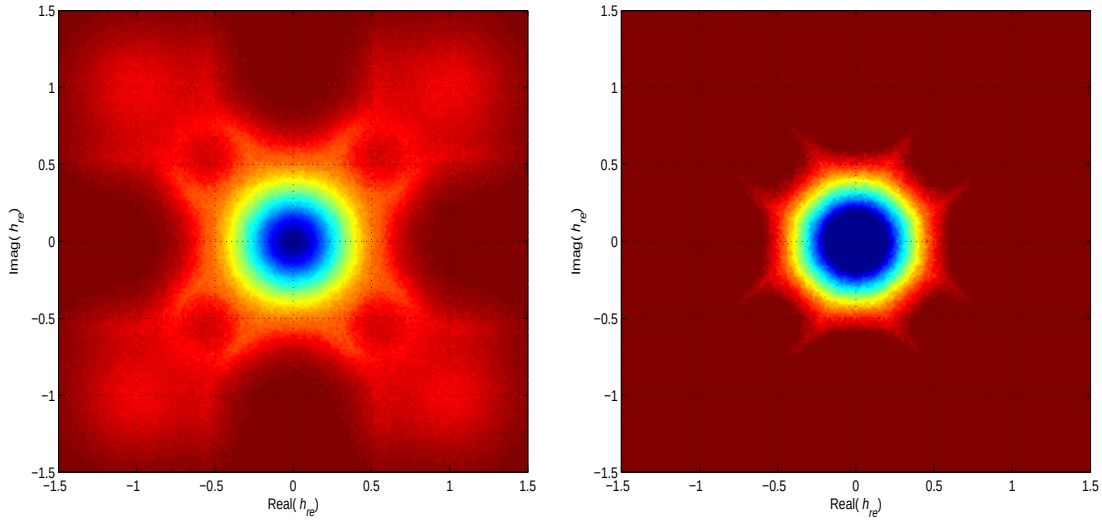

(a) LPNC-EM

(b) 5QAM-DNF

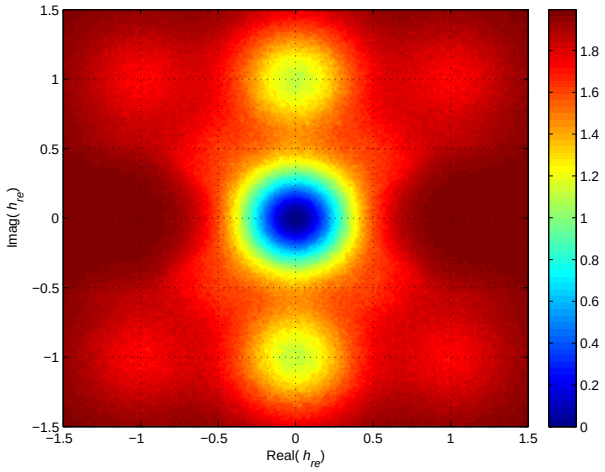

(c) Original PNC (bit-wise XOR)

Figure 4.1: The rate $R_i^{(1)}, i \in \{A, B\}$ against the real and imaginary parts of h_{re} when SNR=10dB.

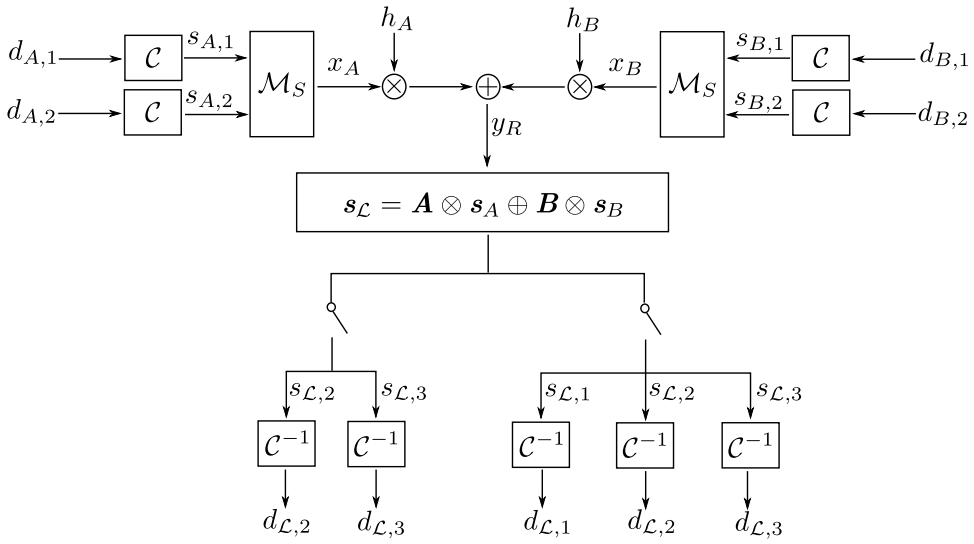

Figure 4.2: System Diagram of Multilevel Coded LPNC-EM.

4.5 Multilevel Coded LPNC-EM

In this section, we provide the detailed design of multilevel coded LPNC-EM. The LNCC in (4.5) forms a group of linear functions for user data bits $\boldsymbol{s}_i = \begin{bmatrix} s_{i,1} \\ s_{i,2} \end{bmatrix}, i \in \{A, B\}$. This inspires us to employ the independent coding levels for $s_{i,1}$ and $s_{i,2}$ to construct the HDF paradigm as in [7]. The details of the proposed multilevel coded LPNC-EM are described as follows.

In the proposed multilevel coded LPNC-EM, the user data bits $\boldsymbol{s}_{i,1}$ and $\boldsymbol{s}_{i,2}$ are the coded data stream, which are generated by independently encoding the input binary bits $\boldsymbol{d}_{i,1}$ and $\boldsymbol{d}_{i,2}$, given by $\boldsymbol{s}_{i,j} = \mathcal{C}(\boldsymbol{d}_{i,j})$, where $j \in \{1, 2\}$ and $\mathcal{C}(\cdot)$ is the channel encoder.

The relay *R* performs the proposed LPNC-EM mapping as in (4.4) and inputs each level of the resulting LNCC $\boldsymbol{s}_{\mathcal{L}}$ into the channel decoder $\mathcal{C}^{-1}(\cdot)$. The independent decoding for each level of $\boldsymbol{s}_{\mathcal{L}}$ is formulated as

$$\begin{bmatrix} \mathcal{C}^{-1}(\boldsymbol{s}_{\mathcal{L},1}) \\ \mathcal{C}^{-1}(\boldsymbol{s}_{\mathcal{L},2}) \\ \mathcal{C}^{-1}(\boldsymbol{s}_{\mathcal{L},3} \end{bmatrix} = \begin{bmatrix} \mathcal{C}^{-1}\left(\boldsymbol{G}(1,:) \otimes \boldsymbol{s}_{AB}\right) \\ \mathcal{C}^{-1}\left(\boldsymbol{G}(2,:) \otimes \boldsymbol{s}_{AB}\right) \\ \mathcal{C}^{-1}\left(\boldsymbol{G}(3,:) \otimes \boldsymbol{s}_{AB}\right) \end{bmatrix}, \tag{4.15}$$

where $\boldsymbol{G}(m,:), m \in \{1, 2, 3\}$, is the *m*-the row of $\boldsymbol{G}$.

As each bit level of $\boldsymbol{s}_{\mathcal{L}}$ is a linear function of the coded data stream $\boldsymbol{s}_{i,j}$, the output of the decoder function is then a linear combination of $\boldsymbol{d}_{i,j}$. This because LPNC-EM does not break the linearity of channel codes. Based on these, (4.15) can be expanded as

$$\begin{bmatrix} \mathcal{C}^{-1}(\boldsymbol{s}_{\mathcal{L},1}) \\ \mathcal{C}^{-1}(\boldsymbol{s}_{\mathcal{L},2}) \\ \mathcal{C}^{-1}(\boldsymbol{s}_{\mathcal{L},3} \end{bmatrix} = \boldsymbol{G} \otimes \begin{bmatrix} \mathcal{C}^{-1}(\boldsymbol{s}_{A,1}) \\ \mathcal{C}^{-1}(\boldsymbol{s}_{A,2}) \\ \mathcal{C}^{-1}(\boldsymbol{s}_{B,1}) \\ \mathcal{C}^{-1}(\boldsymbol{s}_{B,2}) \end{bmatrix} = \boldsymbol{G} \otimes \begin{bmatrix} \boldsymbol{d}_{A,1} \\ \boldsymbol{d}_{A,2} \\ \boldsymbol{d}_{B,1} \\ \boldsymbol{d}_{B,2} \end{bmatrix} \triangleq \boldsymbol{D}_{\mathcal{L}}, \tag{4.16}$$

where we denote the linear combination of $\boldsymbol{d}_{i,j}$ as $\boldsymbol{D}_{\mathcal{L}}$ and $\boldsymbol{D}_{\mathcal{L}} = \begin{bmatrix} \boldsymbol{d}_{\mathcal{L},1} \\ \boldsymbol{d}_{\mathcal{L},2} \\ \boldsymbol{d}_{\mathcal{L},3} \end{bmatrix}$ in which $\boldsymbol{d}_{\mathcal{L},n}, n \in \{1,2,3\}$ is the n-th bit level of $\boldsymbol{D}_{\mathcal{L}}$.

The results of (4.15) and (4.16) show the fundamental principle of multilevel coded LPNC-EM. Based on this, we plot the system structure of the multilevel coded LPNC-EM, as shown in Fig. 4.2.

4.6 Performance Evaluation

In this section, we evaluate the frame error rate (FER) performance for the proposed strategy and the benchmarks in the Rayleigh fading 2-WRC. Due to the nature of network coding, we note that the transmission of the BC phase in 2-WRC is in fact the same as that of the point-to-point channel. The authors in [8] pointed out that the MAC phase is the performance bottleneck of 2-WRC for PNC strategy. For this reason, we pay more attention to the performance in the MAC phase than that in the BC phase, that is, we assume that the BC phase is free from error and the LNCC or network coded symbol can be perfectly received by each user. Fig. 4.3 shows the FER performance for the proposed strategy and the benchmarks when the BC phase is error-free. The length of the original data packet is 512 bits. A rate 1/3 convolutional code with generator polynomials $(133, 171, 145)_8$ is applied. We choose the original PNC and 5QAM-DNF in [8] as the benchmarks.

Based on Fig. 4.3, we observe that uncoded LPNC-EM is superior to uncoded orig-

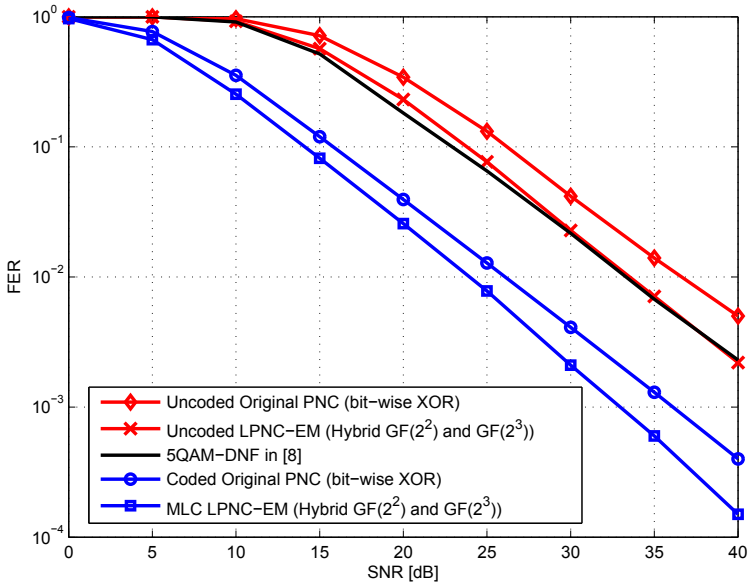

Figure 4.3: FER for different strategies

inal PNC. Compared with 5QAM-DNF, uncoded LPNC-EM still achieves almost equal performance. We also clearly observe the coding gain by the chosen convolutional codes. Similar to uncoded scenario, multilevel coded LPNC-EM outperforms the coded original PNC.

Fig. 4.4 shows the sum-rate for different strategies in the MAC phase. Based on Fig. 4.4, we see that LPNC-EM outperforms the original PNC and achieves an almost equal performance (with a negligible rate degradation) compared with 5QAM-DNF. This is in accordance with our FER results.

4.7 Summary

In this Chapter, we proposed a novel LPNC-EM for Rayleigh fading 2-WRC. The relay node adaptively selects the linear generator matrix and directly maps the superimposed signal of the two users into the linear network coded combination over the hybrid Galois Field ($\mathrm{GF}(2^2)$ or $\mathrm{GF}(2^3)$). The selection criterion ensures unambiguous decoding and maximizes the individual rate of each user. The LPNC-EM forms two or three independent coding levels which facilitates the multilevel coded structure. This enables the HDF

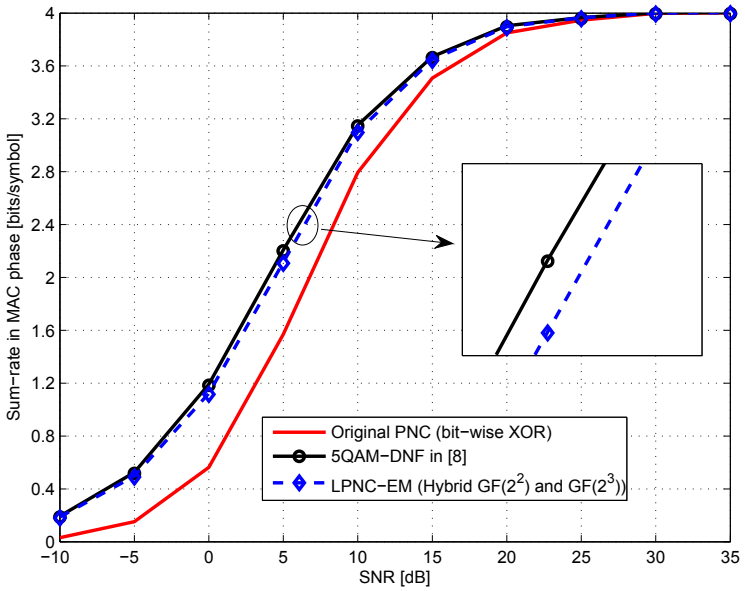

Figure 4.4: Average Rate for two users v.s. h_re

paradigm as in [7]. The numerical results show that the uncoded LPNC-EM outperforms the original PNC and can achieve equal error performance compared with 5QAM-DNF in [8]. Furthermore, the multilevel coded LPNC-EM also provides a superior error performance over the coded original PNC.

Chapter 5

Linear Physical-layer Network Coding in Hybrid Finite Ring for Rayleigh fading 2-way Relay Channels

Contents

5.1 Overview

In this chapter, we propose a novel LPNC scheme over hybrid finite ring (HFR-LPNC) for Rayleigh fading two-way relay channels. The relay maps the superimposed signal of the two users to a linear network coded combination (LNCC) over hybrid finite ring, rather than using the simple bit-wise XOR mapping [1]. The optimal linear coefficients are selected to generate the LNCC, aiming to: 1) maximize the sum-rate in the MAC phase; and 2) ensure unambiguous decoding. To avoid the performance degradation caused by

high-order irregular mappings, properly designed source coding is used for compressing the LNCC alphabet over the hybrid finite ring into the unifying 4-ary alphabet. We derive the constellation constrained sum-rates for HFR-LPNC in comparison with 5QAM denoise-and-forward (5QAM-DNF) [8], which we use as a reference scheme. Furthermore, we explicitly characterize the rate difference between HFR-LPNC and 5QAM-DNF. Our analysis and simulation show that: 1) HFR-LPNC has a superior ability to mitigate the singular fading compared with 5QAM-DNF; and 2) HFR-LPNC is superior to 5QAM-DNF over a wide range of SNRs.

5.2 Introduction

In order to deal with the fading in the MAC phase of the 2-WRC, the authors of [8] proposed a novel, non-linear 5QAM-DNF scheme for PNC, which can mitigate these singular fade states by extending the mapping from 4-ary to 5-ary. The authors in [56,57] proposed a new non-linear PNC constructed from the Latin square, which has similar capability to mitigate the singular fading. However, the drawbacks of 5QAM-DNF and Latin square based PNC are also clear: both the nonlinear mapping and the 5QAM constellation used on the BC phase introduce irregularities in the communication system which mean that they cannot readily be implemented in conventional systems. Moreover, the selection criterion of their non-linear mapping is based on the maximization of minimum Euclidean distance which cannot guarantee the maximum sum-rate in the MAC phase.

The algebraic approach to network coding proposed in [25, 26], namely, the so-called compute-and-forward (CPF), has extended the PNC beyond the 2-WRC to general Gaussian multiple access channels (GMAC). However, we note that their scheme requires a high dimensional lattice construction which may not be practical. The degrees of freedom (DoF) of CPF was investigated in [27], in which the authors proved that the DoF of CPF using lattice codes for a K transmitters and K relays network is at most $2/(1 + 1/K)$. In [28], the authors proposed a novel distributed space-time coding for two-way relay channels, which mitigates the singular fading at the user side without any channel state information at the transmitter (CSIT) and only adopts simple XOR mapping at the relay. The authors in [4,32] proposed a combined PNC approach with interference alignment for

multi-antenna base stations and relays. In [29], the authors proposed a novel decoding algorithm for PNC which can deal with the symbol and phase synchronization. The authors in [30] proposed a joint design of channel coding and PNC for frequency selective channels. The authors in [31] proposed a precoding based PNC for the generalized MIMO Y channels, where the precoding at each user and the relay is carefully constructed to ensure that the users are grouped in pairs and the interference among user pairs can be canceled. The authors in [33] investigated the error probability bound at the relay which uses a punctured codebook method for explicitly computing the distance spectrum of the PNC. The symbol error rate (SER) of PNC with BPSK and QPSK modulation in non-fading 2-WRC was studied in [35]. The author in [37] analyzed the SER for QAM modulated PNC with the phase error. An exact bit error rate (BER) performance of the PNC for the fading 2-WRC was derived in [36]. The concept of linear network coding in the switching networks was originally proposed in [38, 39] and further extended to the wireless 2-WRC in [34], namely, linear physical-layer network coding (LPNC). However, their designed LPNC can only be optimized for the prime q-ary modulation (e.g., 5PAM in [34]) at sources. This restricts its application with common modulation schemes such as QPSK, 16QAM and etc. Moreover, their LPNC design is based on the maximization of minimum Euclidean distance which cannot guarantee the maximum sum-rate in the MAC phase.

To tackle the aforementioned challenge of singular fading for PNC, in this chapter, we propose HFR-LPNC for the Rayleigh fading 2-WRC. Unlike the 5PAM modulation in [34], we restrict the two users of 2-WRC to employ simple QPSK signalling. By properly selecting the linear coefficients belonging to the hybrid finite ring, the relay directly maps the superimposed signal of the two users into the linear network coded combination (LNCC) over these finite rings. The selection criterion ensures unambiguous decodablility and maximizes the sum-rate in the MAC phase. We explicitly characterize the sum-rates of LPNC and 5QAM-DNF. Based on our analysis and numerical results, we demonstrate that: 1) HFR-LPNC has a superior ability to mitigate the singular fading compared with 5QAM-DNF [8]; and 2) HFR-LPNC is superior to 5QAM-DNF over a wide range of SNRs. The four major contributions of this chapter are summarized as follows:

1. We design a new linear mapping over the hybrid finite ring for the superimposed signal of two users. This makes the decoding of neighboring network coded com-

binations more reliable, as the hybrid finite ring offers multiple decoding choices for a specific superimposed signal.

2. We optimize the designed linear mapping using the criterion of maximizing the sum-rate in the MAC phase. We also redesign 5QAM-DNF based on rate maximization rather than maximizing the minimum Euclidean distance [8].

3. We introduce source coding (SC) for compressing the LNCC alphabet over the hybrid finite ring into the unifying 4-ary alphabet. This avoids performance degradation for the BC phase transmission.

4. We derive the constellation constrained sum-rate for HFR-LPNC and 5QAM-DNF [8] (as the benchmark) and explicitly characterize the rate difference between them.

5.3 Preliminaries, System Model and Design

In this section, we first provide some preliminary definitions of modern algebra; then, we describe the system model and the design of the proposed scheme in detail.

5.3.1 Algebraic Preliminaries

Let $\mathcal{S}(q) \triangleq \{0, 1, 2, ..., q-1\}$ denote a finite set of the consecutive integers from 0 to $q-1$. The cardinality of $\mathcal{S}(q)$ is denoted by $|S(q)| = q$. Clearly, the finite set $\mathcal{S}(q)$ is *closed* under modulo-q addition and multiplication [42], given by

$$a \boxplus b \triangleq \mathrm{mod}(a+b, q),$$

and

$$a \boxdot b \triangleq \mathrm{mod}(a \cdot b, q),$$

respectively, where a, $b \in \mathcal{S}(q)$.

Based on the defined modulo-q operations on the finite set $\mathcal{S}(q)$, the following axioms are satisfied for a, b, $c \in \mathcal{S}(q)$

1. *Associative law:* $(a \boxplus b) \boxplus c = a \boxplus (b \boxplus c)$ and $(a \boxdot b) \boxdot c = a \boxdot (b \boxdot c)$;

2. *Commutative law:* $a \boxplus b = b \boxplus a$ and $a \boxdot b = b \boxdot a$.

Definition 1 [41]. A *semigroup* is a set with an associative binary operation $*$ defined on it.

Definition 2 [41]. A *monoid* is a semigroup $\mathcal{G}$ that contains an element e such that for any element a in $\mathcal{G}$,

$$e * a = a * e = a.$$

Then e is called an *identity element* of $\mathcal{G}$ with respect to the operation $*$.

Definition 3 [41]. A *group* is a monoid $\mathcal{G}$ in which for any element a of $\mathcal{G}$, there exists an element a' in $\mathcal{G}$ such that

$$a * a' = a' * a = e,$$

where a' is called an *inverse* of a, and vice versa, with respect to the operation $*$. A group $\mathcal{G}$ is said to be *commutative* if the binary operation $*$ defined on it is commutative.

Definition 4 [41]. A set $\mathcal{R}$ with two binary operations $+$ and $\cdot$ forms an algebraic structure $(\mathcal{R}, +, \cdot)$, which is called a *ring* if and only if the following axioms for a, b, $c \in \mathcal{R}$ are satisfied:

1. $(\mathcal{R}, +)$ forms a *commutative group*;

2. $(\mathcal{R}, \cdot)$ forms a *monoid*;

3. the operation $+$ distributes over the operation $\cdot$:

$$(a + b) \cdot c = a \cdot c + b \cdot c,$$

$$a \cdot (b + c) = a \cdot b + a \cdot c.$$

4. If the operation $\cdot$ also satisfies the commutative law, then the ring is called commutative.

Definition 5 [41].: A *bijection* is a function that defines an exact one-to-one correspondence between members of two sets of the same size.

Remark 1: $(\mathcal{S}(q), \boxplus, \boxdot)$ forms a finite commutative ring since: 1) $(\mathcal{S}(q), \boxplus)$ forms a commutative group, in which the identity element with respect to $\boxplus$ is 0; 2) $(\mathcal{S}(q), \boxdot)$ forms a monoid since $\boxdot$ is associative and the identity element is 1; and 3) it is easy to verify that the operation $\boxplus$ distributes over $\boxdot$.

Remark 2: $(\mathcal{S}(q), \boxdot)$ for non-prime q is not a group, since not all elements have inverses. For example, in $\mathcal{S}(6) = \{0, 1, 2, 3, 4, 5\}$ neither the even elements $(2, 4)$ nor 3 have inverses, since no multiple of these numbers, taken modulo-6, can be 1. However the subset $\{1, 5\}$ forms a group under $\boxdot$, again with 1 as the identity, since 5 is then its own inverse. In general, the non-zero elements in $\mathcal{S}(q)$ which are relatively prime to q form a group under $\boxdot$.

Remark 3: Multiplication (using $\boxdot$) by a member a of $\mathcal{S}(q)$ constitutes a bijection of $\mathcal{S}(q)$ to itself if and only if a has an inverse under $\boxdot$ (a multiplicative inverse), since a bijective function is reversible, and clearly multiplication by the inverse must reverse the multiplication. Hence multiplication by any non-zero element in $\mathcal{S}(q)$ which is relatively prime to q constitutes a bijection. Similarly addition ($\boxplus$) of any member of $\mathcal{S}(q)$ constitutes a bijection, since all elements have an additive inverse (under $\boxplus$).

Definition 6. The set $\mathcal{S}_{\mathrm{H}}(q_1, q_2, \cdots, q_n)$ with the operations $\boxplus$ and $\boxdot$, where $q_1, q_2, \cdots, q_n$ are integers, defined as

$$\mathcal{S}_{\mathrm{H}}(q_1, q_2, \cdots, q_n) \triangleq \{(\mathcal{S}(q_1), \boxplus, \boxdot), (\mathcal{S}(q_2), \boxplus, \boxdot), \cdots, (\mathcal{S}(q_n), \boxplus, \boxdot)\},$$

is called a hybrid finite ring.

5.3.2 MAC Phase

The 2-WRC involves two users (*A* and *B*) and one relay (*R*). It is assumed that both users adopt the Gray coded QPSK constellation with unity energy constraint. The constellation mapper is denoted as $\mathcal{M}_S(\cdot)$. In the MAC phase, the PNC allows *A* and *B* to simultaneously transmit signals. The electromagnetic signals are superimposed and received by the

relay, given by

$$y_R = h_A x_A + h_B x_B + n_R, \tag{5.1}$$

where $x_i = \mathcal{M}_S(s_i)$ is the modulated symbol of user *i*, $i \in \{A, B\}$ and s_i represents the user data, which serves as the *complementary side information* (C-SI) for user i. Let h_i, $i \in \{A, B\}$ denote the channel gain between user i and *R*. We assume that two channels experience independent and identically distributed (i.i.d.) frequency-flat Rayleigh fading with unit variance. The ratio $h_{re} \triangleq h_B/h_A$ is referred to as the relative fading factor. The received signal is corrupted by complex Additive White Gaussian Noise (AWGN) n_R with variance σ_w^2 per complex dimension. For simplicity, each user adopts the same transmission power of one unit. We define the average signal-to-noise-ratio (SNR) per information symbol as $\frac{1}{2\sigma_w^2}$. We refer to

$$x_{AB} \triangleq h_A x_A + h_B x_B \tag{5.2}$$

as the noiseless *superimposed signal (SS)*.

5.3.3 Linear Mapping at Relay

The authors in [8] pointed out that if both users employ QPSK modulation, the original PNC [1] using bit-wise eXclusive-OR (XOR) mapping has a significant performance degradation when h_{re} takes the values: $\pm j$, $\pm\frac{1}{2}(1 \pm j)$ and $\pm 1 \pm j$, which are referred to as the *singular points*. In addition, when $h_{re} \to 0$ or ∞, performance is necessarily degraded, since one of the source-relay channels is severely faded.

Around these singular points, the bit-wise XOR mapping cannot distinguish the nearest neighboring SSs associated with different network coded combinations. Because of this drawback, we propose to extend the linear mapping for PNC over the hybrid finite ring, which provides multiple decoding choices to distinguish the nearest neighboring SSs. Each SS is mapped into an element of the finite ring $\mathcal{S}(q)$. Note that the cardinality q may lie in the range 4 (described in [8] as a minimal mapping) to 16 (a full mapping). Hence, the initial hybrid finite ring is then given as $\mathcal{S}_{\text{H}}(4, \cdots, 16) = \{\mathcal{S}(4), \mathcal{S}(5), \mathcal{S}(6), \mathcal{S}(7), \mathcal{S}(8), \mathcal{S}(9), \mathcal{S}(10), \mathcal{S}(11), \mathcal{S}(12), \mathcal{S}(13), \mathcal{S}(14), \mathcal{S}(15), \mathcal{S}(16)\}$.

In the proposed design, the relay *R* performs the linear mapping $\mathcal{L}$ to generate a *linear*

network coded combination (LNCC) (where linearity is in the finite ring sense), taking the form

$$s_{\mathcal{L}}^{(q)} = \mathcal{L}_q\left(s_A, s_B\right) = \alpha_q \boxdot s_A \boxplus \beta_q \boxdot s_B, \quad \forall \alpha_q, \beta_q \in \mathcal{Z}_q, \tag{5.3}$$

where α_q and β_q represent the *linear coefficients* of LNCC and $\mathcal{Z}_q \triangleq \mathcal{S}(q)/\{0\}$ denotes the domain of α_q and β_q. The LNCC alphabet of $s_{\mathcal{L}}^{(q)}$ is denoted as $\mathcal{S}_{\mathcal{L}}^{(q)} = \left\{s_{\mathcal{L}}^{(q)}\right\}$ and its cardinality is $\left|\mathcal{S}_{\mathcal{L}}^{(q)}\right|$.

Given the received signal y_R at the relay, the relay estimates the LNCC $s_{\mathcal{L}}^{(q)}$ based on the maximal likelihood (ML) rule. Integrating the designed linear mapping in (5.3) into the ML detection, we have

$$\hat{s}_{\mathcal{L}}^{(q)} = \arg\max_{s_{\mathcal{L}}^{(q)}} p(y_R|s_{\mathcal{L}}^{(q)}) = \arg\max_{s_{\mathcal{L}}^{(q)}} \sum_{x_A, x_B : s_{\mathcal{L}}^{(q)} = \mathcal{L}_q(s_A, s_B)} P(x_A)P(x_B)p(y_R|x_{AB}), \tag{5.4}$$

where $\hat{s}_{\mathcal{L}}^{(q)}$ represents the decoded version of $s_{\mathcal{L}}^{(q)}$; $p(y_R|s_{\mathcal{L}}^{(q)})$ is the likelihood function; and the summation includes all transmitted symbol pairs (x_A, x_B) such that the SS is mapped into the LNCC $s_{\mathcal{L}}^{(q)}$. The conditional probability density function (PDF) $p(y_R|x_{AB})$ is given by

$$p(y_R|x_{AB}) = \frac{1}{2\pi\sigma_w^2} \exp\left(-\frac{|y_R - x_{AB}|^2}{2\sigma_w^2}\right). \tag{5.5}$$

The proposed HFR-LPNC generates several LNCCs in different finite rings and selects the one which can (in order of priority) 1) ensure the unambiguous decodability; 2) maximize the sum-rate in the MAC phase and 3) minimize the cardinality q of the ring (so as to minimize the required capacity in the BC phase). The details of the selection criteria for the coefficients of (5.3) are described in the following subsections.

5.3.4 Unambiguous Decodability of Linear Mapping

Each user should be able to decode the desired signal from the other user by exploiting the received LNCC and its C-SI. This requires the linear mapping in (5.3) to be unambiguously decodable, that is:

$$\begin{aligned} \mathcal{L}_q\left(s_A, s_B\right) &\neq \mathcal{L}_q\left(s'_A, s_B\right), \ \forall s_A \neq s'_A \\ \mathcal{L}_q\left(s_A, s_B\right) &\neq \mathcal{L}_q\left(s_A, s'_B\right), \ \forall s_B \neq s'_B, \end{aligned} \tag{5.6}$$

which is called the *exclusive law* in [8]. For given s_B, it defines a bijection from s_A to $s_{\mathcal{L}}^{(q)} = \mathcal{L}_q(s_A, s_B)$, and similarly for given s_A, a bijection from s_B to $s_{\mathcal{L}}^{(q)} = \mathcal{L}_q(s_A, s_B)$,

Clearly, the unambiguous decoding is possible if and only if the pair (α_q, β_q) is properly selected such that the linear mapping in (5.3) satisfies (5.6). Recall from **Remark 3** above and the domain of α_q and β_q, that multiplication by α_q or β_q constitutes a bijection (and therefore satisfies (5.6)) if and only if the coefficient has a multiplicative inverse with respect to $\boxdot$. This applies only to the non-zero elements of $\mathcal{S}(q)$ which are also relatively prime to q. Hence, the updated valid domain of α_q and β_q, denoted by $\mathcal{Z}_q^{'}$, is given by

$$\alpha_q, \beta_q \in \mathcal{Z}_q^{'} = \begin{cases} \{\text{odd integers in } \mathcal{S}(4)\}, \text{if } q = 4 \\ \mathcal{S}(5)/\{0\}, \text{if } q = 5 \\ \{\text{odd integers in } \mathcal{S}(6)\}/\{3\}, \text{if } q = 6 \\ \mathcal{S}(7)/\{0\}, \text{if } q = 7 \\ \{\text{odd integers in } \mathcal{S}(8)\}, \text{if } q = 8 \\ \mathcal{S}(9)/\{0,3\}, \text{if } q = 9 \\ \{\text{odd integers in } \mathcal{S}(10)\}/\{5\}, \text{if } q = 10 \\ \mathcal{S}(11)/\{0\}, \text{if } q = 11 \\ \{\text{odd integers in } \mathcal{S}(12)\}/\{3\}, \text{if } q = 12 \\ \mathcal{S}(13)/\{0\}, \text{if } q = 13 \\ \{\text{odd integers in } \mathcal{S}(14)\}/\{7\}, \text{if } q = 14 \\ \mathcal{S}(15)/\{0,3,5\}, \text{if } q = 15 \\ \{\text{odd integers in } \mathcal{S}(16)\}, \text{if } q = 16 \end{cases}. \quad (5.7)$$

Since the addition of any given element from $\mathcal{S}(q)$ also constitutes a bijection, then if α_q and β_q are selected from the above domain, (5.6) is automatically satisfied.

5.3.5 Search Space of Linear coefficients

For a given q, we have $(\alpha_q, \beta_q) \in \mathcal{Z}_q^{'} \times \mathcal{Z}_q^{'}$, where $\mathcal{Z}_q^{'} \times \mathcal{Z}_q^{'}$ indicates the search space of pair (α_q, β_q). However, searching (α_q, β_q) over such large search space requires a high computational complexity. The following **Theorem 1** shows that the size of the search space can be reduced from $\left|\mathcal{Z}_q^{'}\right|^2$ to $\left|\mathcal{Z}_q^{'}\right|$.

Theorem 1. The linear coefficient pairs $(\alpha_q, \beta_q) \in 1 \times \mathcal{Z}_q^{'}$ and $(\alpha_q, \beta_q) \in \mathcal{Z}_q^{'} \times \mathcal{Z}_q^{'}$ yield the same LNCC alphabet.

Proof. let $\alpha_q = 1$ and $\beta_q \in \mathcal{Z}_q^{'}$, we generate the following LNCC alphabet

$$\mathcal{S}_{\mathcal{L}}^{(q)} = \left\{ s_{\mathcal{L}}^{(q)} | \left(s_{\mathcal{L}}^{(q)} = 1 \boxdot s_A \boxplus \beta_q \boxdot s_B \right) \right\} \tag{5.8}$$

Multiplying $s_{\mathcal{L}}^{(q)}$ by $\lambda \in \mathcal{Z}_q^{'}$, we generate a new LNCC alphabet $\mathcal{S}'^{(q)}_{\mathcal{L}}$, given as

$$\mathcal{S}'^{(q)}_{\mathcal{L}} = \left\{ s'^{(q)}_{\mathcal{L}} | s'^{(q)}_{\mathcal{L}} = \lambda \boxdot s_{\mathcal{L}}^{(q)} = \lambda \boxdot (1 \boxdot s_A \boxplus \beta_q \boxdot s_B) \right\} \tag{5.9}$$

The algebraic associative law indicates that

$$\lambda \boxdot (1 \boxdot s_A \boxplus \beta_q \boxdot s_B) = (\lambda \boxdot 1) \boxdot s_A \boxplus (\lambda \boxdot \beta_q) \boxdot s_B \tag{5.10}$$

where we define $\alpha_q' \triangleq \lambda \boxdot 1$and $\beta_q' \triangleq \lambda \boxdot \beta_q$. Hence, $\mathcal{S}'^{(q)}_{\mathcal{L}}$ is re-expressed as

$$\mathcal{S}'^{(q)}_{\mathcal{L}} = \left\{ s'^{(q)}_{\mathcal{L}} | s'^{(q)}_{\mathcal{L}} = \alpha_q' \boxdot s_A \boxplus \beta_q' \boxdot s_B \right\} \tag{5.11}$$

where $(\alpha_q', \beta_q') \in \mathcal{Z}_q^{'} \times \mathcal{Z}_q^{'}$. From Section II.A above, we know that $\mathcal{S}_q$ in (5.9) is closed under the multiplication operation. Hence we have $\mathcal{S}_{\mathcal{L}}^{(q)} = \mathcal{S}'^{(q)}_{\mathcal{L}}$ and the proof of **Theorem 1** is complete. □

5.3.6 LPNC for Maximizing the Sum-rate in MAC Phase

Recall from the rate region of PNC established in [5, 7] that for HFR-LPNC, the sum-rate in the MAC phase strongly depends on the rate of LNCC, i.e., the mutual information between y_R and $s_{\mathcal{L}}^{(q)}$, denoted as $I(Y_R; S_{\mathcal{L}}^{(q)})$. The mutual information $I(Y_R; S_{\mathcal{L}}^{(q)})$ is calculated as

$$I(Y_R; S_{\mathcal{L}}^{(q)}) = H(Y_R) - H(Y_R | S_{\mathcal{L}}^{(q)}). \tag{5.12}$$

The entropy $H(Y_R)$ of the received signal is given by

$$H(Y_R) = -\int_{y_R \in \mathbb{C}} p(y_R) \log_2 \left(p(y_R) \right) dy_R. \tag{5.13}$$

The PDF of y_R in (5.13) is calculated as

$$p(y_R) = \sum_{x_A, x_B} P(x_{AB}) p(Y_R|x_{AB}) = \sum_{x_A, x_B} P(x_A) P(x_B) p(x_R|x_{AB}), \tag{5.14}$$

where $p(y_R|x_{AB})$ is defined in (5.5).

The conditional entropy $H(Y_R|S_{\mathcal{L}}^{(q)})$ in (7.13) can be calculated as

$$\begin{aligned} H(y_R|s_{\mathcal{L}}^{(q)}) =& -\sum_{s_{\mathcal{L}}^{(q)}} \int_{y\in\mathbb{C}} p\left(y_R, s_{\mathcal{L}}^{(q)}\right) \log_2\left(p\left(y_R|s_{\mathcal{L}}^{(q)}\right)\right) dy_R \\ =& -\sum_{s_{\mathcal{L}}^{(q)}} P(s_{\mathcal{L}}^{(q)}) \int_{y\in\mathbb{C}} p\left(y_R|s_{\mathcal{L}}^{(q)}\right) \log_2\left(p\left(y_R|s_{\mathcal{L}}^{(q)}\right)\right) dy_R, \end{aligned} \tag{5.15}$$

where $p\left(y_R|s_{\mathcal{L}}^{(q)}\right)$ is defined in (5.4).

Note that neither $H(Y_R)$ in (5.13) nor $H(Y_R|S_{\mathcal{L}}^{(q)})$ in (5.15) can be written in closed form. Hence, we use Monte-Carlo integration instead for computing (5.13) in (5.15). As such, the mutual information in (7.13) is computed as

$$I(Y_R; S_{\mathcal{L}}^{(q)}) = -\mathbb{E}\left[\log_2\left(p(Y_R)\right)\right] + \mathbb{E}\left[\log_2\left(p\left(Y_R|S_{\mathcal{L}}^{(q)}\right)\right)\right], \tag{5.16}$$

where M_i, $i \in \{A, B\}$, is the cardinality of the user alphabet assuming that the channel input is uniformly distributed, a common assumption for current communication systems.

Based on the calculated $I(Y_R; S_{\mathcal{L}}^{(q)})$, the following **Theorem 2** provides the rate region of the two users in the MAC phase given that HFR-LPNC is decoded at *R*. Note that unlike conventional multiple access channels, the sum-rate or individual rate in the MAC phase of 2-WRC is in fact the rate achieved by the two users assuming that the BC phase is free from error. Similarly, the sum-rate or individual rate in the BC phase is in fact the rate achieved by the two users assuming that decoding at the relay is error-free. The individual achievable rate of user $i, i \in \{A, B\}$ in the MAC phase is denoted by $R_i^{(1)}$ and the sum-rate in the MAC phase is denoted by $R_{AB}^{(1)}$.

The proof of **Theorem 2** is detailed in the Appendix.

Theorem 2. For the proposed HFR-LPNC, the rate region in the MAC phase is given

by

$$\begin{aligned} R_A^{(1)} &\leq \frac{1}{2} I\left(Y_R; \hat{S}_A | S_B\right) \\ R_B^{(1)} &\leq \frac{1}{2} I\left(Y_R; \hat{S}_B | S_A\right) \\ R_{AB}^{(1)} &\leq \frac{1}{2} \cdot \frac{4}{H\left(S_{\mathcal{L}}^{(q)}\right)} I\left(Y_R; S_{\mathcal{L}}^{(q)}\right), \end{aligned} \tag{5.17}$$

where the quantity 4 is the entropy of 4-bit binary tuple (s_A, s_B); and $H(s_{\mathcal{L}}^{(q)}) = -\sum_{s_{\mathcal{L}}^{(q)}} P(s_{\mathcal{L}}^{(q)}) \log_2\left(P(s_{\mathcal{L}}^{(q)})\right)$ is the entropy of $s_{\mathcal{L}}^{(q)}$. The quantity $\hat{s}_i$ denotes the recovered version of s_i.

For a given channel state, the objective of the proposed design is to find an optimal linear mapping such that the sum-rate bound of **Theorem 2** is maximized. The results of (5.3) and (5.16) indicate that $I(Y_R; S_{\mathcal{L}}^{(q)})$ depends on different LNCC, which in turn depends on the linear coefficient pair (α_q, β_q). Therefore, we re-express the mutual information $I(Y_R; S_{\mathcal{L}}^{(q)})$ in terms of the linear coefficient pair (α_q, β_q), which we write as $I^{(\alpha_q,\beta_q)}(Y_R; S_{\mathcal{L}}^{(q)})$. Based on these, our final selection criterion to maximize the sum-rate is given by

$$(\tilde{\alpha}_q, \tilde{\beta}_q) = \underset{(\alpha_q,\beta_q)\in 1\times\mathcal{Z}_q'}{\arg\max} \underbrace{\left[\frac{4}{H(s_{\mathcal{L}}^{(q)})} I^{(\alpha_q,\beta_q)}(Y_R; S_{\mathcal{L}}^{(q)})\right]}_{\Delta(\alpha_q,\beta_q)}, \tag{5.18}$$

where $(\tilde{\alpha}_q, \tilde{\beta}_q)$ is the returned linear coefficient pair. The objective function for optimization, defined as $\Delta(\alpha_q, \beta_q)$, is in fact the scaled (doubled) bound of sum-rate as given in (5.17).

5.3.7 The size-reduced HFR-LPNC

In this subsection, we provide an approach which can reduce the size of the initial hybrid finite ring $\mathcal{S}_{\mathrm{H}}(4, \cdots, 16)$ and hence results in a lower computational complexity. Here, we use 5QAM-DNF as the performance benchmark. The sum rate of 5QAM-DNF in the MAC phase is denoted as $R_{AB,\mathrm{DNF}}^{(1)}$. The following algorithm is proposed to reduce the size of $\mathcal{S}_{\mathrm{H}}(4, \cdots, 16)$ based on comparing the rate difference with $R_{AB}^{(1)}$ and $R_{AB,\mathrm{DNF}}^{(1)}$.

We note that the above algorithm only selects those finite rings that could result in

Algorithm 1 Reduce the size of $\mathcal{S}_{\mathrm{H}}(4, \cdots, 16)$

for all SNR=-10dB:40dB **do**
  for all $q \in \{4, ..., 16\}$ **do**
    for all $\mathrm{Re}(h_{re}) = -2 : 2$ **do**
      for all $\mathrm{Im}(h_{re}) = -2 : 2$ **do**
        Make a set empty: $\mathcal{Q} = \varphi$;
        Generate the LNCC $s_{\mathcal{L}}^{(q)} = \mathcal{L}_q\left(s_A, s_B\right)$;
        Compute $R_{AB}^{(1)}(q)$ and $R_{AB,\mathrm{DNF}}^{(1)}$;
        if $R_{AB}^{(1)}(q) \geq R_{AB,\mathrm{DNF}}^{(1)}$ for a given q **then**;
          Include this q in the set: $\mathcal{Q} \leftarrow \{\mathcal{Q} \cup q\}$;
        end if
      end for
    end for
  end for
end for
Let $\mathcal{Q} \leftarrow \mathrm{unique}(\mathcal{Q})$, which corresponds to the selected finite rings.

a superior performance for HFR-LPNC relative to 5QAM-DNF. **Algorithm 1** returns a size-reduced hybrid finite ring, given as $\mathcal{S}_{\mathrm{H}}(4, 5, 8) = \{\mathcal{S}(4), \mathcal{S}(5), \mathcal{S}(8)\}$ and excludes other finite rings in the initial hybrid finite ring $\mathcal{S}_{\mathrm{H}}(4, \cdots, 16)$. We refer to the LPNC using hybrid finite ring $\mathcal{S}_{\mathrm{H}}(4, 5, 8)$ as the *size-reduced HFR-LPNC*. We plot the scaled sum-rate bound of the size-reduced HFR-LPNC in the MAC phase as shown in Fig. 5.1, over the complex plane of h_{re} when SNR=10dB. We are interested especially in singular fading points as discussed in Section II.C above, which tend to result in local minima of the sum-rate. Based on Fig. 5.1, we have the following observations:

1) LPNC in $\mathcal{S}(4)$ cannot mitigate any singular fading points mentioned in Section II.C above. However, we note that it has a higher sum-rate bound (a scaled version in fact) around $|h_{re}| = 0$ compared with that in $\mathcal{S}(5)$.

2) LPNC in $\mathcal{S}(5)$ mitigates the singular points around $h_{re} = \pm j$, $h_{re} = \pm\frac{1}{2}(1 \pm j)$ and $h_{re} = \pm 1 \pm j$. However, the sum-rate bound for $\mathcal{S}(5)$ is lower than those in other finite rings around $|h_{re}| = 0$.

3) LPNC in $\mathcal{S}(8)$ mitigates the singular points around $h_{re} = \pm j$, $h_{re} = \pm\frac{1}{2}(1 \pm j)$ and $h_{re} = \pm 1 \pm j$ but its mitigation on these points is weaker than that of LPNC in $\mathcal{S}(5)$. However, LPNC in $\mathcal{S}(8)$ has the highest sum-rate bound around $|h_{re}| = 0$ compared with those in other finite rings.

4) HFR-LPNC combines the advantages of LPNC over rings $\mathcal{S}(4)$, $\mathcal{S}(5)$ and $\mathcal{S}(8)$.

It is interesting to note that despite causing exclusive law failure, singular fading does not reduce the sum-rate to zero. This is because typically only some symbol combinations are affected, resulting effectively in erasures of those symbols only. Note also that the sum-rate of the MAC phase is non-zero for $h_{re} = 0$. In this case $R_B^{(1)} = 0$ since $h_B = 0$, but $R_A^{(1)}$ is non-zero; similarly for $h_A = 0$.

Based on *Theorem 2*, the size-reduced HFR-LPNC only needs to search over $\sum_{q=4,5,8} \left|\mathcal{Z}_q^{'}\right| = 10$ pairs of linear coefficients to select the optimal one. The computation complexity is thus reduced.

5.3.8 The Selection Algorithm for HFR-LPNC

In this subsection, we provide a selection algorithm for HFR-LPNC based on the selection criterion in (5.18) and **Theorem 2**. We note that after scaling by $1/h_A$, the SS in (5.2) can be re-expressed in terms of h_{re}, and given as $x_{AB}^*(h_{re}) = x_A + h_{re}x_B$. This indicates that the objective function in (5.18) is also a function of h_{re}, and can be re-expressed as $\Delta(\alpha_q, \beta_q, h_{re})$.

Given a specific relative fading factor h_{re}, the **Algorithm 2** is proposed to determine the optimal HFR-LPNC to: 1) satisfy the unambiguous decoding in (5.6); 2) maximize the sum-rate in the MAC phase; and 3) minimize the cardinality q.

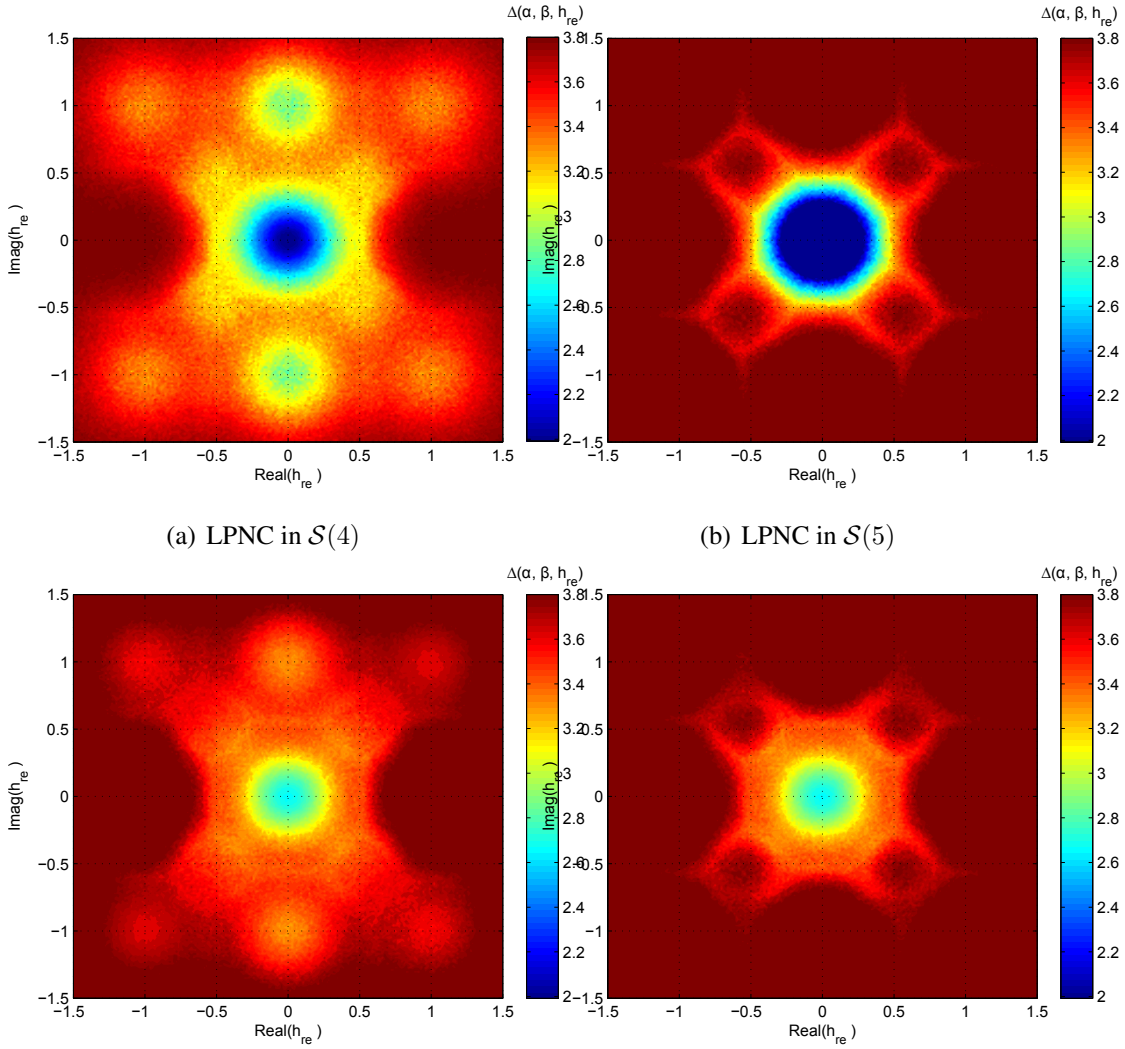

(a) LPNC in $\mathcal{S}(4)$

(b) LPNC in $\mathcal{S}(5)$

(c) LPNC in $\mathcal{S}(8)$

(d) HFR-LPNC after selection $(\mathcal{S}(q), q \in \{4, 5, 8\})$

Figure 5.1: The scaled bound of sum-rate, $\Delta(\alpha_q, \beta_q, h_{re})$, for LPNC in different finite rings v.s. h_{re} when SNR=10dB.

Algorithm 2 Optimal LPNC over Hybrid Finite Ring $\mathcal{S}_{\mathrm{H}}(4,5,8)$

1: Given h_{re};
2: **for all** $q \in \{4,5,8\}$ **do**
3: Make the rate set empty: $\mathcal{F}_I = \varphi$;
4: **for all** $(\alpha_q, \beta_q) \in 1 \times \mathcal{Z}_q^{'}$ **do**
5: Generate the LNCC $s_{\mathcal{L}}^{(q)} = \mathcal{L}_q\left(s_A, s_B\right)$;
6: Compute $\Delta(\alpha_q, \beta_q, h_{re})$;
7: Include it in the rate set: $\mathcal{F}_I \leftarrow \mathcal{F}_I \cup \{\Delta(\alpha_q, \beta_q, h_{re})\}$;
8: **end for**
9: **end for**
10: Let $\Delta(\alpha_q, \beta_q, h_{re})_{max}$ be the maximum value among all the rates: $\Delta(\alpha_q, \beta_q, h_{re})_{max} = \max\left(\mathcal{F}_I\right)$;
11: Select $(\alpha_q, \beta_q) \in 1 \times \mathcal{Z}_q^{'}$ whose rate corresponds to $\Delta(\alpha_q, \beta_q, h_{re})_{max}$ and with the smallest q (for minimal cardinality).

5.3.9 BC Phase and Decoding of the Desired Signal

In the BC phase, transmitting HFR-LPNC poses a challenge as the linear mapping in hybrid finite ring requires irregular modulation and sacrifices spectral efficiency. This is similar to 5QAM in [8]. To tackle this challenge, we propose to use source coding (SC) to compress the LNCC alphabet over the hybrid finite ring into an unifying 4-ary alphabet. In this subsection, we firstly systematically describe the joint design of SC and the HFR-LPNC; and then we determine the compression efficiency using SC; finally, we discuss decoding procedure of the desired signal for each user.

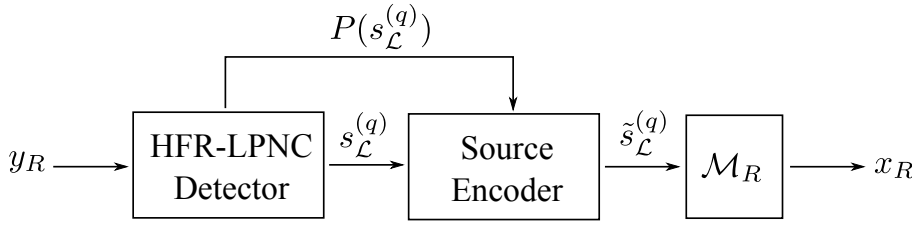

Figure 5.2: The Block Diagram of jointly designed HFR-LPNC and SC.

The block diagram of the jointly designed HFR-LPNC and SC is shown in Fig. 5.2. Based on different channel conditions, the HFR-LPNC detector generates the LNCC that maximizes the sum-rate in the MAC phase and also outputs the a priori probability of each

LNCC. The conditional probability of LNCC over different $\mathcal{S}(q)$ is denoted as $p(S_{\mathcal{L}}^{(q)}|q)$. Since $\mathcal{S}(4)$ and $\mathcal{S}(5)$ are subsets of $\mathcal{S}(8)$, the source encoder treats the hybrid finite ring $\mathcal{S}_{\mathrm{H}}(4,5,8)$ as a general $\mathcal{S}(8)$. We can obtain the a priori probability of the unified LNCC as follows

$$\begin{aligned}
P(S_{\mathcal{L}}^{(q)}=m) &= \sum_{q=4,5,8} p(S_{\mathcal{L}}^{(q)}=m|q)P(q), m\in\{0,1,2,3\}\\
P(S_{\mathcal{L}}^{(q)}=4) &= \sum_{q=5,8} p(S_{\mathcal{L}}^{(q)}=4|q)P(q),\\
P(S_{\mathcal{L}}^{(q)}=5) &= p(S_{\mathcal{L}}^{(q)}=5|q=8)P(q=8),\\
P(S_{\mathcal{L}}^{(q)}=6) &= p(S_{\mathcal{L}}^{(q)}=6|q=8)P(q=8),\\
P(S_{\mathcal{L}}^{(q)}=7) &= p(S_{\mathcal{L}}^{(q)}=7|q=8)P(q=8).
\end{aligned} \tag{5.19}$$

where $P(q)$ denotes the probability of the ring $\mathcal{S}(q)$ being selected, which can be obtained by a Monte-Carlo method averaging over a large number of channel realizations for Rayleigh fading 2-WRC. Note that the entropy of $s_{\mathcal{L}}^{(q)}$ obtained from its distribution for each channel and averaged over all channels is the same as that obtained from the distribution averaged over all channels.

In the proposed design, we apply classical Huffman coding to compress the LNCC alphabet into a unifying 4-ary alphabet using the above a priori probability. The output sequence of source encoder, namely, the compressed LNCC, is denoted as $\tilde{s}_{\mathcal{L}}^{(q)}$.

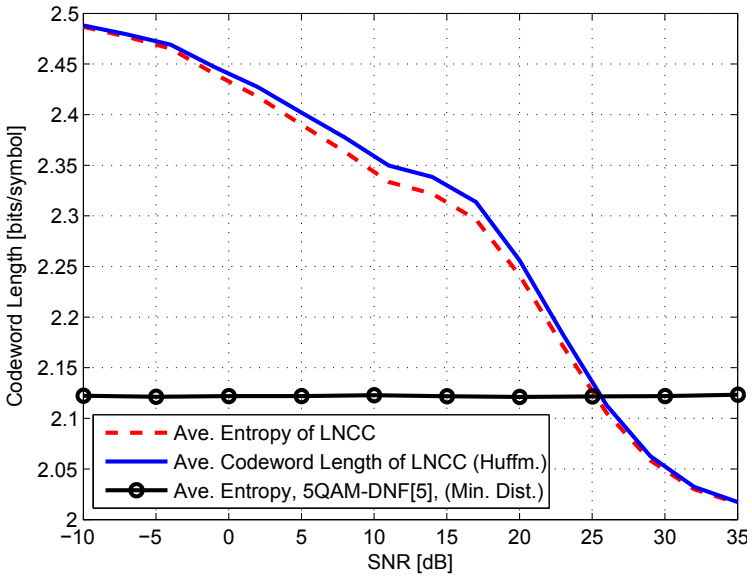

Figure 5.3: Entropy and Codeword Length of LNCC v.s. SNR.

The entropy of LNCC provides a bound on the compressed length for jointly designed

HFR-LPNC and SC. Based on the a priori probability in (5.19), we simulate the entropy and average length of compressed LNCC, as shown in Fig. 5.3, which shows that the average length of compressed LNCC is very close to the entropy of LNCC and they both strongly depend on the SNR: they vary inversely with the SNR. This can also be confirmed by the distribution of LNCC $s_{\mathcal{L}}^{(q)}$, as illustrated in Fig. 5.4. From Fig. 5.4, we can observe that when SNR is high, LNCC $s_{\mathcal{L}}^{(q)}$ is more uniformly distributed over $\mathcal{S}(4)$.

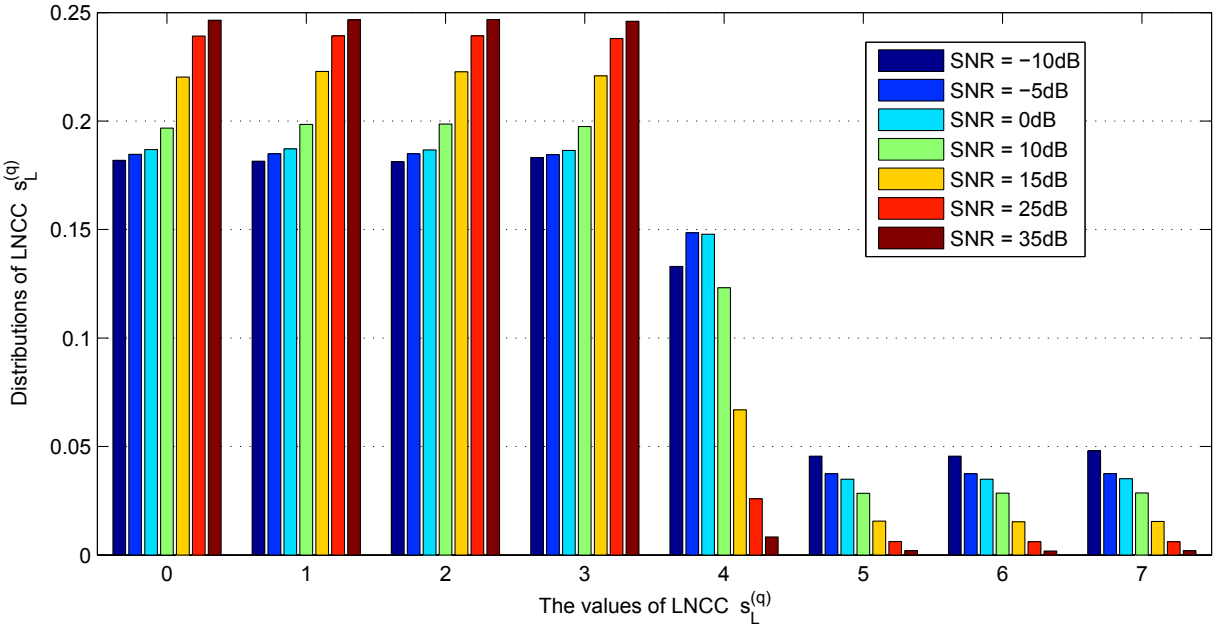

Figure 5.4: Distributions of LNCC with different SNRs.

We note that for rings other than $\mathcal{S}(4)$ and $\mathcal{S}(8)$ the distribution of $s_{\mathcal{L}}^{(q)}$ over the elements is not uniform, and that this non-uniformity increases with SNR, thus reducing entropy. We note also that the minimum cardinality constraint in **Algorithm 2** causes $\mathcal{S}(4)$ to be selected more often at higher SNR, and hence entropy tends to 2 bits/symbol as SNR increases. On the other hand at low SNR the larger rings $\mathcal{S}(5)$ and $\mathcal{S}(8)$ result in less 'quantization error', which offers a superior denoise performance and hence higher mutual information, and hence they are more frequently selected and entropy is increased.

For comparison, the entropy per network coded symbol of 5QAM-DNF [8] is also shown in Fig. 5.3, in which the selection criterion of the mapping is the minimum-distance algorithm. For this algorithm, the mapping depends only on the channel, and is not affected by the SNR, and hence the average entropy is constant with SNR. In contrast, our HFR-LPNC scheme using the mutual information criterion is able to adapt the sum-rate in MAC phase according to the SNR.

The relay *R* maps the compressed LNCC onto the modulated symbol, given as $x_R = \mathcal{M}_R(\tilde{s}_{\mathcal{L}}^{(q)})$, where $\mathcal{M}_R(\cdot)$ is the relay constellation mapper using QPSK modulation. The relay then broadcasts x_R to *A* and *B*. The received signal at each user is given by

$$y_i = h_i x_R + n_i, \tag{5.20}$$

where n_i is the complex AWGN at user i, $i \in \{A, B\}$.

Each user decompresses the received unified 4-ary LNCC to recover the original LNCC $s_{\mathcal{L}}^{(q)}$ over the hybrid finite ring $\mathcal{S}_{\mathrm{H}}(4, 5, 8)$. Thanks to the unambiguous decodability in (5.6), user *A* decodes its desired signal s_B by exploiting $s_{\mathcal{L}}^{(q)}$ and its C-SI s_A according to

$$\hat{s}_B = \underset{s_B \in \mathcal{S}(4)}{\arg\min}\, d_H\left(\mathcal{L}(s_A, s_B), s_{\mathcal{L}}^{(q)}\right), \tag{5.21}$$

where $d_H(X, Y)$ denotes the Hamming distance between the quantities X and Y and $\hat{s}_B$ represents the decoded version of s_B . User *B* applies the same decoding pattern to recover its desired signal s_A.

5.3.10 HFR-LPNC with diversity reception

In this subsection, we investigate diversity reception for HFR-LPNC, where the relay can observe multiple replicas of the transmitted signals. Regarding frequency-selective multipath fading scenarios, we consider the same scenario as in [8] where a perfect equalizer is assumed. In such circumstance, the proposed HFR-LPNC should have the capability of diversity reception. Given that the relay uses D-branch diversity, the received signal is expressed as

$$\mathbf{y}_R = \mathbf{h}_A x_A + \mathbf{h}_B x_B + \mathbf{n}_R, \tag{5.22}$$

where $\mathbf{y}_R = \begin{bmatrix} y_{R,1} & \cdots & y_{R,D} \end{bmatrix}^T$, $\mathbf{h}_i = \begin{bmatrix} h_{i,1} & \cdots & h_{i,D} \end{bmatrix}^T$ and $\mathbf{n}_R = \begin{bmatrix} n_{R,1} & \cdots & n_{R,D} \end{bmatrix}^T$. Then the maximum likelihood (ML) detector where the linear mapping is integrated, is given by

$$\hat{s}_{\mathcal{L}}^{(q)} = \underset{s_{\mathcal{L}}^{(q)}}{\arg\max}\, p(y_R | s_{\mathcal{L}}^{(q)}) = \underset{s_{\mathcal{L}}^{(q)}}{\arg\max} \sum_{x_A, x_B : S_{\mathcal{L}}^{(q)} = \mathcal{L}_q(s_A, s_B)} \frac{1}{2\pi\sigma_w^2} \exp\left(-\frac{\|\mathbf{y}_R - \mathbf{h}_A x_A + \mathbf{h}_B x_B\|^2}{2\sigma_w^2}\right). \tag{5.23}$$

Based on (5.23), the metric of the mapping selection of the proposed HFR-LPNC in (5.18), is rewritten as

$$\Delta\left(\alpha_q, \beta_q\right) = \frac{4}{H\left(S_{\mathcal{L}}^{(q)}\right)} I\left(\mathbf{Y}_R; S_{\mathcal{L}}^{(q)}\right), \tag{5.24}$$

where the mutual information $I\left(\mathbf{Y}_R; S_{\mathcal{L}}^{(q)}\right)$ is calculated as

$$I\left(\mathbf{Y}_R; S_{\mathcal{L}}^{(q)}\right) = -\mathbb{E}\left[\log_2\left(p(\mathbf{Y}_R)\right)\right] + \mathbb{E}\left[\log_2\left(p\left(\mathbf{Y}_R | S_{\mathcal{L}}^{(q)}\right)\right)\right]. \tag{5.25}$$

5.3.11 HFR-LPNC with 16QAM

In this subsection, we investigate HFR-LPNC using 16QAM. We adopt the **Algorithm 1** to check the finite ring with size $q = 16$ to 32, where those finite rings which can provide a superior sum-rate compared with the 29QAM-DNF in [8] are picked out. Based on this and the algebraic preliminaries in Section II, we list valid domain as $\mathcal{Z}_q'$ of α_q and β_q of selected finite rings, given by

$$\alpha_q, \beta_q \in \mathcal{Z}_q' = \begin{cases} \{\text{odd integers in } \mathcal{S}(16)\}, \text{if } q = 16 \\ \mathcal{S}(17)/\{0\}, \text{if } q = 17 \\ \{\text{odd integers in } \mathcal{S}(18)\}/\{3,9\}, \text{if } q = 18 \\ \mathcal{S}(19)/\{0\}, \text{if } q = 19 \\ \{\text{odd integers in } \mathcal{S}(20)\}/\{5\}, \text{if } q = 20 \\ \mathcal{S}(21)/\{0,3,7\}, \text{if } q = 21 \\ \{\text{odd integers in } \mathcal{S}(22)\}/\{11\}, \text{if } q = 22 \\ \mathcal{S}(23)/\{0\}, \text{if } q = 23 \\ \{\text{odd integers in } \mathcal{S}(24)\}/\{3\}, \text{if } q = 24 \\ \mathcal{S}(25)/\{0,5\}, \text{if } q = 25 \\ \{\text{odd integers in } \mathcal{S}(26)\}/\{13\}, \text{if } q = 26 \\ \mathcal{S}(27)/\{0,3,9\}, \text{if } q = 27 \\ \{\text{odd integers in } \mathcal{S}(28)\}/\{7\}, \text{if } q = 28 \\ \mathcal{S}(29)/\{0\}, \text{if } q = 29 \\ \{\text{odd integers in } \mathcal{S}(30)\}/\{0,3,5,15\}, \text{if } q = 30 \end{cases}, \tag{5.26}$$

where we note that the proposed HFR-LPNC with 16QAM would need to search over $\sum_{q=16}^{30} |\mathcal{Z}'_q| = 230$ codes while the 29QAM-DNF needs to search over 400 codes.

5.4 Benchmarks

In this section, we introduce several schemes in existing literature to use as the benchmarks.

5.4.1 Benchmark 1: Rate based 5QAM-DNF

Algorithm 3 Rate based 5QAM-DNF Mapping Selection

1: Obtain possible best codes by using the design method based on the Closest-neighbour clustering [8]: $\mathcal{C}_0, ..., \mathcal{C}_9$, where $\mathcal{C}_q$ ($q \in \mathcal{Z}_{10}$) is the mapping function of 5QAM-DNF, which is shown in the Table I of [8])
2: Given h_{re}
3: **for all** $\mathcal{C}_q$ where $q \in \mathcal{Z}_{10}$ **do**
4: Make the rate set empty: $D_I = \varphi$;
5: **for all** $\mathcal{C}_q(s_A, s_B) \neq \mathcal{C}_q(s'_A, s'_B)$, where $(s_A, s_B) \times (s'_A, s'_B) \in \mathcal{Z}_4 \times \mathcal{Z}_4$ **do**
6: Compute the $I(y_R; s_{\mathcal{C}_q})$.
7: Include it in the rate set: $D_I \leftarrow D_I \cup \{I(y_R; s_{\mathcal{C}_q})\}$.
8: **end for**
9: **end for**;
10: Let $I(Y_R; S_{\mathcal{C}_q})_{\max}$ be the maximum value among all the rates.
11: Select $\mathcal{C}_q$ whose rate corresponds to $I(Y_R; S_{\mathcal{C}_q})_{\max}$.
12: Select one of such codes with the minimum cardinality.

The selection criterion for the original 5QAM-DNF in [8], namely, the minimum-distance algorithm, is intended to maximize the minimum Euclidean distance (MED). The pros and cons of HFR-LPNC and 5QAM-DNF can be summarized as: 1) the proposed HFR-LPNC requires selection of coefficients for the linear equation (3), based on the ring while 5QAM-DNF requires an exhaustive search over a wider range of possible mappings; 2) the mapping selection method of HFR-LPNC is based on sum-rate maxi-

mization while that of 5QAM-DNF is based on distance profile; and 3) the joint design of HFR-LPNC and source coding can avoid the irregular mapping, e.g., 5QAM.

However, we note that the MED based mapping selection approach for 5QAM-DNF cannot guarantee the maximum sum-rate in the MAC phase. To this end, we improve the selection criterion of 5QAM-DNF. **Algorithm 3** is the improved selection algorithm. Using this improved selection criterion, we obtain a rate based 5QAM-DNF, which is used as a benchmark.

5.4.2 Benchmark 2: DSTC based PNC

The novel DSTC-PNC proposed by Muralidharan and Rajan in [28] is also considered as a benchmark. Clearly, the DSTC-PNC scheme has several advantages: 1) the relay only employs the bit-wise XOR mapping which does not need to adapt to the channels; 2) both users do not necessarily know the CSI; and 3) DSTC based PNC exploits the distance profile to avoid the singular fade states.

To measure the rate of the network codded symbol, we rewrite the ML decoding for DSTC-PNC [28] as

$$\widehat{\mathbf{s}}_R = \arg\max_{\mathbf{s}_R} \sum_{\substack{\mathbf{x}_A, \mathbf{x}_B : \\ s_{R_1} = s_{A_1} \oplus s_{B_1} \\ s_{R_2} = s_{A_2} \oplus s_{B2}}} \exp\left[-\frac{1}{2\sigma^2} \left\| \mathbf{y}_R - \mathbf{h}_{AB} \begin{bmatrix} \mathbf{M}_A \mathbf{x}_A \\ \mathbf{M}_B \mathbf{x}_B \end{bmatrix} \right\|^2 \right], \quad (5.27)$$

where $\widehat{\mathbf{s}}_R$ is the decoded network coded symbol and $H(\mathbf{S}_R) = 4$ bits/symbol; the matrices $\mathbf{M}_A$ and $\mathbf{M}_B$ are the coding matrices of DSTC-PNC. We note that the DSTC-PNC based on constructions 1 and 2 in [11] achieve the almost equal performance in Rayleigh fading 2-WRC. Therefore we only choose construction 2 for simplicity.

5.4.3 Benchmark 3: Precoding based PNC

In [31], Wang, Ding, Dai and Vasilakos proposed a precoding based PNC for the generalized MIMO Y channels. We also use this precoding based PNC as a benchmark. Similar to DSTC-PNC, the precoding based PNC resolves the singular fade states when two users transmit their signals. Hence, the relay only needs to employ the simple XOR mapping. However, such precoding based PNC scheme requires CSIT.

5.5 Sum-rate Analysis and Evaluation

In this section, we analyze and evaluate the sum-rate of the proposed HFR-LPNC in 2-WRC.

5.5.1 Sum-rate Analysis for HFR-LPNC

Based on **Theorem 2** and the returned linear coefficients for maximizing the sum-rate in (5.18), the rate region of HFR-LPNC in the MAC phase is given by

$$\begin{aligned} R_A^{(1)} &\leq \tfrac{1}{2} I\left(Y_R; \hat{S}_A | S_B\right) \\ R_B^{(1)} &\leq \tfrac{1}{2} I\left(Y_R; \hat{S}_B | S_A\right) \\ R_{AB}^{(1)} &\leq \tfrac{1}{2} \cdot \tfrac{4}{H\left(S_{\mathcal{L}}^{(q)}\right)} I^{(\tilde{\alpha}_q, \tilde{\beta}_q)}\left(Y_R; S_{\mathcal{L}}^{(q)}\right). \end{aligned} \tag{5.28}$$

Due to the nature of network coding, the individual achievable rates of users *A* and *B* in the BC phase are in fact bounded by the point-to-point channel capacities, given by

$$\begin{aligned} R_A^{(2)} &\leq \tfrac{1}{2} I(Y_A; X_R), \\ R_B^{(2)} &\leq \tfrac{1}{2} I(Y_B; X_R), \end{aligned} \tag{5.29}$$

where $I(y_i; x_R)$ is the mutual information between received signal at user i and the transmitted signal from *R*. The quantity $R_i^{(2)}$ denotes the individual achievable rate of user i in the BC phase.

The sum-rate in the BC phase, denoted by $R_{AB}^{(2)}$, is then given by

$$R_{AB}^{(2)} \leq \frac{1}{2}\left[I(Y_A; X_R) + I(Y_B; X_R)\right]. \tag{5.30}$$

Based on the results of (5.28)-(5.30), the rate region (in terms of end-to-end transmission) of HFR-LPNC in 2-WRC yields

$$\begin{aligned} R_A &\leq \tfrac{1}{2}\min\left[I\left(Y_R; \hat{S}_A|S_B\right), I(Y_A; X_R)\right] \\ R_B &\leq \tfrac{1}{2}\min\left[I\left(Y_R; \hat{S}_B|S_A\right), I(Y_B; X_R)\right] \\ R_{AB} &\leq \tfrac{1}{2}\min\left\{\tfrac{4}{H\left(S_{\mathcal{L}}^{(q)}\right)} I^{(\tilde{\alpha}_q, \tilde{\beta}_q)}\left(Y_R; S_{\mathcal{L}}^{(q)}\right), \left[I(Y_A; X_R) + I(Y_B; X_R)\right]\right\}, \end{aligned} \tag{5.31}$$

where the mutual information is determined using Monte-Carlo integration. The quantity R_i represents the end-to-end achievable rate of user i and R_{AB} is the overall sum-rate.

5.5.2 Sum-rate Comparison

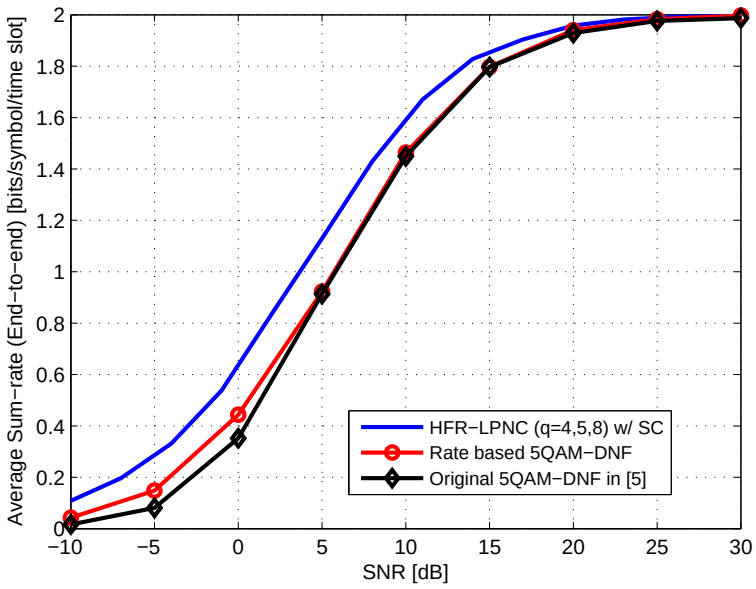

Figure 5.5: End-to-end average sum-rate against SNR in Rayleigh fading channels. (QPSK used at the MAC phase)

In this subsection, we evaluate and compare the average sum-rates (in terms of end-to-end transmission) for the jointly designed HFR-LPNC and SC, the original and improved

5QAM-DNF schemes in 2-WRC. We assume that all channel links in the 2-WRC experience quasi-static i.i.d. frequency-flat Rayleigh fading, i.e., each channel coefficient is modelled as a zero-mean complex Gaussian random variable with unit variance. Fig. 5.5 shows the average sum-rates against SNR for all schemes on the Rayleigh fading 2-WRC. Based on Fig. 5.5, we have the following observations: 1) the joint HFR-LPNC/SC scheme outperforms the others; and 2) the improved 5QAM-DNF is superior to the original design in the low SNR regime. The sum-rate of the joint design of HFR-LPNC and SC is higher than that of the original 5QAM-DNF by about 0.3 bits/symbol at best (where SNR$\approx$0dB). We can see that HFR-LPNC achieves a performance equal to the DSTC-PNC over a wide range of SNRs. However, it is difficult to say which of HFR-LPNC and DSTC-PNC is to be preferred. This is because: 1) HFR-LPNC needs to adapt to the channels while DSTC-PNC does not; 2) DSTC-PNC would require four phases to form a whole data exchange; 3) DSTC-PNC requires the channel coefficients in the first two MAC phases to remain static (although it can split a MAC phase into two sub-MAC phases this requires precise network synchronization); and 4) it is not known whether or not DSTC-PNC is delay-robust. The precoding based PNC definitely provides the best performance as it completely eliminates the singular fading at each user. However, it requires CSIT. We know that when the compression is not employed, the relay might choose QPSK, 5QAM or 8PSK to transmit the LNCC in the BC phase, depending on the selected linear mapping. We can observe that the HFR-LPNC without compression is slightly degraded compared with that with the compression. This implies that the BC might be a bottleneck in the low SNR regime. However, in the moderate-to-high SNR regime, the degradation of the HFR-LPNC without the compression reduces. This is because in the moderate-to-high SNR regime, the ring $\mathcal{S}(4)$ is more frequently selected such that even though the compression is not employed, the performance degradation is not too great.

Fig. 5.6 depicts the end-to-end average sum-rate against SNR in flat-fading Rayleigh fading channels where 16QAM is used in the MAC phase. The simulation results show that when the 16QAM is adopted by both users, the proposed HFR-LPNC still outperforms both rate based 5QAM-DNF and the original 5QAM-DNF. Clearly, the proposed design has the capability to accommodate in a higher-order modulation system.

Fig. 5.7 shows the end-to-end average sum-rate against SNR in frequency-selective 3-path Rayleigh fading channels with different exponential decaying (ED) profiles. As

in [8], we assume that all the nodes employ the optimum equalizer to deal with the delayed waves. The simulation results show that the proposed HFR-LPNC still outperforms 5QAM-DNF in frequency-selective fading scenario, which confirms that our proposed HFR-LPNC has the capability of diversity reception.

Fig. 5.8 shows the end-to-end average sum-rate against SNR in Rayleigh fading channels with the estimation error of noise variance (EENV), denoted by $\Delta\sigma^2$. We observe that if the EENV is not too large ($\Delta\sigma^2 < 0.015$), the performance degradation due to the EENV is negligible. We also observe that in the low-to-moderate SNR regime, the proposed HFR-LPNC still outperforms 5QAM-DNF which is based on the MED selection criterion, even for larger EENV. Note that because the mapping selection criterion depends on noise variance, it is sensitive to EENV. However we have shown that the performance degradation in HFR-LPNC due to this is negligible for EENV < 0.015, and the scheme still outperforms 5QAM-DNF for low to medium SNR, even with larger EENV.

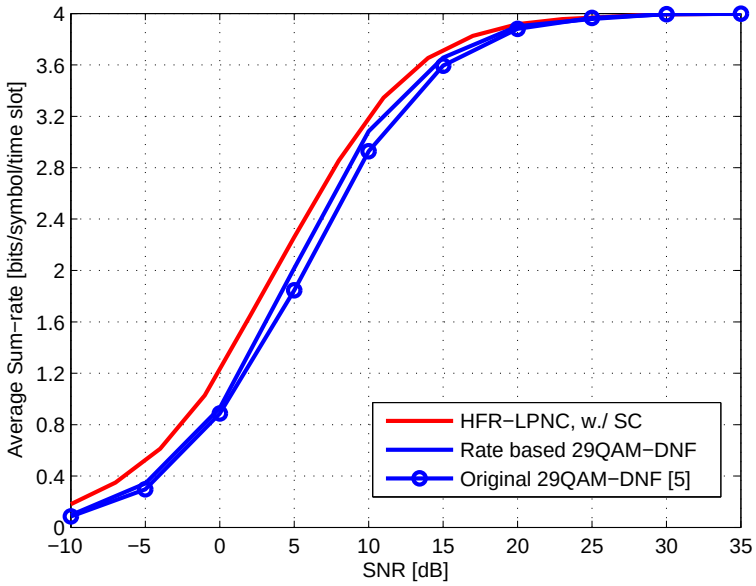

Figure 5.6: End-to-end average sum-rate against SNR in Rayleigh fading channels. (16QAM used at the MAC phase)

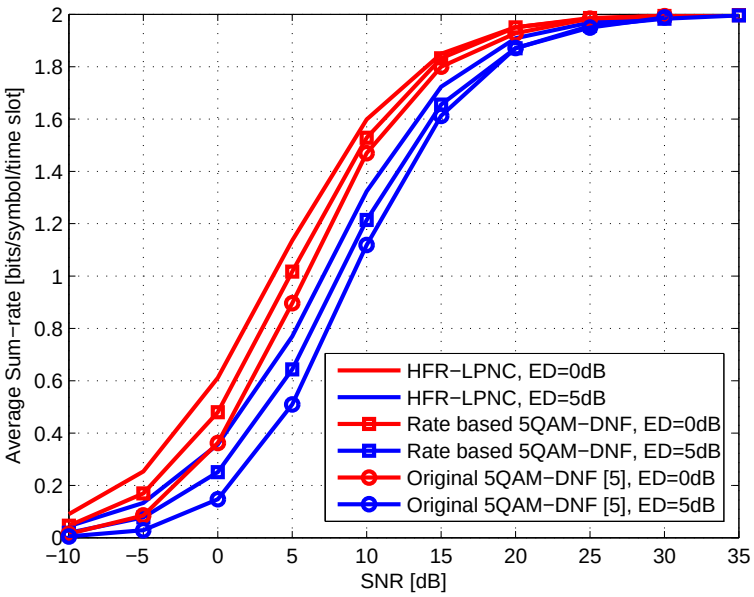

Figure 5.7: End-to-end average sum-rate against SNR in frequency-selective 3-path Rayleigh fading channels with exponential decaying profile. (QPSK used at the MAC phase)

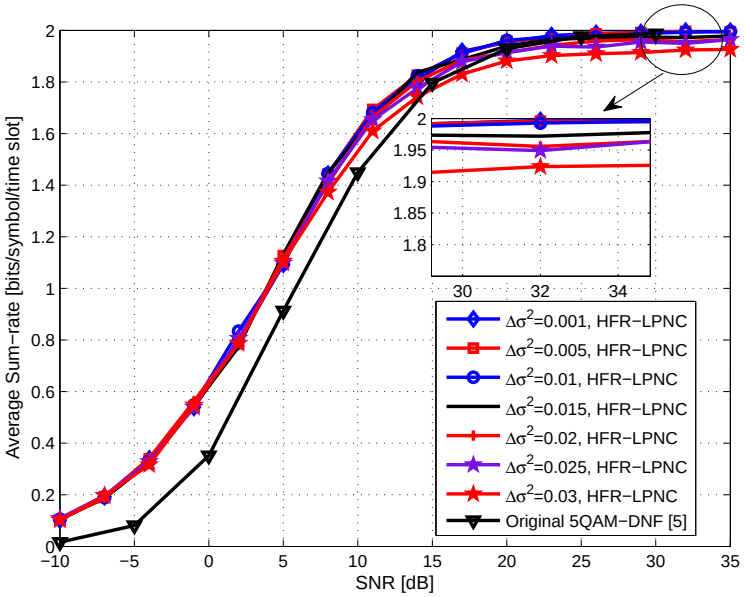

Figure 5.8: End-to-end average sum-rate against SNR in Rayleigh fading channels with the estimation error of noise variance. (QPSK used at the MAC phase)

5.6 Summary

We have proposed a novel HFR-LPNC for Rayleigh fading two-way relay channels. The relay node generates linear network coded combinations over a hybrid finite ring by properly selecting the linear coefficients. The selection criterion ensures unambiguous decoding and maximizes the sum-rate in the MAC phase. To prevent the performance degradation caused by high-order mapping employed in the BC phase, jointly designed HFR-LPNC and source coding is used to compress the LNCC alphabet over the hybrid finite ring into a unified 4-ary alphabet. We have derived constellation constrained sum-rates for HFR-LPNC and 5QAM denoise-and-forward (5QAM-DNF) [8] and further explicitly characterized the rate difference between HFR-LPNC and 5QAM-DNF. Our analysis and simulation show that our HFR-LPNC is superior to 5QAM-DNF scheme over a wide range of SNRs.

Chapter 6

PNC in Multiuser Hierarchical Wireless Network

Contents

6.1 Overview

The hierarchical wireless network (HWN) is a network architecture which includes cell extension relaying and in-band backhauling and can be treated as a set of multiuser 2-WRC. Bi-directional relaying protocols may thus be used, i.e., PNC and ANC, performed at RNs. However, the multiple relay nodes (RN) give rise to co-channel interference (CCI) which severely degrades the network performance. In this Chapter, two efficient interference exploitation strategies based on network coding are proposed to address the above

challenge: 1) PNC with joint decoding (PNC-JD); and 2) ANC with interference-aware maximum likelihood detection (ANC-IAML). The proposed strategies transform the naturally occurring CCIs into the useful signal instead of suppressing them, and exploit the network topology to provide extra diversity. A straightforward design, the TDMA-PNC, is also introduced as a benchmark for comparison. We further derive and compare the constellation constrained sum-rate for each scheme, which clearly demonstrates the substantial performance enhancement provided by the proposed strategies over the TDMA-PNC in HWN.

6.2 Introduction

The bi-directional relaying protocols in the 2-WRC have attracted considerable attention in recent years. Two state-of-the-art bi-directional relaying protocols, PNC [1] and ANC [6], both exhibit a significant spectral efficiency improvement compared to the traditional network coding using three time slots, as they require only two transmission time slots. In PNC, the relay node (RN) performs network coding functions on the Galois field by extracting the network coded symbols (NCS) directly from the superimposed electromagnetic signals and then broadcasts the NCS to the two users. Based on the exclusive law [3], any user in the 2-WRC can recover the other user's signal by exploiting the received NCS and side information (SI). ANC on the other hand allows the RN to linearly amplify the superimposed electromagnetic signals, and then forwards the resulting signal to the two users. By subtracting the SI (self-interference cancellation), the two users can obtain their desired signals.

Based on the concepts of PNC and ANC, several significant developments have been proposed recently. The constellation constrained capacity regions for PNC in 2-WRC were established in [7]. A denoise-and-forward scheme with irregular mapping for PNC to combat fading in 2-WRC was proposed in [8]. The pseudo-XOR (PXOR) algorithm for LDPC coded PNC in faded 2-WRC was introduced in [15]. A novel eigen-direction alignment enhanced PNC for MIMO was introduced in [34]. The authors of [33] investigated the error probability bound at the relay which uses a punctured codebook for explicitly computing the distance spectrum of the PNC. The authors in [43] proposed non-

coherent detection at the relay for PNC in 2-WRC. The authors in [44] provided a new non-coherent detector for ANC in 2-WRC. The authors of [45] investigated the outage probability and optimal power allocation for ANC in 2-WRC. However, it is worth noting that these developments are constrained by the original PNC/ANC design, i.e., their proposed strategies only support the two users in the 2-WRC, and both users need to employ the same modulation scheme. In [25, 26], an algebraic approach to network coding, namely compute-and-forward (CPF), extends PNC beyond the 2-WRC to general Gaussian multiple access channels (GMAC). The authors in [46] provided the outage probability of CPF in generalized multi-way relay channels. However, we note that CPF [25, 26] is based on lattices of very large dimension, and has yet to be demonstrated in practice. Some practical code designs for CPF were proposed in [58]. However, these designs require multi-dimensional constellations and hence cannot be directly adopted by current communication systems which commonly use low dimensional constellations. Motivated by these, we focus on designing more realistic network coding (PNC and ANC) protocols, which can make use of regular modulation schemes, such as PSK or QAM, and can support multiple users in a more complex network model compared to 2-WRC.

As a promising layered network architecture, the HWN [47–49] encompasses both cell extension using relays and wireless in-band backhauling in which a single hub base station (HBS) is deployed to communicate with multiple relay nodes (RN), which in turn are responsible for information exchange between the HBS and mobile stations (MS). This can be considered as an important element of cooperative multipoint (CoMP). The HWN can be treated as a set of 2-WRCs. As all network nodes cooperate, the whole network supports numerous MSs by deploying only a small number of HBSs at the vertex of the HWN. Without requiring multiple antennas per network node, the HWN provides a cost-effective approach to improve the connectivity, transmission reliability and quality-of-service (QoS). The spectral efficiency of the HWN can be enhanced by the bi-directional relaying protocol, i.e., PNC or ANC. However, we note that the high density deployment of RNs in HWN gives rise to aggressive frequency reuse resulting in large co-channel interference (CCI) between neighbouring RNs. From the receivers' perspective, CCIs are conventionally treated as noise, which impairs the decodability of the desired signal and hence degrades the network performance. A straightforward design to completely avoid CCI is to allocate different orthogonal frequency bands/time slots for each data exchange. However, this leads to poor spectral efficiency. Therefore, a fundamental question in

such a system design is how to mitigate CCI in the HWN while improving its spectral efficiency.

Motivated by the above challenge, we propose two interference exploitation strategies: 1) PNC-JD and 2) ANC-IAML. In PNC-JD, each RN decodes the joint network coded symbol (J-NCS) for the useful symbol pair and the interfering symbol pair. To mitigate the error-propagation, we propose a novel rate based relay selection (RS) scheme. The proposed RS allows only the RN with the higher instantaneous rate related to the J-NCS to transmit in the next time slot. The HBS and MSs can recover their desired signals by exploiting the received J-NCS and their SI. In ANC-IAML, all RNs amplify the linear sum of the signals transmitted from the HBS and MSs and forward it to the HBS and MSs. The different copies of the amplified sum signal are naturally combined at the HBS and MSs, which offers extra transmit diversity. After cancelling out the self-interference, the HBS/MS performs interference aware ML detection to extract its desired signal. For comparison purposes, we also consider a benchmark scheme: the time-division multiple access based PNC (TDMA-PNC) which uses orthogonal time slots to avoid frequency reuse among different data exchanges. There are four main contributions in this Chapter, summarized as follows:

1) We propose two new network coding strategies, PNC-JD and ANC-IAML, which can fully utilize the CCI and the network infrastructure by naturally transforming the CCI into useful signals. Moreover, both PNC-JD and ANC-IAML can provide transmit diversity.

2) We extend the PNC and ANC protocols beyond the traditional 2-WRC to a more complex multiuser network, namely, the HWN, which also is a model for CoMP networks. Such a network structure may be used to allow data exchange among several groups of users.

3) We propose novel decoding strategies which allow the PNC and ANC protocols to support multiple users without involving any *irregular constellations*. Moreover, the proposed designs allow the HBS and MSs to employ different modulation schemes.

4) We derive the constellation-constrained sum-rates for the proposed PNC-JD and ANC-IAML, which provide a more realistic performance metric compared with the con-

stellation unconstrained sum-rates for HWN.

We compare our proposed protocols with the TDMA-PNC. The analytical and simulated results clearly demonstrate that our proposed PNC-JD and ANC-IAML strategies can substantially enhance the sum-rate compared with the TDMA-PNC. Moreover, the inherent denoise characteristic [4] of PNC makes the sum-rate of PNC-JD superior to that of ANC-IAML.

6.3 System Model and General Assumptions

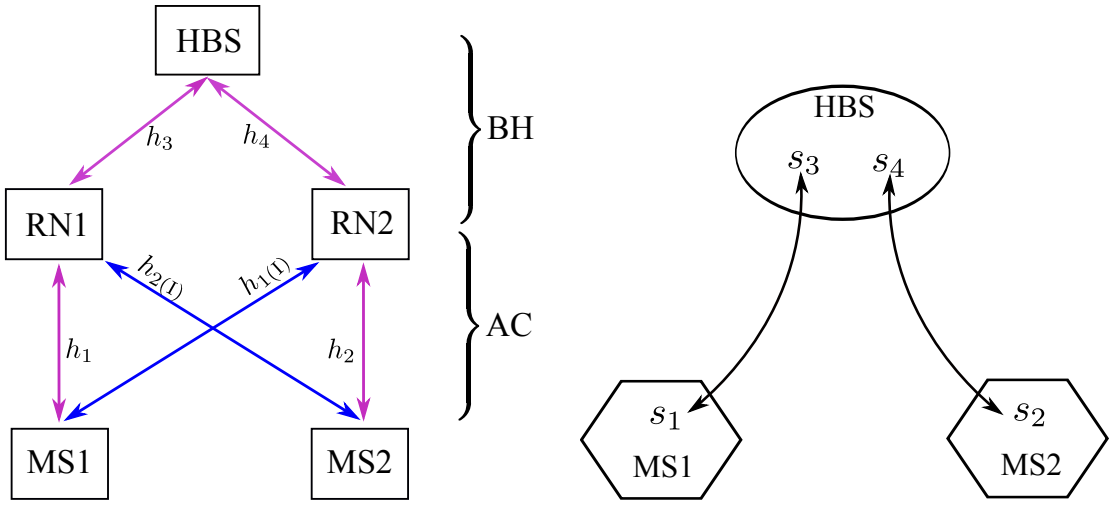

Figure 6.1: (a) System Model of HWN; (b) Expected data exchange between the HBS and MSs.

Fig. 6.1(a) depicts a simplified system model of the HWN consisting of two MSs, one HBS and two RNs. We assume that each node is equiped with an omni-directional half-duplex antenna. The links between the HBS and the RNs are defined as the backhaul network (BH), while the links between the RNs and the MSs are defined as the access network (AC). It is expected that the binary data streams s_1/s_2 from MS1/MS2 are correspondingly exchanged with s_3/s_4 from the HBS with the help of RN1/RN2, as shown in Fig. 6.1(b). We note that the two node groups ($\{$MS1, RN1, HBS$\}$ and $\{$MS2, RN2, HBS$\}$) should work independently without interfering with each other. However, in practice, the multiple access signals from MS1 and HBS to RN1 causes interference to RN2

while the broadcast from RN1 to MS1 and HBS causes interference to MS2 and *vice versa* (see the blue lines in Fig. 6.1(a)).

The structure of the HWN is equivalent to a set of 2-WRCs in the presence of interference. Similar to the traditional 2-WRC, we assume the transmission channels in HWN are *reciprocal.* As such, we denote the channel coefficients between MS1 and RN1 as h_1, MS2 and RN2 as h_2, HBS and RN1 as h_3, HBS and RN2 as h_4, RN1 and MS2 as $h_{1(\mathrm{I})}$ and MS2 and RN1 as $h_{2(\mathrm{I})}$, respectively. We assume that all channel links experience quasi-static, independent and identically distributed (i.i.d.) frequency-flat fading. We also assume that the received signals at each node are corrupted by circularly symmetric Additive Gaussian White Noise (AWGN) with variance N_0. The cardinality of the modulation alphabet for a symbol x is denoted as M_x. The rate of a symbol x in the m-th time slot is denoted as $R_x^{(m)}$.

We assume that the RNs can transmit the signalling to the HBS but cannot communicate with each other. The HBS deals with all the signalling from the RNs and decides whether the RNs can transmit or not.

6.4 The Benchmark: TDMA based PNC (TDMA-PNC)

6.4.1 System Description

The TDMA-PNC is a *straightforward* design and is easy to implement in the HWN. The TDMA-PNC scheme, depicted in Fig. 6.2, uses four orthogonal time slots and ensures that the two nodes groups ($\{$MS1, RN1, HBS$\}$ and $\{$MS2, RN2, HBS$\}$) do not interfere with each other.

Without loss of generality, we assume the MSs and HBS employ the same BPSK modulation $\mathcal{M}_{\mathrm{B}}(\cdot)$, where $\mathcal{M}_{\mathrm{B}}(\cdot)$ is the BPSK mapper. As such, each modulated symbol with unit variance is given by

$$x_i = \mathcal{M}_{\mathrm{B}}(s_i), i \in \{1, 2, 3, 4\}. \tag{6.1}$$

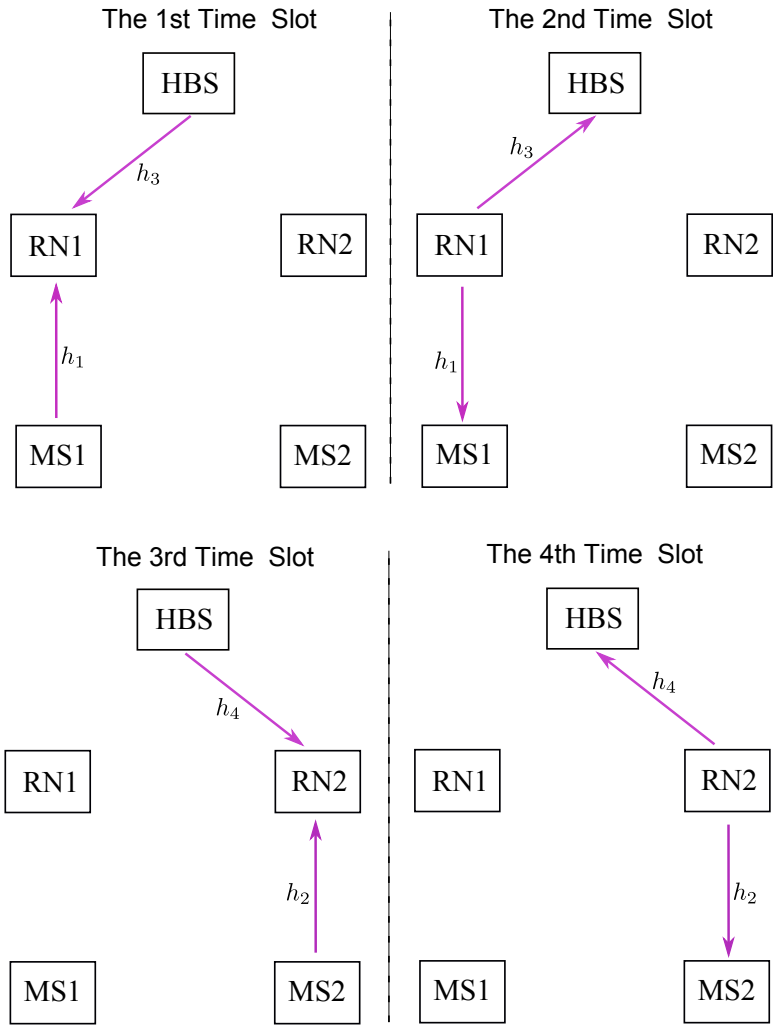

Figure 6.2: The straightforward design: TDMA based PNC strategy.

In the first time slot, MS1 and HBS simultaneously transmit symbols x_1 and x_3 to RN1. The received signal at RN1 can be expressed as

$$y_{\mathrm{RN1}} = h_3 x_3 + h_1 x_1 + n_{\mathrm{RN1}}, \tag{6.2}$$

where n_{RN1} is the AWGN at RN1. In the absence of CCIs, RN1 decodes the NCS $s_{\oplus,13} \triangleq s_1 \oplus s_3$ by performing PNC detection on y_{RN1}. For simplicity, we omit the simple traditional PNC detection here. Please refer to [7] for details.

In the second time slot, RN1 broadcasts the modulated NCS $x_{\oplus,13} = \mathcal{M}_{\mathrm{B}}(s_{\oplus,13})$ to MS1 and HBS.

Due to the symmetrical structure of the HWN, all operations at RN2 are the same as those at RN1. The PNC decoding performed at RN2 is used to obtain the NCS $s_{\oplus,24} \triangleq s_2 \oplus s_4$ in the third time slot. Then RN2 broadcasts the modulated NCS $x_{\oplus,24} = \mathcal{M}_{\mathrm{B}}(s_{\oplus,24})$ to MS2 and the HBS in the fourth time slot.

6.4.2 Sum-rate Analysis

In this subsection, we analyze the constellation constrained sum-rate, i.e., the sum-rate when the HBS and MSs employ finite size constellations with uniform distribution over their elements. The sum-rate with respect to all valid symbols can be calculated as

$$R_{\mathrm{Sum}} = \sum_{i=1}^{4} R_{x_i}, \tag{6.3}$$

where R_{x_i} is the achievable rate of the symbol x_i.

The author in [7] pointed out that the rate region in the uplink of 2-WRC for two transmitting nodes has a rectangular shape when PNC is decoded at the relay, i.e., both users' rates are bounded by the computation rate of NCS. Hence the rate region of TDMA-PNC in the first time slot yields

$$R_{x_1}^{(1)} = R_{x_3}^{(1)} \leq I(Y_{\mathrm{RN1}}; S_{\oplus,13}), \tag{6.4}$$

where $I(Y_{\mathrm{RN1}}; S_{\oplus,13})$ is the mutual information between the received signal y_{RN1} and the NCS $s_{\oplus,13}$, which indicates the computation rate of $s_{\oplus,13}$. To this end, we can measure the rate region of x_1 and x_3 by equivalently examining $I(Y_{\mathrm{RN1}}; S_{\oplus,13})$.

As in [7], Monte-Carlo integration is used to calculate the mutual information $I(Y_{\mathrm{RN1}}; S_{\oplus,13})$, using:

$$I(Y_{\mathrm{RN1}}; S_{\oplus,13}) = \log_2(M_{s_{\oplus,13}}) + \mathbb{E}\left[\log_2\left(\frac{p\left(Y\,|S_{\oplus,13}\right)}{\sum\limits_{S'_{\oplus,13}} p\left(Y\,|S'_{\oplus,13}\right)}\right)\right], \tag{6.5}$$

where $\mathbb{E}_{p(Y_{\mathrm{RN1}}|s_{\oplus,13})}(\cdot)$ is the the empirical mean of $p\left(Y_{\mathrm{RN1}}|S_{\oplus,13}\right)$ provided that we generate random variable Y_{RN1} with the distribution $p(y_{\mathrm{RN1}}|s_{\oplus,13})$. Here we set the cardinality of the NCS $M_{s_{\oplus,13}} = 4$ since there are four distinct superimposed signals for x_1 and x_3. The cardinalities of the users' alphabets are $M_{x_1} = M_{x_3} = 2$ as x_1 and x_3 are BPSK symbols.

Since RN1 broadcasts the modulated NCS $x_{\oplus,13}$ to HBS and MS1 in the third time slot, the achievable rates of x_1 and x_3 are bounded by the point-to-point channel capacities $I(Y_{\mathrm{HBS}}; X_{\oplus,13})$ and $I(Y_{\mathrm{MS1}}; X_{\oplus,13})$, respectively. Based on these, the equivalent end-to-end achievable rates of x_1 and x_3 can be calculated as

$$R_{x_1} \leq \frac{1}{4}\min\left[I(Y_{\mathrm{RN1}}; S_{\oplus,13}), I(Y_{\mathrm{HBS}}; X_{\oplus,13})\right] \tag{6.6}$$

and

$$R_{x_3} \leq \frac{1}{4}\min\left[I(Y_{\mathrm{RN1}}; S_{\oplus,13}), I(Y_{\mathrm{MS1}}; X_{\oplus,13})\right] \tag{6.7}$$

respectively. Here the factor $\frac{1}{4}$ is due to the use of four time slots.

Due to the symmetrical structure of the HWN, we calculate the end-to-end achievable rates R_{x_2} and R_{x_4} using an approach similar to R_{x_1} and R_{x_3}. Substituting the achievable rates of each symbol into (6.3), the constellation constrained sum-rate is thus calculated.

6.5 PNC with Joint Decoding

In the previous section, TDMA-PNC splits the data exchanges into two independent groups ($\{$MS1, RN1, HBS$\}$ and $\{$MS2, RN2, HBS$\}$) by using four orthogonal time slots which help the HWN to completely avoid CCI. However, the TDMA-PNC strategy (or generally speaking, the orthogonal multiple access scheme with PNC) consumes a large number of time-slots which implies a poor spectral efficiency. We note that the PNC

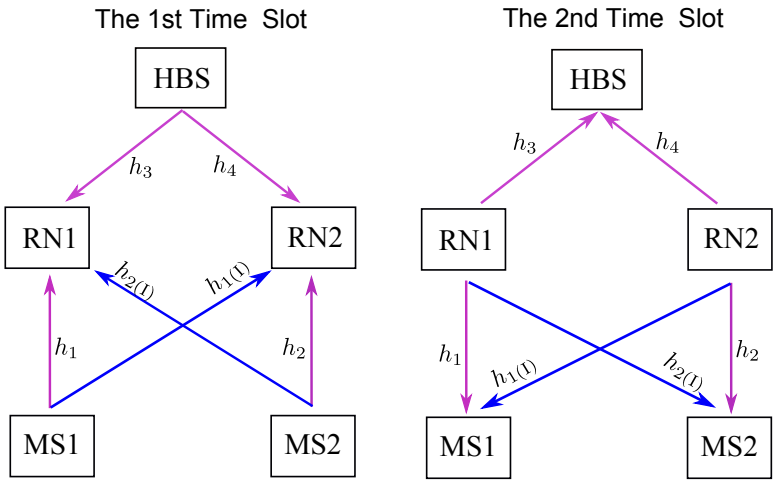

Figure 6.3: Two time slots interference exploitation strategies (including PNC-JD in section V and ANC-IAML in section VI.)

strategy can improve the spectral efficiency for HWN. Nevertheless, traditional PNC only supports two users with the same modulation scheme in the traditional 2-WRC. Hence, the proposed strategy aims to: 1) jointly mitigate CCI and improve spectral efficiency; and 2) modify the traditional PNC to support multiple users with different modulation.

6.5.1 System Description

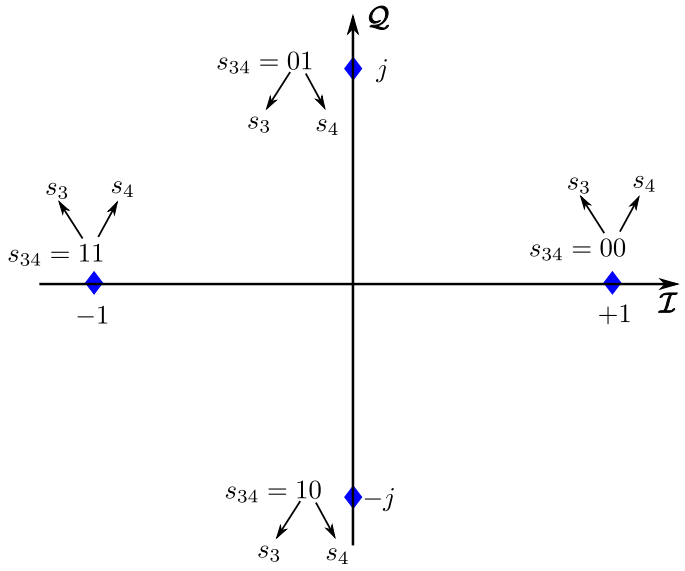

Figure 6.4: The constellation of Gray coded symbol x_{34}: the first bit of the 2-bit binary tuple s_{34} carries s_3 while the second bit of it carries s_4.

In the proposed design, MS1 and MS2 employ BPSK modulation for data stream s_1 and s_2, respectively, i.e, $x_1 = \mathcal{M}_{\rm B}(s_1)$ and $x_2 = \mathcal{M}_{\rm B}(s_2)$. The modulation scheme at the HBS is shown in Fig. 6.4. In order to exchange the data packets with MSs within two time slots, the HBS applies QPSK modulation to transmit s_3 and s_4 simultaneously, i.e., the first and second bits of the 2-bit binary tuple s_{34} carry the bit data streams of s_3 and s_4, respectively. Then s_{34} is modulated to a Gray coded QPSK symbol x_{34}, i.e., $x_{34} = \mathcal{M}_{\rm Q}(s_{34})$, where $\mathcal{M}_{\rm Q}(\cdot)$ is the QPSK mapper. In this way, the data streams of s_3 and s_4 are in fact combined together for transmission.

Processing at RNs

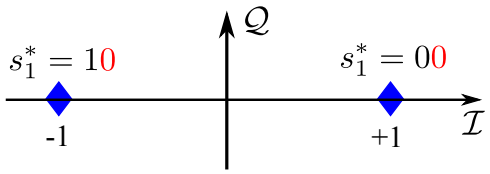

Figure 6.5: Virtually postfix a redundant 0 to s_1 (see the red 0 in the figure).

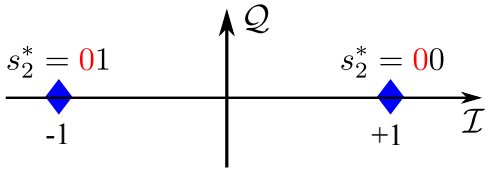

Figure 6.6: Virtually prefix a redundant 0 to s_2 (see the red 0 in the figure).

In the first time slot, the received signal at RN1 is given by

$$y_{\rm RN1} = h_3 x_{34} + h_1 x_1 + h_{2({\rm I})} x_2 + n_{\rm RN1}. \tag{6.8}$$

where we observe that there are two interference components for signals x_1 and x_3: one is the signal x_2 from MS2 and the other appears in the quadrature part of x_{34} (the second bit of s_{34}) from the HBS. Motivated by this, we aim to exploit these interference signals in detecting the useful signal. To this end, in the proposed design, PNC detection is performed to obtain the NCS of s_1 and s_3 jointly with the NCS of s_2 and s_4. We thus call the proposed design PNC with joint decoding.

The procedure of PNC-JD can be summarized as follows:

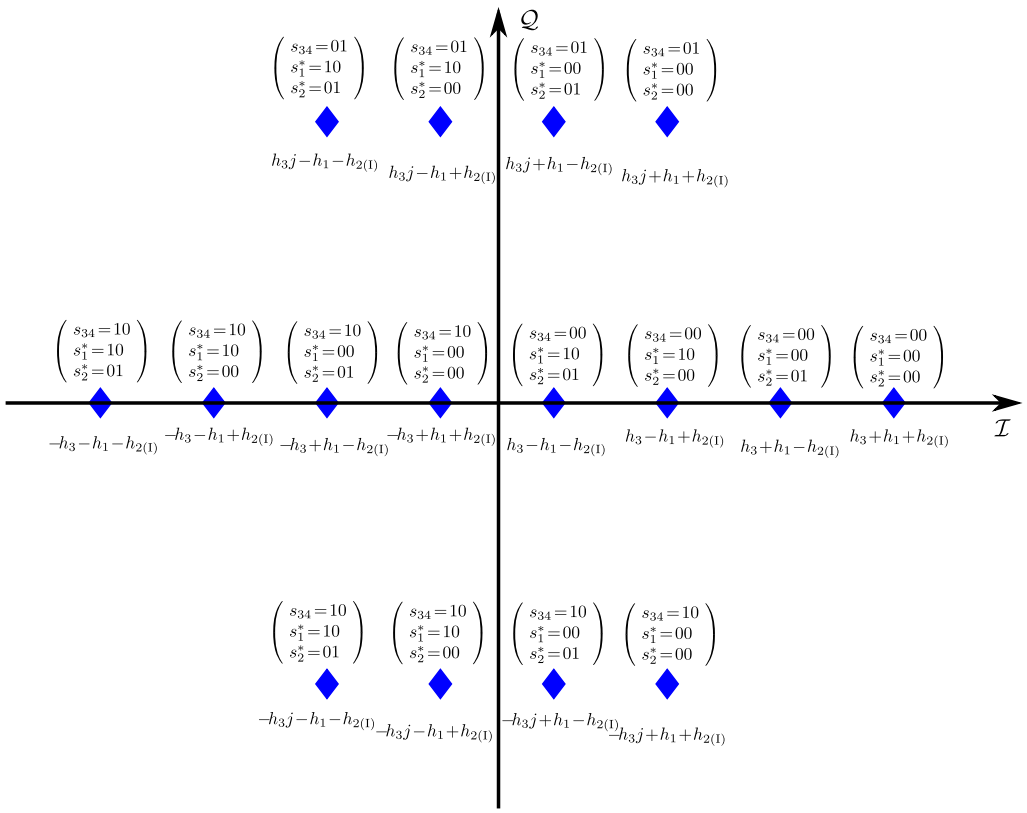

Figure 6.7: Fullly exploiting the superimposed constellation at RN1: performing PNC-JD. Note that this figure is intended to represent a generic constellation, not corresponding to any specific channel realization.

1. The RN virtually treats the BPSK symbol x_1 as a 2-bit binary tuple in which the first bit carries the real data stream s_1 and the second bit is a redundant postfix bit, set to 0, giving $s_1^* = (s_1, 0)$. The virtual mapping relationship between s_1^* and x_1 is denoted by $\mathcal{M}_{\mathrm{B,V}}^{(1)}(s_1^*) = x_1$, given as $\mathcal{M}_{\mathrm{B,V}}^{(1)}(10) = -1 \ \text{ and } \ \mathcal{M}_{\mathrm{B,V}}^{(1)}(00) = +1$, as shown in Fig. 6.5. On the other hand, the data word s_2 is virtually prefixed with a redundant bit 0, i.e., $s_2^* = (0, s_2)$, as shown in Fig. 6.6. The virtual mapping function between s_2^* and x_2 is denoted by $\mathcal{M}_{\mathrm{B,V}}^{(2)}(s_2^*) = x_2$, giving $\mathcal{M}_{\mathrm{B,V}}^{(2)}(01) = -1 \ \text{ and } \ \mathcal{M}_{\mathrm{B,V}}^{(2)}(00) = +1$.

2. The *joint network coded symbol* (J-NCS) of s_1^*, s_2^* and s_{34} is denoted as $s_{\oplus,\mathrm{JNC}}$, obtained by the eXclusive-OR (XOR) operation:

$$s_{\oplus,\mathrm{JNC}} \triangleq s_1^* \oplus s_2^* \oplus s_{34}, \tag{6.9}$$

   where it is clear that $s_{\oplus,13} = s_1 \oplus s_3$ is the first bit of $s_{\oplus,\mathrm{JNC}}$ and $s_{\oplus,24} = s_2 \oplus s_4$ is the second bit of $s_{\oplus,\mathrm{JNC}}$.

3. Instead of treating the interference as noise, all points on the superimposed constellation of RN1 are explicitly taken into account. In this way, PNC-JD can fully exploit the superimposed constellation in the presence of interference. This is shown in Fig. 6.7. We observe that each superimposed signal is mapped into a J-NCS in which its first bit carries $s_{\oplus,13}$ and its second bit carries $s_{\oplus,24}$. The ML estimate of the J-NCS $s_{\oplus,\mathrm{JNC}}$ can be calculated as

$$\begin{aligned}\hat{s}_{\oplus,\mathrm{JNC}} &= \arg\max_{s_{\oplus,\mathrm{JNC}}} p(y_{\mathrm{RN1}}|s_{\oplus,\mathrm{JNC}}) \\ &= \arg\max_{s_{\oplus,\mathrm{JNC}}} \frac{1}{M_{x_1} M_{x_2} M_{x_{34}}} \sum_{x_1,x_2,x_{34}:s_{\oplus,\mathrm{JNC}}=s_1^*\oplus s_1^*\oplus s_{34}} p(y_{\mathrm{RN1}}|x_{34}, x_1, x_2),\end{aligned} \tag{6.10}$$

where we observe that the summation includes all signals in the superimposed constellation which map to the same J-NCS $s_{\oplus,\mathrm{JNC}}$, as shown in Fig. 6.7. The conditional probability $p(y_{\mathrm{RN1}}|x_{34}, x_1, x_2)$ is given by

$$\begin{aligned}&p(y_{\mathrm{RN1}}|x_{34}, x_1, x_2) \\ &= \frac{1}{\pi N_0} \exp\left(-\frac{\left| y_{\mathrm{RN1}} - h_3 x_{34} - h_1 x_1 - h_{2(\mathrm{I})} x_2 \right|^2}{N_0} \right) \\ &= \frac{1}{\pi N_0} \exp\left(-\frac{\left| y_{\mathrm{RN1}} - h_3 \mathcal{M}_{\mathrm{Q}}(s_{34}) - h_1 \mathcal{M}_{\mathrm{B,V}}^{(1)}(s_1^*) - h_{2(\mathrm{I})} \mathcal{M}_{\mathrm{B,V}}^{(2)}(s_2^*) \right|^2}{N_0} \right).\end{aligned} \tag{6.11}$$

Due to the symmetrical structure of the HWN, RN2 applies the same PNC-JD approach to decode the RN2's J-NCS $\hat{s}_{\oplus,\mathrm{JNC}}$.

RN Selection

Due to the nature of the decode-and-forward strategy, we note that after performing PNC-JD, the residual decoding error broadcasted to the MSs and HBS can give rise to severe error propagation. The relay selection (RS) technique can be used to mitigate error propagation from the relay. Moreover, due to the reciprocity of channels in the HWN, RS can guarantee the best transmission in both the first and the second time slot. Those RNs with a poorer channel condition will remain silent in the second time slot.

Several RS algorithms have been proposed in the literatures, e.g., the Max-Min algorithm in [50, 51] and CRC check algorithm in [52, 53]. However, for the Max-Min algorithm, acquisition of global channel state information (CSI) at each relay is necessary, which gives rise to an excessive burden. For the CRC check method, at the low SNR, there may be residual errors at all RNs, and hence none will transmit in the second time slot. Motivated by this, we propose a novel RS scheme based on the instantaneous rate, which is summarized as Algorithm 1, listed below. As synchronization is not the main issue of this thesis, we assume that perfect network synchronization is achievable.

Compared with the Max-Min algorithm, instantaneous rate based RS only requires RNs to exchange a small amount of data with the HBS, and does not require global CSI. Moreover, in the scenario of multi-relay assisted HWN, as the number of RNs is less than that of MS, thus the proposed RS algorithm is still affordable.

In the second time slot, the selected RN modulates its own J-NCS $s_{\oplus,\mathrm{JNC}}$ as $x_{\oplus,\mathrm{JNC}} = \mathcal{M}_{\mathrm{Q}}(s_{\oplus,\mathrm{JNC}})$ and broadcasts $x_{\oplus,\mathrm{JNC}}$ to the MSs and HBS.

Table 6.1: The proposed RS algorithm.

Algorithm 1: Instantaneous Rate based Relay Selection

1. Given h_1, h_3 and $h_{1(I)}$, RN1 calculates $I(Y_{\mathrm{RN1}}; S_{\oplus,\mathrm{JNC}})$ and forwards it to HBS.
2. Given h_2, h_4 and $h_{2(I)}$, RN2 calculates $I(Y_{\mathrm{RN2}}; S_{\oplus,\mathrm{JNC}})$ and forwards it to HBS.
3. **if** $I(Y_{\mathrm{RN1}}; s_{\oplus,\mathrm{JNC}}) > I(Y_{\mathrm{RN2}}; S_{\oplus,\mathrm{JNC}})$ **then**
4. HBS broadcasts one bit '0' to RN1 and RN2.
5. RN1 transmits $s_{\oplus,\mathrm{JNC}}$ in the second time slot while the RN2 keeps silent.
6. **elseif** $I(Y_{\mathrm{RN1}}; S_{\oplus,\mathrm{JNC}}) < I(Y_{\mathrm{RN2}}; S_{\oplus,\mathrm{JNC}})$ **then**
7. HBS broadcasts one bit '1' to RN1 and RN2.
8. RN2 transmits $s_{\oplus,\mathrm{JNC}}$ in the second time slot while RN1 keeps silent.
9. **else**
10. The HBS broadcasts two bits '11' to RN1 and RN2.
11. Both of them transmit $s_{\oplus,\mathrm{JNC}}$ in the second time-slot.
6. **end if**

Processing at MSs and HBS

The received signals at HBS and MS1 are represented as

$$y_{\mathrm{HBS}} = h_{\mathrm{MS1}} x_{\oplus,\mathrm{JNC}} + n_{\mathrm{HBS}} \tag{6.12}$$

and

$$y_{\mathrm{MS1}} = h_{\mathrm{HBS}} x_{\oplus,\mathrm{JNC}} + n_{\mathrm{MS1}} \tag{6.13}$$

respectively. Here h_{MS1} and h_{HBS} are determined by the selected RN, given by $h_{\mathrm{MS1}} \in \{h_1, h_{1(\mathrm{I})}, h_1 + h_{1(\mathrm{I})}\}$ and $h_{\mathrm{HBS}} \in \{h_3, h_4, h_3 + h_4\}$.

We note that when RN1 and RN2 achieve equal instantaneous rate, in our designed RS scheme, we have $h_{\mathrm{MS1}} = h_1 + h_{1(\mathrm{I})}$ and $h_{\mathrm{HBS}} = h_3 + h_4$. According to [54], the sum of two Gaussian random variable (R.V.) with zero mean and variance Ω is still a Gaussian R.V. with zero mean and variance 2Ω. This indicates that the selected superimposed channels $h_{\mathrm{MS1}} = h_1 + h_{1(\mathrm{I})}$ and $h_{\mathrm{HBS}} = h_3 + h_4$ still experience Rayleigh fading (the variance is doubled) when both RNs transmit. The detection of $x_{\oplus,\mathrm{JNC}}$ at the HBS is the same as the detection for QPSK symbol on the point-to-point fading channel. The first and second bit of decoded $s_{\oplus,\mathrm{JNC}}$ are $s_{\oplus,13}$ and $s_{\oplus,24}$, respectively. By performing the XOR operation

with s_3 and s_4 respectively, the HBS' desired data s_1 and s_2 can be obtained. MS1 and MS2 perform the same operation to obtain s_3 and s_4, respectively.

6.5.2 Sum-rate Analysis

In this subsection, we examine the constellation-constrained sum-rate for the PNC-JD strategy in the HWN.

Analysis for the first time slot

We can evaluate the rates with respect to x_3 and x_4 in the first time slot by examining the rates related to x_{34} as x_3 and x_4 are jointly embedded in x_{34}. As we employ an RS algorithm based on instantaneous rate, the rate region for symbols x_1, x_2, x_3 and x_4 in the first time slot should obey

$$\begin{aligned} R_{x_1}^{(1)} = R_{x_3}^{(1)} &\leq \max\left[\frac{1}{2}I(Y_{\mathrm{RN1}}; S_{\oplus,\mathrm{JNC}}), \frac{1}{2}I(Y_{\mathrm{RN2}}; S_{\oplus,\mathrm{JNC}})\right] \\ R_{x_2}^{(1)} = R_{x_4}^{(1)} &\leq \max\left[\frac{1}{2}I(Y_{\mathrm{RN1}}; S_{\oplus,\mathrm{JNC}}), \frac{1}{2}I(Y_{\mathrm{RN2}}; S_{\oplus,\mathrm{JNC}})\right] \end{aligned}, \tag{6.14}$$

where $I(Y_{\mathrm{RN1}}; S_{\oplus,\mathrm{JNC}})$ and $I(Y_{\mathrm{RN2}}; S_{\oplus,\mathrm{JNC}})$ are the mutual information between the received signal and the J-NCS, at RN1 and RN2, respectively. Since $s_{\oplus,13}$ and $s_{\oplus,24}$ are the first and second bits of the 2-bit binary tuple $s_{\oplus,\mathrm{JNC}}$, the rates of $s_{\oplus,13}$ and $s_{\oplus,24}$ are half of $I(Y_{\mathrm{RN1}}; S_{\oplus,\mathrm{JNC}})$ or $I(Y_{\mathrm{RN2}}; S_{\oplus,\mathrm{JNC}})$. As such, $I(Y_{\mathrm{RN1}}; S_{\oplus,\mathrm{JNC}})$ and $I(Y_{\mathrm{RN2}}; S_{\oplus,\mathrm{JNC}})$ are scaled by the factor $\frac{1}{2}$ in (6.14).

In the following, we derive $I(y_{\mathrm{RN1}}; s_{\oplus,\mathrm{JNC}})$ in detail. We expand $I(y_{\mathrm{RN1}}; s_{\oplus,\mathrm{JNC}})$ as

$$I(Y_{\mathrm{RN1}}; S_{\oplus,\mathrm{JNC}}) = H(Y_{\mathrm{RN1}}) - H(Y_{\mathrm{RN1}}|S_{\oplus,\mathrm{JNC}}). \tag{6.15}$$

The entropy $H(Y_{\mathrm{RN1}})$ of the received signal is given by

$$H(Y_{\mathrm{RN1}}) = -\int_{y_{\mathrm{RN1}}} p(y_{\mathrm{RN1}})\log_2\left(p(y_{\mathrm{RN1}})\right) dy_{\mathrm{RN1}}. \tag{6.16}$$

The probability density function (PDF) $p(y_{\mathrm{RN1}})$ of the received signal is given by

$$p(y_{\mathrm{RN1}}) = \frac{1}{M_{x_{34}} M_{x_1} M_{x_2}} \sum_{x_1, x_2, x_{34}} p(y_{\mathrm{RN1}} | x_{34}, x_1, x_2), \tag{6.17}$$

where $p(y_{\mathrm{RN1}}|x_{34}, x_1, x_2)$ is defined in (6.11).

The conditional entropy $H(Y_{\mathrm{RN1}}|S_{\oplus,\mathrm{JNC}})$ can be calculated as

$$H(Y_{\mathrm{RN1}}|S_{\oplus,\mathrm{JNC}}) = -\sum_{s_{\oplus,\mathrm{JNC}}} \int_{y_{\mathrm{RN1}}} p\left(y_{\mathrm{RN1}}, s_{\oplus,\mathrm{JNC}}\right) \log_2 \left(p\left(y_{\mathrm{RN1}}|s_{\oplus,\mathrm{JNC}}\right)\right) dy_{\mathrm{RN1}}, \tag{6.18}$$

where $p\left(y_{\mathrm{RN1}}|s_{\oplus,\mathrm{JNC}}\right)$ is defined in (6.10).

Note that both $H(Y_{\mathrm{RN1}})$ in (6.16) and $H(Y_{\mathrm{RN1}}|S_{\oplus,\mathrm{JNC}})$ in (6.18) cannot be written in closed forms. Hence, we use Monte-Carlo integration and the mutual information in (6.15) thus can be calculated as

$$I(Y_{\mathrm{RN1}}; S_{\oplus,\mathrm{JNC}}) = -\mathbb{E}\left[\log_2\left(p(Y_{\mathrm{RN1}})\right)\right] + \mathbb{E}\left[\log_2\left(p\left(Y_{\mathrm{RN1}}|S_{\oplus,\mathrm{JNC}}\right)\right)\right], \tag{6.19}$$

where $M_{x_1} = M_{x_2} = 2$ since x_1 and x_2 are BPSK symbols and $M_{x_{34}} = 4$ since x_{34} is QPSK symbol. The cardinality of J-NCS is $M_{s_{\oplus,\mathrm{JNC}}} = 16$ as there are 16 distinct superimposed signals for x_1, x_2 and x_{34}.

Due to the symmetrical structure of the HWN, we can proceed similarly for $I(y_{\mathrm{RN2}}; s_{\oplus,\mathrm{JNC}})$. Then the rate region for symbols x_1, x_2, x_3 and x_4 in the first time slot in (6.14) can be calculated.

Analysis for the second time slot

In the second time slot, based on (6.10), we note that the first bit of the decoded $s_{\oplus,\mathrm{JNC}}$ is $s_{\oplus,13}$. As such, the achievable rate of x_1 is in fact equal to half of that of $x_{\oplus,\mathrm{JNC}}$, given by

$$R_{x_1}^{(2)} \leq \frac{1}{2} I(Y_{\mathrm{HBS}}; X_{\oplus,\mathrm{JNC}}) = \frac{1}{2}\left[H(X_{\oplus,\mathrm{JNC}}) - H(X_{\oplus,\mathrm{JNC}}|Y_{\mathrm{HBS}})\right], \tag{6.20}$$

where $H(X_{\oplus,\mathrm{JNC}}) = \log_2(M_{x_{\oplus,\mathrm{JNC}}})$ and $H(X_{\oplus,\mathrm{JNC}}|Y_{\mathrm{HBS}})$ is given by

$$\begin{aligned} H(X_{\oplus,\mathrm{JNC}}|Y_{\mathrm{HBS}}) &= \int_{y_{\mathrm{HBS}}} p(x_{\oplus,\mathrm{JNC}}, y_{\mathrm{HBS}}) \log_2 \left(\frac{1}{p(x_{\oplus,\mathrm{JNC}}|y_{\mathrm{HBS}})}\right) dy_{\mathrm{HBS}} \\ &= \int_{y_{\mathrm{HBS}}} p(x_{\oplus,\mathrm{JNC}}, y_{\mathrm{HBS}}) \log_2 \left(\frac{\sum\limits_{x'_{\oplus,\mathrm{JNC}}} p(y_{\mathrm{HBS}}|x'_{\oplus,\mathrm{JNC}})}{p(y_{\mathrm{HBS}}|x_{\oplus,\mathrm{JNC}})}\right) dy_{\mathrm{HBS}}. \end{aligned} \tag{6.21}$$

Using Monte-Carlo integration, (6.20) can be calculated as

$$R_{x_1}^{(2)} \leq \frac{1}{2} I(Y_{\text{HBS}}; X_{\oplus,\text{JNC}}) = \frac{1}{2}\log_2(M_{x_{\oplus,\text{JNC}}}) - \frac{1}{2}\mathbb{E}\left[\frac{\sum\limits_{X'_{\oplus,\text{JNC}}} p(Y_{\text{HBS}}|X'_{\oplus,\text{JNC}})}{p(Y_{\text{HBS}}|X_{\oplus,\text{JNC}})}\right]. \quad (6.22)$$

Similarly, the achievable rates of x_3 in the second time slot is also bounded by the point-to-point channel, given by

$$R_{x_3}^{(2)} \leq \frac{1}{2} I(Y_{\text{MS1}}; X_{\oplus,\text{JNC}}) = \frac{1}{2}\log_2(M_{x_{\oplus,\text{JNC}}}) - \frac{1}{2}\mathbb{E}\sum_{X_{\oplus,\text{JNC}}}\left[\frac{\sum\limits_{X'_{\oplus,\text{JNC}}} p(Y_{\text{MS1}}|X'_{\oplus,\text{JNC}})}{p(Y_{\text{MS1}}|X_{\oplus,\text{JNC}})}\right]. \quad (6.23)$$

The end-to-end results

Based on (6.14) and (6.22), the equivalent end-to-end achievable rate of x_1 is bounded by

$$R_{x_1} \leq \frac{1}{2}\min\left\{\max\left[\frac{1}{2}I(Y_{\text{RN1}}; S_{\oplus,\text{JNC}}), \frac{1}{2}I(Y_{\text{RN2}}; S_{\oplus,\text{JNC}})\right], \frac{1}{2}I(Y_{\text{HBS}}; X_{\oplus,\text{JNC}})\right\}, \quad (6.24)$$

where the first coefficient $\frac{1}{2}$ is due to the consumed time slots for the PNC-JD strategy.

Based on (6.14) and (6.23), the equivalent end-to-end achievable rate of x_3 can be calculated as

$$R_{x_3} \leq \frac{1}{2}\min\left\{\max\left[\frac{1}{2}I(Y_{\text{RN1}}; S_{\oplus,\text{JNC}}), \frac{1}{2}I(Y_{\text{RN2}}; S_{\oplus,\text{JNC}})\right], \frac{1}{2}I(Y_{\text{MS1}}; X_{\oplus,13})\right\}. \quad (6.25)$$

Due to the symmetrical structure of the HWN, the achievable rates of x_2 and x_4 can be obtained by the same approach as x_1 and x_3. Substituting the achievable rates of each symbol into (6.3), the constellation constrained sum-rate for PNC-JD is thus calculated.

6.6 ANC with Interference-Aware ML detection (ANC-IAML)

The ANC strategy can be well-suited for bi-directional data exchange in HWN when RNs do not have detection capability or the relay node is constrained by a low system complexity. Motivated by this, in this section, we propose the ANC-IAML strategy in HWN.

6.6.1 System Description

Suppose that MS1 and MS2 employ BPSK modulation for data stream s_1 and s_2, respectively, i.e, $x_1 = \mathcal{M}_{\mathrm{B}}(s_1)$ and $x_2 = \mathcal{M}_{\mathrm{B}}(s_2)$. As for PNC-JD, in order to exchange the data packets with MSs within two time slots, the HBS applies QPSK modulation (see Fig. 6.4) to transmit s_3 and s_4 simultaneously: the first and second bits of the 2-bit binary tuple s_{34} carry the binary data streams of s_3 and s_4, respectively. Then s_{34} is modulated to a Gray coded QPSK symbol x_{34}, i.e., $x_{34} = \mathcal{M}_{\mathrm{Q}}(s_{34})$.

In the first time slot, the received signal at RN1 is given by

$$y_{\mathrm{RN1}} = h_3 x_{34} + h_1 x_1 + h_{2(\mathrm{I})} x_2 + n_{\mathrm{RN1}}. \tag{6.26}$$

Then RN1 amplifies and forwards the received signal to the MSs and HBS, with a normalization factor:

$$\beta_{\mathrm{RN1}} = \left[\left(|h_3|^2 + |h_1|^2 + |h_{2(\mathrm{I})}|^2\right) + N_0\right]^{-\frac{1}{2}}. \tag{6.27}$$

In addition, RN1 sends the CSIs h_3, h_1 and $h_{(\mathrm{I}),2}$ to the MSs and HBS prior to the data frame. Note that although forwarding CSIs consumes extra resources (both time and bandwidth) for the whole system, this cost can be ignored compared with the cost of the data transmission, assuming a block fading channel with a large channel coherence time.

The signal received by RN2 is given as

$$y_{\mathrm{RN2}} = h_4 x_{34} + h_{1(\mathrm{I})} x_1 + h_2 x_2 + n_{\mathrm{RN2}}. \tag{6.28}$$

Then RN2 amplifies and forwards the received signal to the MSs and HBS, with a normalization factor:

$$\beta_{\mathrm{RN2}} = \left[\left(|h_4|^2 + |h_2|^2 + |h_{1(\mathrm{I})}|^2\right) + N_0\right]^{-\frac{1}{2}}. \tag{6.29}$$

Due to the symmetrical structure of HWN, all operations at RN2 is the same with that at RN1. The available CSIs at RN2, i.e., h_4, h_2 and $h_{1(\mathrm{I})}$, are broadcasted to the MSs and HBS.

Processing at MSs

In the second time slot, the received signal at MS1 can be expressed as

$$y_{\mathrm{MS1}} = h_1\beta_{\mathrm{RN1}}y_{\mathrm{RN1}} + h_{1(\mathrm{I})}\beta_{\mathrm{RN2}}y_{\mathrm{RN2}} + n_{\mathrm{MS1}}. \tag{6.30}$$

As MS1 knows its side information x_1, after canceling out the self-interference, the received signal at MS1 can be rewritten as

$$\begin{aligned} y^*_{\mathrm{MS1}} &= h_1\beta_{\mathrm{RN1}}(h_3x_{34} + h_{2(\mathrm{I})}x_2 + n_{\mathrm{RN1}}) + h_{1(\mathrm{I})}\beta_{\mathrm{RN2}}(h_4x_{34} + h_2x_2 + n_{\mathrm{RN2}}) + n_{\mathrm{MS1}} \\ &= (h_1\beta_{\mathrm{RN1}}h_3 + h_{1(\mathrm{I})}\beta_{\mathrm{RN2}}h_4)x_{34} + (h_1\beta_{\mathrm{RN1}}h_{2(\mathrm{I})} + h_{1(\mathrm{I})}\beta_{\mathrm{RN2}}h_2)x_2 \\ &\quad + (h_1\beta_{\mathrm{RN1}}n_{\mathrm{RN1}} + h_{1(\mathrm{I})}\beta_{\mathrm{RN2}}n_{\mathrm{RN2}} + n_{\mathrm{MS1}}). \end{aligned} \tag{6.31}$$

Based on the reciprocity of channels and the forwarded channel coefficients, MS1 knows the global CSIs. As such, MS1 can exploit the superimposed constellation. We denote the virtual channel coefficients $h_{\mathrm{V},1} \triangleq h_1\beta_{\mathrm{RN1}}h_3 + h_{1(\mathrm{I})}\beta_{\mathrm{RN2}}h_4$ and $h_{\mathrm{V},2} \triangleq h_1\beta_{\mathrm{RN1}}h_{2(\mathrm{I})} + h_{1(\mathrm{I})}\beta_{\mathrm{RN2}}h_2$. We let $n_{t,\mathrm{MS1}} \triangleq h_1\beta_{\mathrm{RN1}}n_{\mathrm{RN1}} + h_{1(\mathrm{I})}\beta_{\mathrm{RN2}}n_{\mathrm{RN2}} + n_{\mathrm{MS1}}$ which represents the total noise at MS1. Based on these, (6.31) can be represented as

$$y^*_{\mathrm{MS1}} = h_{\mathrm{V1,MS1}}x_{34} + h_{\mathrm{V2,MS1}}x_2 + n_{t,\mathrm{MS1}}. \tag{6.32}$$

Note that we do not need to decode one signal and treat the other as noise. The ML detection we propose here fully exploits the superimposed constellation for signal y^*_{MS1}, resulting in the ML estimate of s_3

$$\hat{s}_3 = \arg\max_{s_3} p(y^*_{\mathrm{MS1}}|s_3) = \arg\max_{s_3} \frac{1}{M_{x_{34}}M_{x_2}} \sum_{x_{34},x_2:s_3} p(y^*_{\mathrm{MS1}}|x_{34},x_2), \tag{6.33}$$

where the summation includes all signals on superimposed constellation corresponding to the same s_3. Based on this, we can split the superimposed constellation into two decision region, i.e., $\mathcal{D}_\ell, \ell \in \{\mathrm{I}, \mathrm{II}\}$, as shown Fig. 6.8, corresponding to x_3 is mapped as 0 or 1. Thus we have $\mathcal{D}_\mathrm{I} = \{h_{\mathrm{V1,MS1}}x_{34} + h_{\mathrm{V2,MS1}}x_2 | s_3 = 0\}$ and $\mathcal{D}_\mathrm{II} = \{h_{\mathrm{V1,MS1}}x_{34} + h_{\mathrm{V2,MS1}}x_2 | s_3 = 1\}$. For $p(y^*_{\mathrm{MS1}}|x_{34}, x_1)$, we have

$$p(y^*_{\mathrm{MS1}}|x_{34}, x_1) = \frac{1}{\pi N_{0,\mathrm{eqv}}} \exp\left(-\frac{|y^*_{\mathrm{MS1}} - h_{\mathrm{V1,MS1}}x_{34} - h_{\mathrm{V2,MS1}}x_2|^2}{N_{0,\mathrm{eqv}}}\right). \tag{6.34}$$

where $N_{0,\mathrm{eqv}} = (|h_1\beta_{\mathrm{RN1}}|^2 + |h_{1(\mathrm{I})}\beta_{\mathrm{RN2}}|^2 + 1)N_0$ is the equivalent noise variance at MS1.

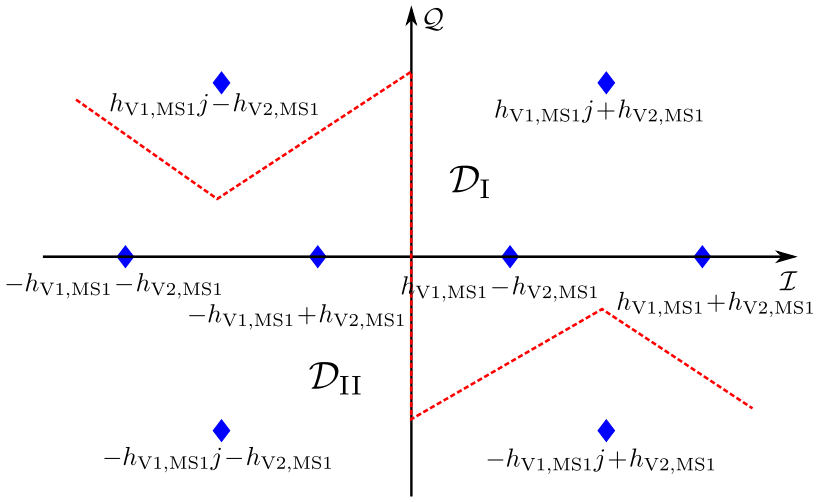

Figure 6.8: Decision Regions for the superimposed constellation of x_{MS1}.

The same detection strategy as (6.33) may be performed at RN2 for symbol x_4, by symmetry.

Processing at the HBS

In the second time slot, the received signal at the HBS is given as

$$y_{\mathrm{HBS}} = h_3\beta_{\mathrm{RN1}}y_{\mathrm{RN1}} + h_4\beta_{\mathrm{RN2}}y_{\mathrm{RN2}} + n_{\mathrm{HBS}_2}. \tag{6.35}$$

As the HBS knows its side information x_{34}, the received signal after self-interference

cancellation is given by

$$\begin{aligned} y^*_{\rm HBS} &= h_3\beta_{\rm RN1}(h_1x_1 + h_{2(\rm I)}x_2 + n_{\rm RN1}) \\ &\quad + h_4\beta_{\rm RN2}(h_{1(\rm I)}x_1 + h_2x_2 + n_{\rm RN2}) + n_{\rm HBS} \\ &= (h_3\beta_{\rm RN1}h_1 + h_4\beta_{\rm RN2}h_{1(\rm I)})x_1 + (h_3\beta_{\rm RN1}h_{2(\rm I)} + h_4\beta_{\rm RN2}h_2)x_2 \\ &\quad + (h_3\beta_{\rm RN1}n_{\rm RN1} + h_4\beta_{\rm RN2}n_{\rm RN2} + n_{\rm HBS}). \end{aligned} \tag{6.36}$$

As for MS1, $y^*_{\rm HBS}$ can be represented in terms of the virtual channels:

$$y^*_{\rm HBS} = h_{\rm V1,HBS}x_1 + h_{\rm V2,HBS}x_2 + n_{t,\rm HBS}. \tag{6.37}$$

where $h_{\rm V1,HBS} \triangleq h_3\beta_{\rm RN1}h_1 + h_4\beta_{\rm RN2}h_{1(\rm I)}$, $h_{\rm V2,HBS} \triangleq h_3\beta_{\rm RN1}h_{2(\rm I)} + h_4\beta_{\rm RN2}h_2$ and $n_{t,\rm HBS} \triangleq h_3\beta_{\rm RN1}n_{\rm RN1} + h_4\beta_{\rm RN2}n_{\rm RN2} + n_{\rm HBS}$.

As x_1 and x_2 are the desired symbols for the HBS, it is optimal to decode x_1 and x_2 at the same time. Similar to RN1 in PNC-JD, the HBS virtually treats the BPSK symbol label corresponding to x_1 as a 2-bit binary tuple in which the first bit carries the real data stream s_1 and the second bit is postfixed with a redundant bit 0, giving $s^*_1 = (s_1, 0)$. As such, the mapping relationship between s^*_1 and x_1 is given as $\mathcal{M}^{(1)}_{\rm B,V}(10) = -1$ and $\mathcal{M}^{(1)}_{\rm B,V}(00) = +1$. On the other hand, the data word s_2 is virtually prefixed with a redundant bit 0, i.e., $s^*_2 = (0, s_2)$. The mapping function between s^*_1 and x_1 is given as $\mathcal{M}^{(1)}_{\rm B,V}(01) = -1$ and $\mathcal{M}^{(1)}_{\rm B,V}(00) = +1$. As such, the NCS of s^*_1 and s^*_2 is denoted as $s_{\oplus,12}$, given by

$$s_{\oplus,12} = s^*_1 \oplus s^*_2. \tag{6.38}$$

Thus it is clear that s_1 is the first bit of $s_{\oplus,12}$ and s_2 is the second bit of $s_{\oplus,12}$. The ML estimate of the NCS $s_{\oplus,12}$ is given by

$$\hat{s}_{\oplus,12} = \arg\max_{s_{\oplus,12}} p(y^*_{\rm HBS}|s_{\oplus,12}) = \arg\max_{s_{\oplus,12}} \frac{1}{M_{x_1}M_{x_2}} \sum_{x_1,x_2:s_{\oplus,12}=s^*_1\oplus s^*_2} p(y^*_{\rm HBS}|x_1,x_2), \tag{6.39}$$

where the conditional PDF $p(y^*_{\rm HBS}|x_1,x_2)$ is calculated as

$$\begin{aligned} p(y^*_{\rm HBS}|x_1,x_2) &= \frac{1}{\pi N_0}\exp\left(-\frac{|y^*_{\rm HBS} - h_{\rm V1,HBS}x_1 - h_{\rm V2,HBS}x_2|^2}{N_0}\right) \\ &= \frac{1}{\pi N_0}\exp\left(-\frac{\left|y^*_{\rm HBS} - h_{\rm V1,HBS}\mathcal{M}^{(1)}_{\rm B,V}(s^*_1) - h_{\rm V2,HBS}\mathcal{M}^{(2)}_{\rm B,V}(s^*_2)\right|^2}{N_0}\right). \end{aligned} \tag{6.40}$$

The PNC detection for the NCS $s_{\oplus,12}$ is illustrated in Fig 6.9.

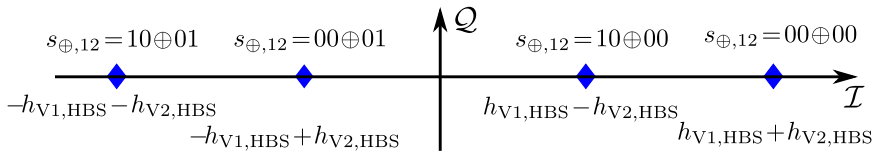

Figure 6.9: Modified PNC detection for $s_{\oplus,12}$ at HBS.

6.6.2 Analysis of Sum-rates

In this subsection, we analyze the constellation constrained sum-rate for the ANC-IAML strategy.

Analysis for end-to-end results at the HBS

Based on the designed decoding strategy at HBS, the achievable rate of x_1 at the HBS is given by

$$R_{x_1} \leq \frac{1}{2} \times \frac{1}{2} I\left(Y^*_{\mathrm{HBS}}; S_{\oplus,12}\right) = \frac{1}{4}\left[H\left(Y^*_{\mathrm{HBS}}\right) - H\left(Y^*_{\mathrm{HBS}}|S_{\oplus,12}\right)\right]. \tag{6.41}$$

where the first coefficient $\frac{1}{2}$ is due to the two time slots used and the second coefficient $\frac{1}{2}$ is due to the fact that the rate of x_1 is half of that of $s_{\oplus,12}$.

The entropy of the received signal is given by

$$H(Y^*_{\mathrm{HBS}}) = -\int_{y^*_{\mathrm{HBS}}} p(y^*_{\mathrm{HBS}}) \log_2\left(p(y^*_{\mathrm{HBS}})\right) dy^*_{\mathrm{HBS}}. \tag{6.42}$$

The PDF of the received signal is given by

$$p(y^*_{\mathrm{HBS}}) = \frac{1}{M_{x_1} M_{x_2}} \sum_{x_1,x_2} p(y^*_{\mathrm{HBS}}|x_1, x_2), \tag{6.43}$$

where $p(y^*_{\mathrm{HBS}}|x_1, x_2)$ is defined in (6.39).

The conditional entropy $H(y^*_{\mathrm{HBS}}|x_{\oplus,12})$ can be calculated as

$$H(Y^*_{\mathrm{HBS}}|S_{\oplus,12}) = -\sum_{s_{\oplus,12}} \int_{y^*_{\mathrm{HBS}}} p\left(y^*_{\mathrm{HBS}}, s_{\oplus,12}\right) \log_2\left(p\left(y^*_{\mathrm{HBS}}|s_{\oplus,12}\right)\right) dy_{\mathrm{HBS}}, \tag{6.44}$$

where $p\left(y^*_{\mathrm{HBS}}|s_{\oplus,12}\right)$ is defined in (6.40).

Note that both $H(Y^*_{\text{HBS}})$ in (6.42) and $H(Y^*_{\text{HBS}}|S_{\oplus,12})$ in (6.43) cannot be written in a closed form. Again, we use Monte-Carlo integration and the mutual information thus can be calculated as

$$I(Y^*_{\text{HBS}}; S_{\oplus,12}) = -\mathbb{E}\left[\log_2\left(p(Y^*_{\text{HBS}})\right)\right] + \mathbb{E}\left[\log_2\left(p\left(Y^*_{\text{HBS}}|S_{\oplus,12}\right)\right)\right]. \tag{6.45}$$

Analysis for end-to-end results at MS1

Based on the designed decoding strategy at MS1, the achievable rates of x_3 at MS1 is given by

$$R_{x_3} \leq \frac{1}{2} I(Y^*_{\text{MS1}}; S_3) = \frac{1}{2}\left[H(S_3) - H(S_3|Y^*_{\text{MS1}})\right], \tag{6.46}$$

where $H(S_3) = \log_2(M_{s_3})$ and $H(S_3|Y^*_{\text{MS1}})$ is given by

$$\begin{aligned} H(S_3|Y^*_{\text{MS1}}) &= \sum_{s_3} \int_{y^*_{\text{MS1}}} p\left(y^*_{\text{MS1}}, s_3\right) \log_2\left(\frac{1}{p\left(s_3|y^*_{\text{MS1}}\right)}\right) dy^*_{\text{MS1}} \\ &= \sum_{s_3} \sum_{x_{34}, x_2 : s_3} \int_{y^*_{\text{MS1}}} p\left(y^*_{\text{MS1}}, x_{34}, x_2\right) \log_2\left(\frac{\sum\limits_{s'_3} p\left(y^*_{\text{MS1}}|s'_3\right)}{p\left(y^*_{\text{MS1}}|s'_3\right)}\right) dy^*_{\text{MS1}}. \end{aligned} \tag{6.47}$$

Using Monte-Carlo integration, the achievable rate of x_3 can be rewritten as

$$R_{x_3} \leq \frac{1}{2} I(Y^*_{\text{MS1}}; S_3) = \frac{1}{2}\log_2(M_{s_3}) - \frac{1}{2}\mathbb{E}\left[\log_2\left(\frac{\sum\limits_{S'_3} p\left(Y^*_{\text{MS1}}|S'_3\right)}{p\left(Y^*_{\text{MS1}}|S_3\right)}\right)\right]. \tag{6.48}$$

By symmetry, we may apply the same approach for the achievable rates R_{x_2} and R_{x_4}. Based on the derived achievable rates of each symbol, the constellation constrained sum-rate in (6.3) is thus calculated.

6.7 Performance Evaluation and Discussion

In this section, we evaluate and compare the sum-rate and outage probability of all strategies, i.e., the TDMA-PNC (benchmark), PNC-JD and ANC-IAML strategies. We assume that all channel links experience quasi-static i.i.d. frequency-flat Rayleigh fading, i.e.,

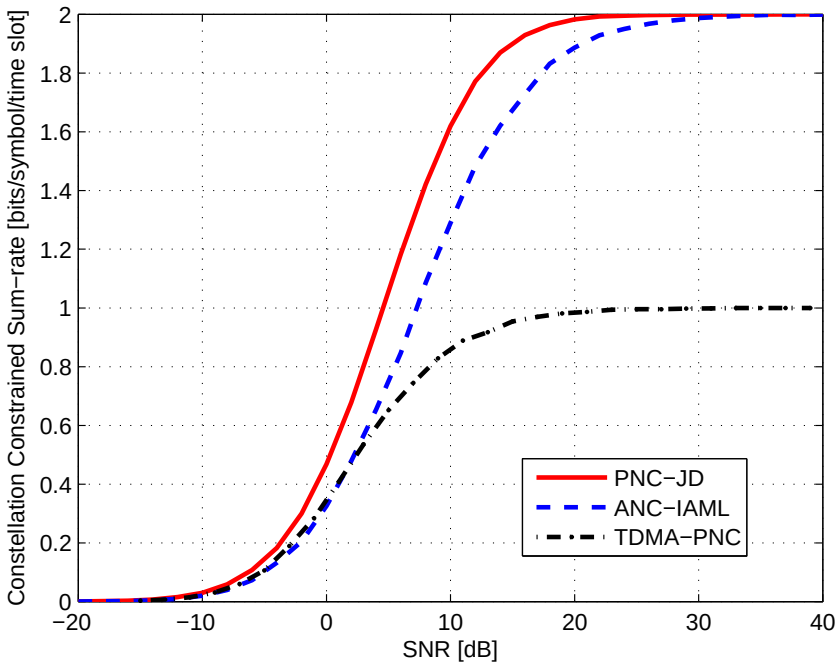

Figure 6.10: Comparison of constellation constrained sum-rates of different strategies.

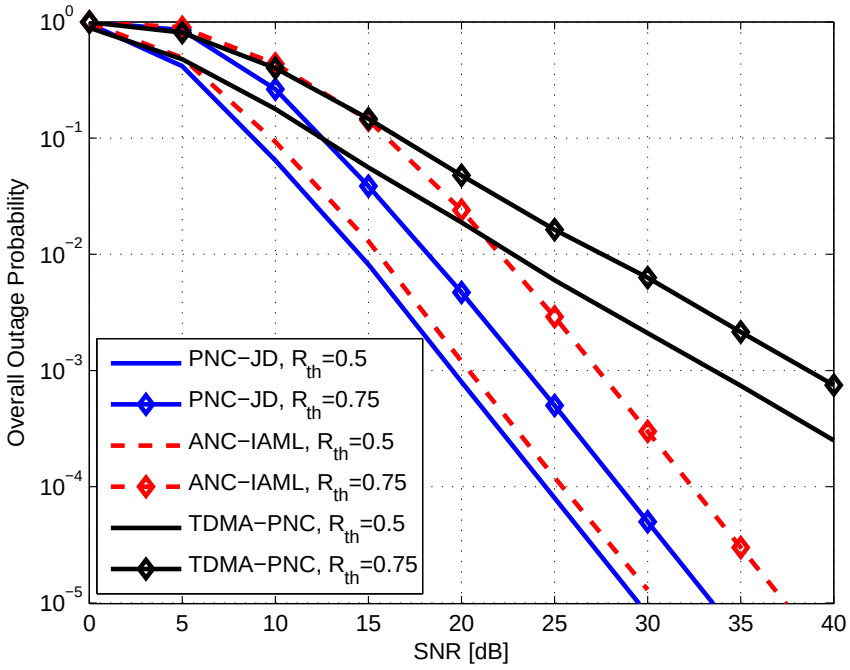

Figure 6.11: Comparison of the overall outage probability for all strategies.

each channel coefficient is modelled as a zero-mean complex Gaussian random variable with unit variance. The average signal-to-noise-ratio (SNR) is denoted as $\frac{1}{N_0}$.

Fig. 6.10 shows the comparison of the ergodic constellation constrained sum-rate of the different strategies. The ergodic constellation constrained sum-rate is obtained by averaging (6.3) over the channel realizations of the HWN, given by $\overline{R}_{\mathrm{Sum}} = \mathbb{E}_{\mathcal{H}}\{R_{\mathrm{Sum}}\}$, where $\mathcal{H} \triangleq \{h_1, h_2, h_3, h_4, h_{1(\mathrm{I})}, h_{2(\mathrm{I})}\}$ denotes the set of channels in the HWN. We observe that in the high SNR regime, due to the finite input constellations adopted by the MSs and HBS, the sum-rates of PNC-JD and ANC-IAML are limited to 2 bits/symbol/time slot which implies that this strategy can maximally guarantee a 4 bit data exchange in 2 time slots while the sum-rate of TDMA-PNC is limited to 1 bit/symbol/time slot. This is clearly because the TDMA scheme inherently requires twice the number of time slots. We observe that PNC-JD outperforms TDMA-PNC at any SNR, but ANC-IAML is slightly worse than TDMA-PNC at lower SNRs. While TDMA-PNC treats signals between RN1 and MS2, and RN2 and MS1, as interference, and uses TDMA to avoid it, both PNC-JD and ANC-IAML exploit these paths to provide additional diversity. We also observe that PNC-JD is superior to ANC-IAML. This is because in the ANC-IAML strategy, RNs not only forward the useful signal but also the amplified noise to the destinations, which lowers the SNR at relevant destinations hence decreases the rates. In PNC-JD, on the other hand, the inherent denoise characteristic of PNC avoids this [4], and the novel RS scheme also mitigates error-propagation from relay.

The outage probability for a given transmission rate is given by the probability of that the achievable rate falls below a given threshold [54]. The overall outage probability can be measured as $P_{out} = \Pr\{R_{\mathrm{sum}} < R_{th}\}$ where R_{th} is the rate threshold. Fig.6.11 shows the resulting curves for the overall outage probability versus SNRs with different rate thresholds. We may observe that PNC-JD and ANC-IAML achieve a lower outage probability compared with TDMA-PNC. In the low SNR regime, TDMA-PNC is just slightly better than ANC-IAML. This is consistent with the discussion and results in Fig. 6.10. The reason is that at a low SNR, the ANC-IMAL amplifies more noise than the useful signal to the HBS and MSs, which results in a higher overall outage probability. We also observe that, because they exploit two signal paths to each MS, PNC-JD and ANC-IAML both achieve second order diversity while TDMA-PNC cannot.

6.8 Summary

In this Chapter, we have proposed two interference exploitation strategies for HWN: 1) PNC-JD and 2) ANC-IAML. In PNC-JD, each RN decodes the J-NCSs for useful symbol pair and interference symbol pair. The proposed mutual information based relay selection scheme only allows the RN with the maximal instantaneous rate to broadcast the J-NCS to the HBS and MSs. The HBS and MSs can recover their desired signal by exploiting the received J-NCS and their SI. In ANC-IAML, all RNs amplify the linear sum of the received signals and forward it back to HBS and MSs. The different copies of the amplified sum signal are naturally combined at HBS and MSs, which results in extra diversity. After cancelling out their corresponding self-interference, HBS/MS performs the interference aware ML detection to extract its desired signal. Our proposed strategies naturally transform the CCIs into the useful signal and enhance the spectral efficiency compared with TDMA-PNC. We have derived the constellation constrained sum-rate as the performance metric for each strategy. The theoretical analysis and simulation confirm that: 1) PNC-JD can provide a substantial sum-rate enhancement compared to TDMA-PNC over a sufficiently wide range of SNR regimes; 2) ANC-IAML achieves a sum-rate almost equal to TDMA-PNC in the low SNR regime while ANC-IAML outperforms TDMA-PNC in the moderate-to-high SNR regime; 3) PNC-JD offers a superior sum-rate relative to ANC-IAML over a wide range of SNR regimes; and 4) PNC-JD and ANC-IAML both provide transmit diversity while TDMA-PNC cannot.

Chapter 7

A New Type of Compute-and-forward using Linear Codes: Multilevel Network Coded Multi-Way Relaying

Contents

7.1 Overview

In this chapter, we propose a novel LPNC over 3-WRC. The relay maps the superimposed signal into the linear network coded combination (LNCC, regarded as network coded symbol) by multiplying the user data by a properly selected generator matrix. A sum-rate based mapping selection scheme is also introduced for generating the optimal LNCC. The unambiguous decodability and minimum cardinality of the proposed LPNC mapping

are investigated. The proposed LPNC facilitates the multilevel coding structure using parallel independent coding levels, in which each level is a linear function of user data. This enables the HDF paradigm [7] for multiuser data exchange. The simulation results show that: 1) the uncoded LPNC achieves equal error performance compared with the Latin cube based PNC [56, 57]; 2) the uncoded LPNC provides a superior sum-rate over the opportunistic scheduling based PNC; and 3) MLC-LPNC shows coding gain over two benchmarks.

7.2 Introduction

PNC [1] in the 2-WRC exhibits a significant throughput enhancement over the conventional three-phase network coding scheme, requiring only two transmission phases: the multiple access channel (MAC) and the broadcast channel (BC) phases.

PNC has attracted enormous attention in recent years. The constellation constrained capacity regions for PNC in 2-WRC were established in [7]. The authors in [7, 8] pointed out that some singular fading in the MAC phase inevitably shortens the minimum distance between different network coded symbols (NCS). A non-linear PNC mapping, namely, the so-called 5QAM denoise-and-forward (5QAM-DNF) scheme, was proposed in [8] to mitigate these singular fade states by extending the PNC mapping from 4-ary to 5-ary. However, the drawback of 5QAM-DNF is also clear: both the nonlinear mapping and the 5QAM constellation used on the BC phase introduce irregularities in the communication system which cannot readily be implemented in conventional systems. Moreover, due to the non-linear mapping, the linear codes cannot be adopted for 5QAM-DNF, which restricts its usage in conventional systems. In [55] and [34], the concept of linear network coding [4] was extended from the wireline network to wireless 2-WRC to form the LPNC. The authors in [55] proposed to use non-binary channel codes to improve the error performance of LPNC. The authors in [34] investigated the asymptotic symbol error rate of LPNC. However, their designed LPNC requires the user to adopt the irregular p-ary immolation, where p is a prime, e.g., 5-PAM modulation. This restricts its usage in conventional systems. Moreover, we note that the aforementioned PNC designs in [34, 55] only focused on the 2-WRC.

A Latin cube based PNC was proposed for 3-WRC [56] and M-WRC [57], respectively, in which the relay adaptively transforms the Latin cube to generate the PNC mapping based on the channel states. The users decode the desired symbols by looking up the Latin cube. However, the channel codes cannot be employed due to the fact that the Latin cube based PNC is in essence a type of non-linear mapping. Moreover, such design requires enlarging the cardinality of NCS alphabet, which results in performance degradation in BC phase. The algebraic approach of PNC was proposed in [25,26], which extends the PNC beyond the 2-WRC to general Gaussian multiple access channels (GMAC), i.e., compute-and-forward (CPF). However, we note that CPF requires infinite dimensional lattices construction which is not practical in the common communications systems. In summary, the existing multi-user PNC strategies either require irregular constellations ([8, 25, 26, 34, 55–58]) or cannot directly adopt the channel codes ([8, 56, 57]).

To tackle the drawbacks of the aforementioned strategies in [8, 25, 26, 34, 55–58], we propose a multilevel coded LPNC for the M-WRC. The superimposed signal at the relay is mapped into the linear network coded combination (LNCC, regarded as NCS) by multiplying the user data by a properly selected generator matrix. The selection criterion guarantees the multiuser exclusive law and maximizes the sum-rate in the MAC phase. The proposed LPNC facilitates the multilevel coding structure using parallel independent coding levels in which each level is a linear function of user data. This enables the hierarchical decode-and-forward paradigm [7] for multiuser data exchange. That is, the resulting LNCC sequence is a valid codeword and can be directly decoded. The minimum cardinality of LNCC alphabet is guaranteed given that LNCC can be unambiguously decoded at each user. As a result, the proposed design improves the spectral efficiency in BC phase compared with the Latin cube based PNC in [56, 57]. The contributions are summarized as four-fold:

1. We propose a new LPNC such that the data exchange in the M-WRC only requires two transmission phases and hence increases the throughput

2. Our proposed LPNC guarantees the linearity of channel codes such that the hierarchical decode and forward paradigm [3] is enabled.

3. We propose a sum-rate maximization based mapping selection approach which generates the optimal LPNC mapping for maximizing the sum-rate in the MAC phase.

4. Our proposed LPNC always ensures the minimum cardinality constraint as in [2] for saving the spectral efficiency in the BC phase.

Based on the our analytical and simulation results, we highlight that 1) the uncoded LPNC achieves the equal error performance compared with the Latin cube based PNC [7,8]; 2) the uncoded LPNC provides a superior sum-rate over the opportunistic scheduling based PNC; and 3) MLC-LPNC shows coding gain over two benchmarks. The proposed design achieves the triple-goal of flexibility, low-complexity and performance.

7.3 System Model and Scheme Description

In this section, we describe the system model of the proposed LPNC in M-WRC. The M-WRC consists of multiple users and one relay. It is assumed that the all users operate in half-duplex mode and there is no direct link among users. The multi-way data exchange takes place among the users with the help of the relay. Each user expects to exchange its own data with those of the other two.

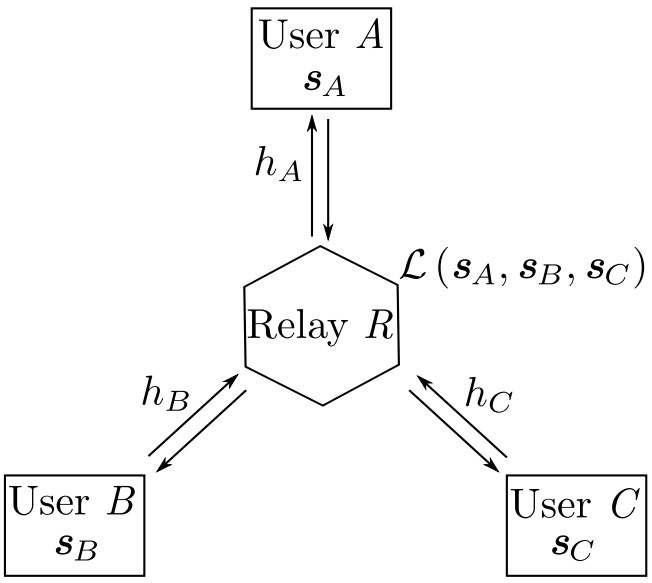

Figure 7.1: System Model of 3-WRC

We focus on a simplified model of M-WRC, i.e., the 3-way relay channels (3-WRC), as shown in Fig. 7.1. We note that the proposed LPNC for 3-WRC can be easily extended to

the general M-WRC. The LPNC facilitates the 3-way data exchange with only two transmission phases, i.e., multiple access (MAC) phase and broadcast (BC) phase. All channels experience quasi-static independent and identically distributed (i.i.d.) frequency-flat Rayleigh fading with unit variance. It is assumed that a binary FEC encoder is employed by each user. The coded symbol is generated by encoding the user's original data.

7.3.1 Multiple Access Phase

In the MAC phase, the three users (*A*, *B* and *C*) simultaneously transmit signals to the relay (*R*). It is assumed that all users adopt QPSK modulation. Due to the QPSK signaling, each channel coded symbol from user i, $i \in \{A, B, C\}$, is thus a member of $\mathrm{GF}\,(2^2)$ and can be expressed by a binary extension field form, i.e., $\boldsymbol{s}_i = \begin{bmatrix} s_{i,1} \\ s_{i,2} \end{bmatrix}$, where $s_{i,j} \in \mathrm{GF}\,(2)$, $j \in \{1, 2\}$, represents the *j*-th binary bit of $\boldsymbol{s}_i$. The channel coded symbol $\boldsymbol{s}_i$ serves as the complementary side information (C-SI) of each user. Let $\mathscr{A}_4$ denote the Gray coded QPSK alphabet with unit energy constraint. The mapping from coded symbol to complex symbols is denoted as $\mathcal{M}_S : \mathrm{GF}\,(2^2) \rightarrow \mathscr{A}_4$. The complex symbols transmitted by user i, denoted as x_i, is then given by $x_i = \mathcal{M}_S(\boldsymbol{s}_i)$.

The electromagnetic signals from users are superimposed at *R*, i.e.,

$$y_R = h_A x_A + h_B x_B + h_C x_C + n_w, \tag{7.1}$$

where h_i, $i \in \{A, B, C\}$ is the channel gain from user i to *R*. We assume that the *channel state information* is perfectly known to the receiver side only. The received superimposed signal is corrupted by complex additive Gaussian white noise (AWGN) n_R with variance σ_w^2 per complex dimension. We refer to

$$x_{ABC} \triangleq h_A x_A + h_B x_B + h_C x_C \tag{7.2}$$

as the noiseless *superimposed signal (SS).*

7.3.2 Proposed Linear Mapping at Relay

In the proposed design, the relay *R* linearly maps the SS into the linear network coded combination (LNCC), given by

$$\mathcal{L} : x_{ABC} \rightarrow \boldsymbol{s}_{\mathcal{L}}, \tag{7.3}$$

where $\boldsymbol{s}_{\mathcal{L}}$ is the LNCC. The alphabet of the LNCC is denoted as $\mathcal{S}_{\mathcal{L}}$, whose cardinality is denoted as $M_{\mathcal{S}_{\mathcal{L}}}$.

Similar to the original PNC in the 2-WRC, the linear mapping $\mathcal{L}$ in (7.3) should ensure that for the given LNCC and C-SI, each user can unambiguously decode the symbols of other users. In other words, the linear mapping $\mathcal{L}$ should be invertible. This is referred to as the *multi-user exclusive law* of the proposed LPNC, given by

$$\begin{aligned}
&\mathcal{L}\left(\boldsymbol{s}_A, \boldsymbol{s}_B, \boldsymbol{s}_C\right) \neq \mathcal{L}\left(\boldsymbol{s}_A, \boldsymbol{s'}_B, \boldsymbol{s'}_C\right), \ \forall (\boldsymbol{s}_B, \boldsymbol{s}_C) \neq (\boldsymbol{s'}_B, \boldsymbol{s'}_C) \ , \\
&\mathcal{L}\left(\boldsymbol{s}_A, \boldsymbol{s}_B, \boldsymbol{s}_C\right) \neq \mathcal{L}\left(\boldsymbol{s'}_A, \boldsymbol{s'}_B, \boldsymbol{s}_C\right), \ \forall (\boldsymbol{s}_A, \boldsymbol{s}_B) \neq (\boldsymbol{s'}_A, \boldsymbol{s'}_B), \\
&\mathcal{L}\left(\boldsymbol{s}_A, \boldsymbol{s}_B, \boldsymbol{s}_C\right) \neq \mathcal{L}\left(\boldsymbol{s'}_A, \boldsymbol{s}_B, \boldsymbol{s'}_C\right), \ \forall (\boldsymbol{s}_A, \boldsymbol{s}_C) \neq (\boldsymbol{s'}_A, \boldsymbol{s'}_C).
\end{aligned} \tag{7.4}$$

This is obtained from extending the original exclusive law [8] from the 2-WRC to 3-WRC. Clearly, the results of (7.4) can be also extended to the M-WRC. The unambiguous decoding of the proposed LPNC is detailed in the next section. To conserve spectral efficiency, the following condition is introduced as the constraint of the cardinality of the LNCC alphabet.

Condition 1. *The resulting LNCC alphabet should satisfy both the multi-user exclusive law and the minimum cardinality.*

Recall that the cardinality of the user alphabet is 4 due to the QPSK signaling. A necessity that the multi-user exclusive law is ensured is that the cardinality of LNCC alphabet is between 4^2 and 4^3, i.e., $4^2 \leq M_{\mathcal{S}_{\mathcal{L}}} \leq 4^3$. *Condition 1* indicates that the cardinality of the resulting LNCC alphabet is restricted to 4^2. As such, $\boldsymbol{s}_{\mathcal{L}}$ returned by $\mathcal{L}$, which is generated from linearly combining $\boldsymbol{s}_A$, $\boldsymbol{s}_B$ and $\boldsymbol{s}_C$, is a member of the binary extension field $\mathrm{GF}\left(2^4\right)$, given by

$$\boldsymbol{s}_{\mathcal{L}} = \boldsymbol{A} \otimes \boldsymbol{s}_A \oplus \boldsymbol{B} \otimes \boldsymbol{s}_B \oplus \boldsymbol{C} \otimes \boldsymbol{s}_C \tag{7.5}$$

where all matrix operations obey modulo-2 arithmetic, i.e., $\boldsymbol{x} \otimes \boldsymbol{y} = \mathrm{mod}(\boldsymbol{x} \cdot \boldsymbol{y}, 2)$ and $x \oplus \boldsymbol{y} = \mathrm{mod}(\boldsymbol{x} + \boldsymbol{y}, 2)$, which are closed within $\mathrm{GF}(2)$. The quantities $\boldsymbol{A}$, $\boldsymbol{B}$ and $\boldsymbol{C}$ are 4×2 binary matrices which are referred to as the parameter matrices. The resulting LNCC $\boldsymbol{s}_{\mathcal{L}}$ can be expanded as

$$\boldsymbol{s}_{\mathcal{L}} = \begin{bmatrix} s_{\mathcal{L},1} \\ s_{\mathcal{L},2} \\ s_{\mathcal{L},3} \\ s_{\mathcal{L},4} \end{bmatrix}, \tag{7.6}$$

where $s_{\mathcal{L},n}$, $n \in \{1,2,3,4\}$, represents the n-th bit level of $\boldsymbol{s}_{\mathcal{L}}$.

We define the generator matrix as $\boldsymbol{G} \triangleq \begin{bmatrix} \boldsymbol{A} & \boldsymbol{B} & \boldsymbol{C} \end{bmatrix}$ and the users' symbol vector as $\boldsymbol{s}_{ABC} \triangleq \begin{bmatrix} \boldsymbol{s}_A \\ \boldsymbol{s}_B \\ \boldsymbol{s}_C \end{bmatrix}$. Hence, (7.6) can be rewritten as $\boldsymbol{s}_{\mathcal{L}} = \boldsymbol{G} \otimes \boldsymbol{s}_{ABC}$

Integrating the linear mapping function (7.6) into the maximal likelihood (ML) detection, we have the following LPNC detection:

$$\boldsymbol{s}_{\mathcal{L}} = \arg\max_{\boldsymbol{s}_{\mathcal{L}}} p(y_R|\boldsymbol{s}_{\mathcal{L}}) = \arg\max_{\boldsymbol{s}_{\mathcal{L}}} \sum_{\forall(x_A,x_B,x_C) \text{ s.t. } \mathcal{L}:y_R \to \boldsymbol{s}_{\mathcal{L}}} P(x_A)P(x_B)P(x_C)p(y_R|x_{ABC}) \tag{7.7}$$

where we note that the summation includes all (x_A, x_B, x_C) such that $\mathcal{L} : y_R \to \boldsymbol{s}_{\mathcal{L}}$. The conditional probability density function (PDF) $p(y_R|x_{AB})$ yields the Gaussian distribution, given by

$$p(y_R|x_{ABC}) = \frac{1}{2\pi\sigma_w^2} \exp\left(-\frac{|y_R - x_{ABC}|^2}{2\sigma_w^2}\right). \tag{7.8}$$

The details of the selection criterion for the linear mapping functions are described in the next section.

7.3.3 Broadcast Phase

In the BC phase, *R* maps the LNCC into the modulated symbol. Due to the cardinality of resulting LNCC, 16QAM modulation is adopted by *R*. Let A_{16} denote the 16QAM alphabet with unit energy constraint. The modulated LNCC, denoted as x_R, is given by

$x_R = \mathcal{M}_R(\boldsymbol{s}_\mathcal{L})$, where $\mathcal{M}_R : \mathrm{GF}(2^4) \rightarrow \mathscr{A}_{16}$ is constellation mapper at *R*. Then x_R is forwarded to all users. The received signal at each user is given by

$$y_i = h_i x_R + n_i \tag{7.9}$$

where n_i is the complex AWGN at user i, where $i \in \{A, B, C\}$. Then user i demodulates the received signal y_i to obtain the LNCC. The demodulated LNCC is denoted as $\hat{\boldsymbol{s}}_\mathcal{L}$.

7.4 Adaptive Selection criterion of Linear Mapping

In this section, we provide the detailed design for the adaptive selection criterion for the linear mapping functions. As all channel states are known to *R*, the mapping functions are then selected to adapt to the channel, i.e., firstly to ensure the multi-user exclusive law, and secondly to maximize the sum-rate.

7.4.1 Unambiguous Decoding Based on Multi-user Exclusive Law

We note that the linear mapping in (7.5) in fact forms a set of linear Diophantine equations with six variables $s_{i,j}$ where $i \in \{A, B, C\}$ and $j \in \{1, 2\}$. Since user i has its own C-SI s_i, (6) is simplified to a set of linear equations with four variables for each user. Hence, fulfilling the multi-user exclusive law is equivalent to choosing the generator matrix $\boldsymbol{G}$ from those for which the linear equation (7.5) is solvable. More specifically, the user i, $i \in \{A, B, C\}$ can successfully recover the desired symbols s_l and s_k (l and $k \in \{A, B, C, \}\backslash\{i\}$) through fully exploiting the C-SI s_i and the received LNCC $\hat{\boldsymbol{s}}_\mathcal{L}$. In the following, we show the detailed recovery procedure for the desired symbols based on the multi-user exclusive law.

User A formulates $\boldsymbol{s}_A$ and $\hat{\boldsymbol{s}}_{\mathcal{L}}$ as in the following signal pattern

$$\begin{aligned}\boldsymbol{r}_A \triangleq \begin{bmatrix}\boldsymbol{s}_A \\ \hat{\boldsymbol{s}}_{\mathcal{L}}\end{bmatrix} &= \begin{bmatrix}\boldsymbol{I}\otimes\boldsymbol{s}_A \\ \boldsymbol{G}\otimes\boldsymbol{s}_{ABC}\end{bmatrix} = \begin{bmatrix}\boldsymbol{I} & \mathbf{0} & \mathbf{0} \\ \boldsymbol{A} & \boldsymbol{B} & \boldsymbol{C}\end{bmatrix}\otimes\begin{bmatrix}\boldsymbol{s}_A \\ \boldsymbol{s}_B \\ \boldsymbol{s}_C\end{bmatrix} \\ &= \begin{bmatrix}\boldsymbol{I} & \mathbf{0} & \mathbf{0} \\ \boldsymbol{A} & \boldsymbol{B} & \boldsymbol{C}\end{bmatrix}\otimes\boldsymbol{s}_{ABC}\end{aligned} \tag{7.10}$$

where $\boldsymbol{I}$ is a 2×2 identity matrix and $\mathbf{0}$ is a null matrix. We note that the equality $\begin{bmatrix}\boldsymbol{I} & \mathbf{0} & \mathbf{0}\end{bmatrix}\otimes\boldsymbol{s}_{ABC} = \boldsymbol{I}\otimes\boldsymbol{s}_A$ holds and we refer to $\boldsymbol{\Gamma}_A \triangleq \begin{bmatrix}\boldsymbol{I} & \mathbf{0} & \mathbf{0} \\ \boldsymbol{A} & \boldsymbol{B} & \boldsymbol{C}\end{bmatrix}$ as user A's decoding matrix. The multi-user exclusive law in (7.4) is then fulfilled if and only if $\boldsymbol{\Gamma}_A$ is invertible, i.e., $\boldsymbol{\Gamma}_A$ is a full rank matrix. The recovered the source symbol vector, denoted as $\hat{\boldsymbol{s}}_{ABC}$, is obtained by multiplying the signal pattern $\boldsymbol{r}_A$ in (7.10) by $\boldsymbol{\Gamma}_A^{-1}$, given by $\hat{\boldsymbol{s}}_{ABC} = \boldsymbol{\Gamma}_A^{-1}\otimes\boldsymbol{r}_A$.

User B formulates $\boldsymbol{s}_B$ and $\hat{\boldsymbol{s}}_{\mathcal{L}}$ as in the following signal pattern

$$\begin{aligned}\boldsymbol{r}_B \triangleq \begin{bmatrix}\hat{\boldsymbol{s}}_{\mathcal{L}}(1:2,:) \\ \boldsymbol{s}_B \\ \hat{\boldsymbol{s}}_{\mathcal{L}}(3:4,:)\end{bmatrix} &= \begin{bmatrix}\boldsymbol{G}(1:2,:)\otimes\boldsymbol{s}_{ABC} \\ \boldsymbol{I}\otimes\boldsymbol{s}_B \\ \boldsymbol{G}(3:4,:)\otimes\boldsymbol{s}_{ABC}\end{bmatrix} \\ &= \begin{bmatrix}\boldsymbol{A}(1:2,:) & \boldsymbol{B}(1:2,:) & \boldsymbol{C}(1:2,:) \\ \mathbf{0} & \boldsymbol{I} & \mathbf{0} \\ \boldsymbol{A}(3:4,:) & \boldsymbol{B}(3:4,:) & \boldsymbol{C}(3:4,:)\end{bmatrix}\otimes\begin{bmatrix}\boldsymbol{s}_A \\ \boldsymbol{s}_B \\ \boldsymbol{s}_C\end{bmatrix} \\ &= \begin{bmatrix}\boldsymbol{A}(1:2,:) & \boldsymbol{B}(1:2,:) & \boldsymbol{C}(1:2,:) \\ \mathbf{0} & \boldsymbol{I} & \mathbf{0} \\ \boldsymbol{A}(3:4,:) & \boldsymbol{B}(3:4,:) & \boldsymbol{C}(3:4,:)\end{bmatrix}\otimes\boldsymbol{s}_{ABC}\end{aligned} \tag{7.11}$$

where the mathematical notation $\boldsymbol{X}(l:n,:)$ represents a sub-matrix of $\boldsymbol{X}$, which contains the l-th to n-th rows of $\boldsymbol{X}$. We note that the equality $\begin{bmatrix}\mathbf{0} & \boldsymbol{I} & \mathbf{0}\end{bmatrix}\otimes\boldsymbol{s}_{ABC} = \boldsymbol{I}\otimes\boldsymbol{s}_B$ holds and we refer to $\boldsymbol{\Gamma}_B \triangleq \begin{bmatrix}\boldsymbol{A}(1:2,:) & \boldsymbol{B}(1:2,:) & \boldsymbol{C}(1:2,:) \\ \mathbf{0} & \boldsymbol{I} & \mathbf{0} \\ \boldsymbol{A}(3:4,:) & \boldsymbol{B}(3:4,:) & \boldsymbol{C}(3:4,:)\end{bmatrix}$ as user B's decoding matrix. Likewise, if and only if $\boldsymbol{\Gamma}_B$ is a full rank matrix, the recovered the source symbol vector $\hat{\boldsymbol{s}}_{ABC}$ is then obtained by multiplying the signal pattern $\boldsymbol{r}_B$ in (7.11) by $\boldsymbol{\Gamma}_B^{-1}$, given by $\hat{\boldsymbol{s}}_{ABC} = \boldsymbol{\Gamma}_B^{-1}\otimes\boldsymbol{r}_B$

User C formulates $\boldsymbol{s}_C$ and $\hat{\boldsymbol{s}}_{\mathcal{L}}$ as in the following signal pattern

$$\begin{aligned}\boldsymbol{r}_C \triangleq \begin{bmatrix}\hat{\boldsymbol{s}}_{\mathcal{L}}\\ \boldsymbol{s}_C\end{bmatrix} &= \begin{bmatrix}\boldsymbol{G}\otimes\boldsymbol{s}_{ABC}\\ \boldsymbol{I}\otimes\boldsymbol{s}_C\end{bmatrix} = \begin{bmatrix}\boldsymbol{A} & \boldsymbol{B} & \boldsymbol{C}\\ \boldsymbol{0} & \boldsymbol{0} & \boldsymbol{I}\end{bmatrix}\otimes\boldsymbol{s}_{ABC}\\ &= \boldsymbol{\Gamma}_C\otimes\boldsymbol{s}_{ABC}\end{aligned} \tag{7.12}$$

where we note that the equality $\begin{bmatrix}\boldsymbol{0} & \boldsymbol{0} & \boldsymbol{I}\end{bmatrix}\otimes\boldsymbol{s}_{ABC} = \boldsymbol{I}\otimes\boldsymbol{s}_C$ holds and we refer to $\boldsymbol{\Gamma}_C \triangleq \begin{bmatrix}\boldsymbol{A} & \boldsymbol{B} & \boldsymbol{C}\\ \boldsymbol{0} & \boldsymbol{0} & \boldsymbol{I}\end{bmatrix}$ as user C's decoding matrix. If and only if $\boldsymbol{\Gamma}_B$ is a full rank matrix, the recovered the source symbol vector $\hat{\boldsymbol{s}}_{ABC}$ is then obtained by multiplying the signal pattern $\boldsymbol{r}_c$ in (7.12) by $\boldsymbol{\Gamma}_C^{-1}$, given by $\hat{\boldsymbol{s}}_{ABC} = \boldsymbol{\Gamma}_C^{-1}\otimes\boldsymbol{r}_C$.

Based on the results of (7.10)-(7.12), we provide the following Remark.

Remark 1. *For any generator matrix $\boldsymbol{G} = \begin{bmatrix}\boldsymbol{A} & \boldsymbol{B} & \boldsymbol{C}\end{bmatrix}$, the multi-user exclusive law is satisfied if and only if the resulting decoding matrices $\boldsymbol{\Gamma}_A$, $\boldsymbol{\Gamma}_B$ and $\boldsymbol{\Gamma}_c$ are all full rank matrices.*

7.4.2 Sum-rate based Selection Criterion

We denote the rate of each user in the MAC phase as $R_i^{(1)}$, $i \in \{A, B, C\}$. The authors in [8] and [7] pointed out that in PNC, the individual rate of each user in the MAC is bounded by the mutual information between the received signal and the network coded combination, denoted as $I(Y_R; \boldsymbol{S}_{\mathcal{L}})$.

The mutual information $I(Y_R; \boldsymbol{S}_{\mathcal{L}})$ is expanded as

$$I(Y_R; \boldsymbol{S}_{\mathcal{L}}) = H(Y_R) - H(Y_R|\boldsymbol{S}_{\mathcal{L}}). \tag{7.13}$$

The entropy $H(y_R)$ of the received signal is given by

$$H(Y_R) = -\int_{y_R\in\mathbb{C}} p(y_R)\log_2\left(p(y_R)\right)dy_R \tag{7.14}$$

where the PDF of the received signal is calculated as

$$p(y_R) = \sum_{x_A, x_B, x_C} P(x_A)P(x_B)P(x_C)p(y_R|x_{ABC}) \tag{7.15}$$

where $p(Y_R|X_{ABC})$ is defined in (7.7).

The conditional entropy $H(Y_R|\boldsymbol{S}_{\mathcal{L}})$ in (7.15) can be calculated as

$$\begin{aligned} H(Y_R|\boldsymbol{S}_{\mathcal{L}}) &= -\sum_{\boldsymbol{s}_{\mathcal{L}}} \int_{y\in\mathbb{C}} p\left(y_R, \boldsymbol{s}_{\mathcal{L}}\right) \log_2\left(p\left(y_R|\boldsymbol{s}_{\mathcal{L}}\right)\right) dy_R \\ &= -\sum_{\boldsymbol{s}_{\mathcal{L}}} P(\boldsymbol{s}_{\mathcal{L}}) \int_{y\in\mathbb{C}} p\left(y_R|\boldsymbol{s}_{\mathcal{L}}\right) \log_2\left(p\left(y_R|\boldsymbol{s}_{\mathcal{L}}\right)\right) dy_R \end{aligned} \tag{7.16}$$

where $p\left(Y_R|\boldsymbol{S}_{\mathcal{L}}\right)$ is defined in (7.8). Note that neither $H(Y_R)$ in (7.14) nor $H(Y_R|\boldsymbol{S}_{\mathcal{L}})$ in (7.15) can be written in closed form. Hence, we use Monte-Carlo integration instead. The mutual information in (7.13) thus can be computed as

$$I(Y_R; \boldsymbol{S}_{\mathcal{L}}) = \mathbb{E}\left[\log_2\left(p(Y_R)\right)\right] - \mathbb{E}\left[\log_2\left(p\left(Y_R|\boldsymbol{S}_{\mathcal{L}}\right)\right)\right], \tag{7.17}$$

where M_i, $i \in \{A, B\}$, is the cardinality of the user alphabet.

Unlike the original PNC, for LPNC-EM, we note that the rate region in the MAC phase is determined by the mapping function in (7.5). Here, we show the impact of the mapping function on the individual achievable rate of each user. The following **Theorem 1** gives the sum-rate in MAC phase given that the proposed LPNC is decoded at *R*.

Theorem 1. *The sum-rate in the MAC phase, denoted by $R^{(1)}_{ABC}$, should be bounded by*

$$R^{(1)}_{ABC} \leq \frac{6}{4} I\left(Y_R; \boldsymbol{S}_{\mathcal{L}}\right), \tag{7.18}$$

*where the factor 6 and 4 are the entropy of $\boldsymbol{s}_{ABC}$ and $\boldsymbol{s}_{\mathcal{L}}$, respectively, as indicated in the proof of **Theorem 1.** .*

The proof of **Theorem 1** is detailed in Appendix B.

As the resulted LNCC $s_{\mathcal{L}}$ is a member of $\mathrm{GF}\left(2^4\right)$, the following observations are obtained: 1) $s_{\mathcal{L}}$ might introduce some redundancy of the binary bit $s_{i,j}, i \in \{A, B, C\}, j \in \{1, 2\}$; and 2) the maximum mutual information $I(Y; \boldsymbol{S}_{\mathcal{L}})$ can achieve 4bits/symbol at best. However, the effective achievable rate of user i, $i \in \{A, B\}$, is equal to the sum of the rates with respect to binary bits $s_{i,1}$ and $s_{i,2}$ in the $\boldsymbol{s}_{\mathcal{L}}$, given by

$$\begin{aligned} R^{(1)}_A &\leq I(Y_R; S_{A,1}(\boldsymbol{S}_{\mathcal{L}})) + I(Y_R; S_{A,2}(\boldsymbol{S}_{\mathcal{L}})) \\ R^{(1)}_B &\leq I(Y_R; S_{B,1}(\boldsymbol{S}_{\mathcal{L}})) + I(Y_R; S_{B,2}(\boldsymbol{S}_{\mathcal{L}})) \\ R^{(1)}_C &\leq I(Y_R; S_{C,1}(\boldsymbol{S}_{\mathcal{L}})) + I(Y_R; S_{C,2}(\boldsymbol{S}_{\mathcal{L}})), \end{aligned} \tag{7.19}$$

where $s_{i,j}(\boldsymbol{s}_{\mathcal{L}}), i \in \{A, B\}, j \in \{1, 2\}$, is the *j*-th data bit of user *i* carried by $\boldsymbol{s}_{\mathcal{L}}$ and $I(Y_R; S_{i,j}(\boldsymbol{S}_{\mathcal{L}}))$ denotes the mutual information between the received signal *R* and the user's binary bit carried by $\boldsymbol{s}_{\mathcal{L}}$. Since $\boldsymbol{s}_{\mathcal{L}}$ is uniformly distributed over $\mathrm{GF}\,(2^4)$, each mapping level in (7.6) is equiprobable. Based on this, we have $I(Y_R; S_{i,j}(\boldsymbol{S}_{\mathcal{L}})) = \frac{1}{4} I(Y_R; \boldsymbol{S}_{\mathcal{L}})$. Hence, the achievable rates of each user can be rewritten as

$$R_A^{(1)} = R_B^{(1)} = R_C^{(1)} \leq \frac{1}{2} I(Y_R; \boldsymbol{S}_{\mathcal{L}}), \tag{7.20}$$

where $\frac{1}{2} I(Y_R; \boldsymbol{S}_{\mathcal{L}})$ equals the effective bits per symbol received by each user if the BC phase is error-free.

Based on (7.20) and **Theorem 1**, we have the following remark.

Remark 2. *The rate region of MAC phase given that the proposed LPNC is decoded at R, takes the following form:*

$$\begin{aligned} R_A^{(1)} = R_B^{(1)} = R_C^{(1)} &\leq \frac{1}{2} I(Y_R; \boldsymbol{S}_{\mathcal{L}}) \\ R_{ABC}^{(1)} &\leq \frac{6}{4} I\left(Y_R; \boldsymbol{S}_{\mathcal{L}}\right). \end{aligned} \tag{7.21}$$

Remark 2 indicates that rate region of the proposed LPNC in the MAC phase in fact forms a cube over a three-dimensional space of $R_A^{(1)}$, $R_B^{(1)}$ and $R_C^{(1)}$.

Based on the result of (7.21), we observe that *maximizing $I(Y_R; \boldsymbol{S}_{\mathcal{L}})$ is equivalent to maximizing the individual achievable rate of each user in the MAC phase, and hence maximizing the sum-rate in the MAC phase*. Since the mutual information $I(Y_R; \boldsymbol{S}_{\mathcal{L}})$ is significantly affected by the generator matrix $\boldsymbol{G}$, we re-express $I(Y_R; \boldsymbol{S}_{\mathcal{L}})$ in terms of $\boldsymbol{G}$, given as $I^{\boldsymbol{G}}(Y_R; \boldsymbol{S}_{\mathcal{L}})$. The selection criterion of maximizing the individual achievable rate of each user returns the optimal $\boldsymbol{G}$, given by

$$\widetilde{\boldsymbol{G}} = \arg\max_{\boldsymbol{G}} \left[I^{\boldsymbol{G}}(Y_R; \boldsymbol{S}_{\mathcal{L}}) \right], \tag{7.22}$$

where $\widetilde{\boldsymbol{G}}$ is the returned generator matrix after exhaustive searching.

In summary, for given channel coefficients, the following selection algorithm is implemented at the relay such that that the sum-rate is maximized and the multiuser exclusive law is ensured.

Algorithm 4 Selection Criterion of $\boldsymbol{G}$ for Maximizing the Sum-rate in the MAC phase.

1: Given h_A, h_B and h_C;
2: **for all** $\boldsymbol{G} \in \{\boldsymbol{G} : \boldsymbol{s}_{\mathcal{L}} = \boldsymbol{G} \otimes \boldsymbol{s}_{ABC}\}$ **do**
3: Make the rate set empty: $\mathcal{F}_I = \varphi$;
4: Generate the LNCC $\boldsymbol{s}_{\mathcal{L}} = \boldsymbol{G} \otimes \boldsymbol{s}_{ABC}$;
5: Check the the satisfaction of multi-user exclusive law (Remark 1) for resulting $\boldsymbol{s}_{\mathcal{L}}$;
6: **if** the multi-user exclusive law (Remark 1) was satisfied **then**
7: Compute $I^{\boldsymbol{G}}(Y_R; \boldsymbol{S}_{\mathcal{L}})$;
8: Include it in the rate set: $\mathcal{F}_I \leftarrow \mathcal{F}_I \cup \{I^{\boldsymbol{G}}(Y_R; \boldsymbol{S}_{\mathcal{L}})\}$;
9: **end if**
10: **end for**
11: Let $I^{\boldsymbol{G}}(Y_R; \boldsymbol{S}_{\mathcal{L}})_{max}$ be the maximum value among all the rates: $I^{\boldsymbol{G}}(Y_R; \boldsymbol{S}_{\mathcal{L}})_{max} = \max(\mathcal{F}_I)$;
12: Select $\widetilde{\boldsymbol{G}}$ whose rate corresponds to $I^{\boldsymbol{G}}(Y_R; \boldsymbol{S}_{\mathcal{L}})_{max}$.

7.5 Multilevel Coded LPNC for 3-WRC

In this section, we introduce multilevel coded LPNC (MLC-LPNC). In the following, we refine the notations from the perspective of the channel coded sequence. The sequence of $s_{i,j}$, where $i \in \{A, B, C\}$ and $j \in \{1, 2\}$, is denoted as $\boldsymbol{s}_{i,j}$. The sequence of $\boldsymbol{s}_{ABC}$ is denoted as $\boldsymbol{S}_{ABC}$, which is a $6 \times n$ binary matrix, i.e., $\boldsymbol{S}_{ABC} = (\boldsymbol{s}_{ABC}[1], \boldsymbol{s}_{ABC}[2], \ldots, \boldsymbol{s}_{ABC}[n])$. The sequence of LNCC $\boldsymbol{s}_{\mathcal{L}}$ is as $\boldsymbol{S}_{\mathcal{L}}$, which is a $4 \times n$ binary matrix, i.e., $\boldsymbol{s}_{\mathcal{L}} = (\boldsymbol{s}_{\mathcal{L}}[1], \boldsymbol{s}_{\mathcal{L}}[2], \ldots, \boldsymbol{s}_{\mathcal{L}}[n])$. The sequence of $s_{\mathcal{L},m}$, $m \in \{1, 2, 3, 4\}$, is denoted as $\boldsymbol{s}_{\mathcal{L},m}$, which is the m-th level of $\boldsymbol{s}_{\mathcal{L}}$.

The system diagram of MLC is illustrated in Fig. 1. Recall from (7.5) and (7.6) that each bit level of $\boldsymbol{S}_{\mathcal{L}}$ is a linear combination of $\boldsymbol{s}_{i,j}$, where $i \in \{A, B, C\}$ and $j \in \{1, 2\}$. This implies that the independent decoding of $\boldsymbol{s}_{\mathcal{L},n}$ is feasible if and only if $\boldsymbol{s}_{\mathcal{L},n}$ is a valid channel coded sequence. Let $\boldsymbol{d}_{i,j} \in \mathrm{GF}^k(2)$ denotes the k-length uncoded binary data sequence from user i,$i \in \{A, B, C\}$. A rate k/n linear code is adopted by each user and the encoder function is denoted as $\mathcal{C} : \mathrm{GF}^k(2) \rightarrow \mathrm{GF}^n(2)$. Then the coded sequence of $\boldsymbol{s}_{i,j}$ is generated from encoding $\boldsymbol{d}_{i,j}$ using $\mathcal{C}(\cdot)$, given by $\boldsymbol{s}_{i,j} = \mathcal{C}(d_{i,j})$.

As the linearity of $\mathcal{C}$ and $\mathcal{L}$ in (7.5) is guaranteed, we know that the hierarchical decode-and-forward paradigm [7] is enabled that is, the bit level $\boldsymbol{s}_{\mathcal{L},n}$ of the resulting LNCC itself is a valid code sequence of $\mathcal{C}$ and can be directly fed into the inverse function of $\mathcal{C}(\cdot)$, i.e., the decoder function $\mathcal{C}^{-1}(\cdot)$. Inspired by this, independent decoding on each level is formulated as

$$\begin{bmatrix} \mathcal{C}^{-1}(\boldsymbol{s}_{\mathcal{L},1}) \\ \mathcal{C}^{-1}(\boldsymbol{s}_{\mathcal{L},2}) \\ \mathcal{C}^{-1}(\boldsymbol{s}_{\mathcal{L},3}) \\ \mathcal{C}^{-1}(\boldsymbol{s}_{\mathcal{L},4}) \end{bmatrix} = \begin{bmatrix} \mathcal{C}^{-1}\left(\boldsymbol{G}(1,:) \otimes \boldsymbol{s}_{ABC}\right) \\ \mathcal{C}^{-1}\left(\boldsymbol{G}(2,:) \otimes \boldsymbol{s}_{ABC}\right) \\ \mathcal{C}^{-1}\left(\boldsymbol{G}(3,:) \otimes \boldsymbol{s}_{ABC}\right) \\ \mathcal{C}^{-1}\left(\boldsymbol{G}(4,:) \otimes \boldsymbol{s}_{ABC}\right) \end{bmatrix} \tag{7.23}$$

where $\boldsymbol{G}(m,:), m \in \{1,2,3\}$, is the m-the row of $\boldsymbol{G}$.

As each bit level of $\boldsymbol{s}_{\mathcal{L}}$ is a linear function of the coded sequence $\boldsymbol{s}_{i,j}$, the output of the decoder function is then a linear combination of $\boldsymbol{d}_{i,j}$. This is due to the fact that the proposed LPNC does not break the linearity of channel code. Based on these, (7.23) can be expanded as

$$\begin{bmatrix} \mathcal{C}^{-1}(\boldsymbol{s}_{\mathcal{L},1}) \\ \mathcal{C}^{-1}(\boldsymbol{s}_{\mathcal{L},2}) \\ \mathcal{C}^{-1}(\boldsymbol{s}_{\mathcal{L},3}) \\ \mathcal{C}^{-1}(\boldsymbol{s}_{\mathcal{L},4}) \end{bmatrix} = \boldsymbol{G} \otimes \begin{bmatrix} \mathcal{C}^{-1}(\boldsymbol{s}_{A,1}) \\ \mathcal{C}^{-1}(\boldsymbol{s}_{A,2}) \\ \mathcal{C}^{-1}(\boldsymbol{s}_{B,1}) \\ \mathcal{C}^{-1}(\boldsymbol{s}_{B,2}) \\ \mathcal{C}^{-1}(\boldsymbol{s}_{C,1}) \\ \mathcal{C}^{-1}(\boldsymbol{s}_{C,2}) \end{bmatrix} = \boldsymbol{G} \otimes \begin{bmatrix} \tilde{\boldsymbol{d}}_{A,1} \\ \tilde{\boldsymbol{d}}_{A,2} \\ \tilde{\boldsymbol{d}}_{B,1} \\ \tilde{\boldsymbol{d}}_{B,2} \\ \tilde{\boldsymbol{d}}_{C,1} \\ \tilde{\boldsymbol{d}}_{C,2} \end{bmatrix} \triangleq \boldsymbol{D}_{\mathcal{L}} \tag{7.24}$$

where $\tilde{X}$ denotes the decoded version of X. Let $\boldsymbol{D}_{\mathcal{L}}$ denote the resulting linear combination of $\boldsymbol{d}_{i,j}$, and it can be expanded as

$$\boldsymbol{D}_{\mathcal{L}} = \begin{bmatrix} \tilde{\boldsymbol{d}}_{\mathcal{L},1} \\ \tilde{\boldsymbol{d}}_{\mathcal{L},2} \\ \tilde{\boldsymbol{d}}_{\mathcal{L},3} \\ \tilde{\boldsymbol{d}}_{\mathcal{L},4} \end{bmatrix} \tag{7.25}$$

where $\tilde{\boldsymbol{d}}_{\mathcal{L},n}$ denotes the$n$-th decoded level of $\boldsymbol{D}_{\mathcal{L}}$.

The results of (7.24)-(7.25) show the parallel independent decoding principle of MLC-LPNC, as shown in Fig. 7.2. After the MLC decoding, $\tilde{\boldsymbol{d}}_{\mathcal{L},n}$ is re-encoded by the linear code $\mathcal{C}$ with rate k/n, given by $\tilde{\boldsymbol{s}}_{\mathcal{L},n} = \mathcal{C}\left(\tilde{\boldsymbol{d}}_{\mathcal{L},n}\right)$. Then coded sequences $(\tilde{\boldsymbol{s}}_{\mathcal{L},4}, \tilde{\boldsymbol{s}}_{\mathcal{L},3}, \tilde{\boldsymbol{s}}_{\mathcal{L},2}, \tilde{\boldsymbol{s}}_{\mathcal{L},1})$ are mapped into the complex symbol sequence, given by

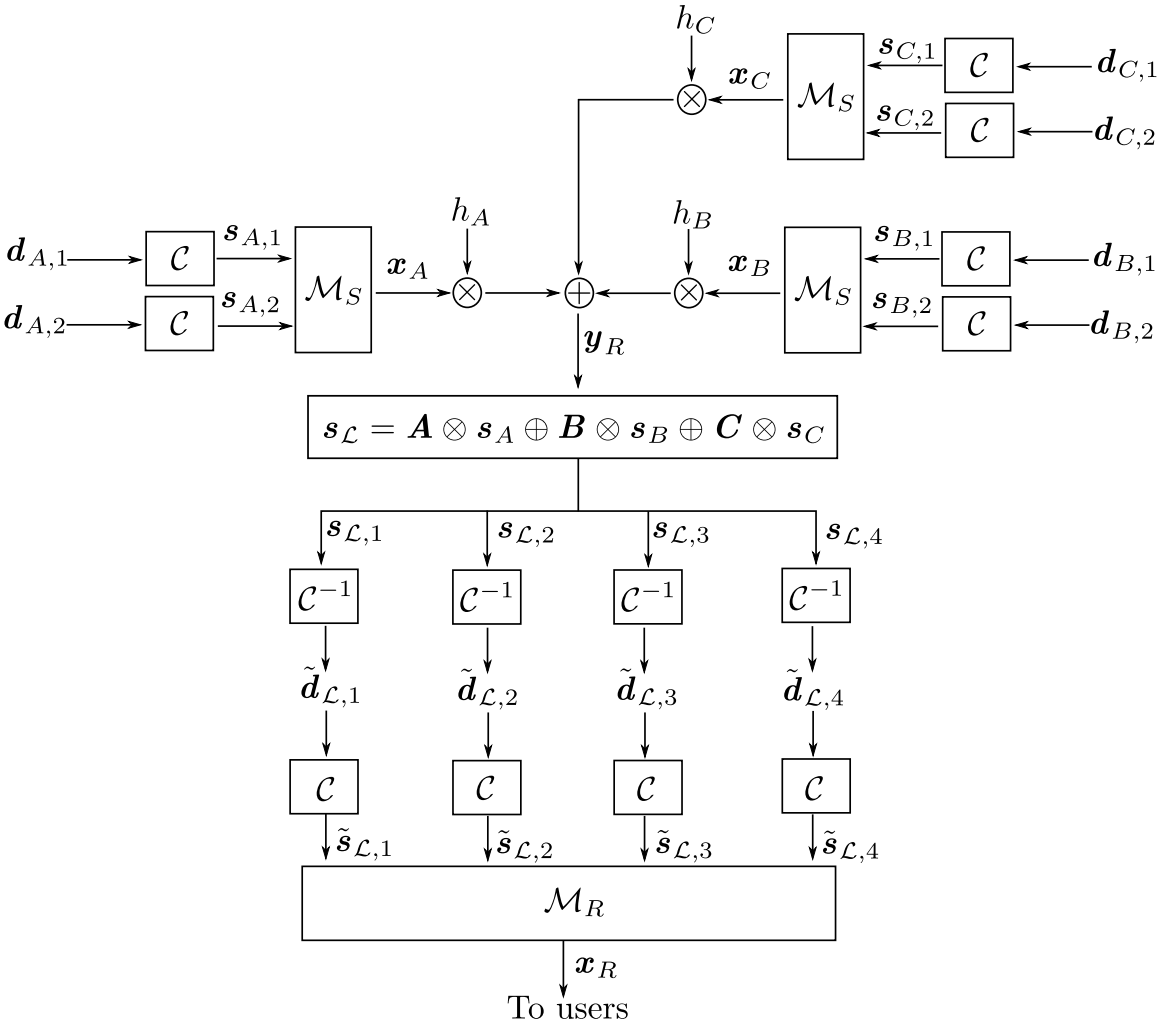

Figure 7.2: The System Diagram of MLC-LPNC

$x_R = \mathcal{M}_R\left(\tilde{\boldsymbol{s}}_{\mathcal{L},4},\tilde{\boldsymbol{s}}_{\mathcal{L},3},\tilde{\boldsymbol{s}}_{\mathcal{L},2},\tilde{\boldsymbol{s}}_{\mathcal{L},1}\right)$, where $\mathcal{M}_R : \mathrm{GF}^n\left(2^4\right) \rightarrow \mathscr{A}_{16}^n$ is the constellation mapper at *R*.

7.6 Low-complexity Approach and Benchmarks

In this section, we first carry out random LPNC, a low-complexity approach for multilevel network coded M-WRC; and secondly, several existing strategies in M-WRC are introduced as the benchmarks.

7.6.1 Random LPNC

It is worth noting that the selection criterion in (7.22) is a fully adaptive approach which requires a high computational capability at the relay. Against this backdrop, we introduce the concept of random LPNC, where the generator matrix is randomly selected from a valid search space, given by

$$\begin{aligned} \tilde{\boldsymbol{G}} \in \{\boldsymbol{G} : \boldsymbol{s}_{\mathcal{L}} = \boldsymbol{G} \otimes \boldsymbol{s}_{ABC}\} \\ \text{s.t. } \hat{\boldsymbol{s}}_{ABC} = \boldsymbol{\Gamma}_A^{-1} \otimes \boldsymbol{r}_A, \\ \hat{\boldsymbol{s}}_{ABC} = \boldsymbol{\Gamma}_B^{-1} \otimes \boldsymbol{r}_B, \\ \hat{\boldsymbol{s}}_{ABC} = \boldsymbol{\Gamma}_C^{-1} \otimes \boldsymbol{r}_C. \end{aligned} \tag{7.26}$$

Clearly, the random selection relaxes the criterion of sum-rate maximization and hence degrades the performance compared with the fully adaptive selection in (7.22).

7.6.2 Benchmarks

Latin Cube based PNC

The Latin cube based PNC for 3-WRC is introduced in [56, 57], in which, the relay adaptively transforms the Latin cube to generate the PNC mapping based on the channel states.

The users decode the desired symbols by looking up the Latin cube. The cardinality of the resulting PNC alphabet is between 16 and 23, which requires the irregular modulation in BC phase. We note that the Latin cube based PNC is in fact a type of non-linear mapping as 5QAM-DNF in 2-WRC [8].

Opportunistic Scheduling for PNC

The authors in [14] introduces an opportunistic user selection scheme for the 3-WRC, where two selection criteria based on the channel norm and the minimum distance are adopted.

7.7 Outage Probability Analysis

In this section, we provide the analysis on outage probability for the proposed MLC-LPNC and benchmarks.

7.7.1 Outage Probability of MLC-LPNC

For MLC-LPNC facilitated 3-WRC, an outage event for data transmission by user i occurs when either the MAC phase or the single transmission from R to user i in the BC phase is in outage. Therefore, in terms of end-to-end transmission, the outage probability for the MLC-LPNC facilitated 3-WRC is calculated as

$$P_{\mathrm{LPNC},i}^{\mathrm{Out}} = 1 - \left(1 - P_{\mathrm{MAC}}^{\mathrm{Out}}(R_{\mathrm{NCS}})\right) \prod_{j \neq i} \left(1 - P_{\mathrm{BC}}^{\mathrm{Out}}(R_{R,j})\right) \tag{7.27}$$

where R_{NCS} and $R_{R,j}$ represent the computation rate with respect to NCS and the transmission rate from R to user j, $(j \neq i)$; $P_{\mathrm{MAC}}^{\mathrm{Out}}(R_{\mathrm{NCS}})$ represents the outage probability in the MAC phase, given by

$$P_{\mathrm{MAC}}^{\mathrm{Out}}(R_{\mathrm{NCS}}) = \Pr\left\{ \frac{1}{2} I^{\widetilde{\boldsymbol{G}}}(Y_R; \boldsymbol{S}_{\mathcal{L}}) < R_{\mathrm{NCS}} \right\} \tag{7.28}$$

where the factor $\frac{1}{2}$ is due to the two channel uses and similarly hereafter. The mutual information $I^{\widetilde{\boldsymbol{G}}}(Y_R; \boldsymbol{S}_{\mathcal{L}})$ is obtained from (7.22), which indicates that an outage event occurs in the MAC phase if the maximized mutual information $\frac{1}{2}I^{\widetilde{\boldsymbol{G}}}(Y_R; \boldsymbol{S}_{\mathcal{L}})$ cannot support the computation rate R_{NCS}. The quantity$P_{\mathrm{BC}}^{\mathrm{Out}}(R_{R,i})$in (12) defines the outage probability in the BC phase, with respect to the single transmission from R to user i, given by

$$P_{\mathrm{BC}}^{\mathrm{Out}}(R_{R,j}) = \Pr\left\{\frac{1}{2}I(Y_j; X_R) < R_{R,j}\right\} \tag{7.29}$$

where $I(Y_j; X_R)$ denotes the mutual information between received signal y_j at user j and transmitted signal x_R at R.

7.7.2 Latin Cube based PNC

For Latin cube based PNC, the outage probability in terms of end-to-end transmission takes the same form as (12). The outage probability for Latin square based PNC, in the MAC phase, is given by

$$P_{\mathrm{MAC}}^{\mathrm{Out}}(R_{\mathrm{NCS}}) = \Pr\left\{\frac{1}{2}I(Y_R; S_{\mathrm{NCS}}) < R_{\mathrm{NCS}}\right\} \tag{7.30}$$

where s_{NCS} is Latin cube generated NCS whose cardinality is between 16 and 23. Clearly, the outage probability in the BC phase should satisfy

$$P_{\mathrm{BC}}^{\mathrm{Out}}(R_{R,j}) = \Pr\left\{\frac{1}{2}I(Y_j; X_R) < R_{R,j}\right\} \tag{7.31}$$

where the relay adaptively transmit the signalx_R with different alphabet cardinalities (16 to 23), based on the generated NCS.

7.7.3 Opportunistic Scheduling for PNC

Clearly, the opportunistic scheduling based PNC groups all users in pairs. Let $U_1 \triangleq \{A, B\}$, $U_2 \triangleq \{A, C\}$ and $U_3 \triangleq \{B, C\}$ define the corresponding user groups and the

index of the user groups is denoted as m.

The outage probability with respect to the opportunistic scheduling for PNC is given by

$$P_{\mathrm{TS},i}^{\mathrm{Out}} = 1 - \prod_{m} \left(1 - P_{\mathrm{MAC}}^{\mathrm{Out}}(R_{\mathrm{NCS},m})\right) \prod_{j \in U_m / \{i\}} \left(1 - P_{\mathrm{BC}}^{\mathrm{Out}}(R_{R,j})\right) \tag{7.32}$$

Here, $P_{\mathrm{MAC}}^{\mathrm{Out}}(R_{\mathrm{NCS}})$ is the outage probability in the MAC phase for the m-the scheduled user pair, given by

$$P_{\mathrm{MAC}}^{\mathrm{Out}}(R_{\mathrm{NCS},m}) = \Pr\left\{\frac{1}{6} I(Y_R; S_{\mathrm{NCS},m}) < R_{\mathrm{NCS},m}\right\} \tag{7.33}$$

where the factor $\frac{1}{6}$ is due to the six channel uses and $s_{\mathrm{NCS},m}$ is the NCS, generated by the non-linear mapping for the m-the scheduled user pair.

The quantity $P_{\mathrm{BC}}^{\mathrm{Out}}(R_{R,j})$in (7) is the outage probability in the BC phase, for broadcasting $s_{\mathrm{NCS},m}$to the m-the scheduled user pair, which is calculated as

$$P_{\mathrm{BC}}^{\mathrm{Out}}(R_{R,j}) = \Pr\left\{\frac{1}{6} I(Y_j; X_R) < R_{R,j}\right\} \tag{7.34}$$

The corresponding evaluations on the derived outage probability for MCL-LPNC, Latin cube based PNC and the opportunistic scheduling based PNC are accordingly provided in the next section.

7.8 Performance Evaluation

In this section, we evaluate the end-to-end symbol error rate (FER) and the sum-rate for the proposed design and the benchmarks in Rayleigh fading 3-WRC. The length of the original data packet is 512 bits. A rate 1/2 convolutional code with generator polynomials $(133, 171)_8$ is adopted.

Based on Fig. 7.3, we observe that the FER of the uncoded LPNC is slightly higher than that of the Latin cube based PNC. This is because: 1) the Latin cube based PNC has a larger cardinality (16 to 23) of NCS such that it has a better interference mitigation

capability compared with the uncoded LPNC. and 2) the uncoded LPNC has a smaller cardinality (16) of LNCC alphabet which results in a superior transmission performance in the BC phase. A key superiority of the proposed LPNC is that it can directly adopt the channel codes whereas the Latin cube based PNC cannot due to its non-linear property. In Fig. 7.3, we also observe that the proposed MLC-LPNC provides a significant coding gain over the Latin cube based PNC.

Fig. 7.4 shows the sum-rate comparison, in terms of end-to-end transmission, for proposed design and benchmarks. We observe that the proposed design outperforms the other two benchmarks. This is due to the minimum cardinality constraint (compared with Latin cube based PNC) and improved spectral efficiency (compared with the opportunistic scheduling based PNC) of the proposed design.

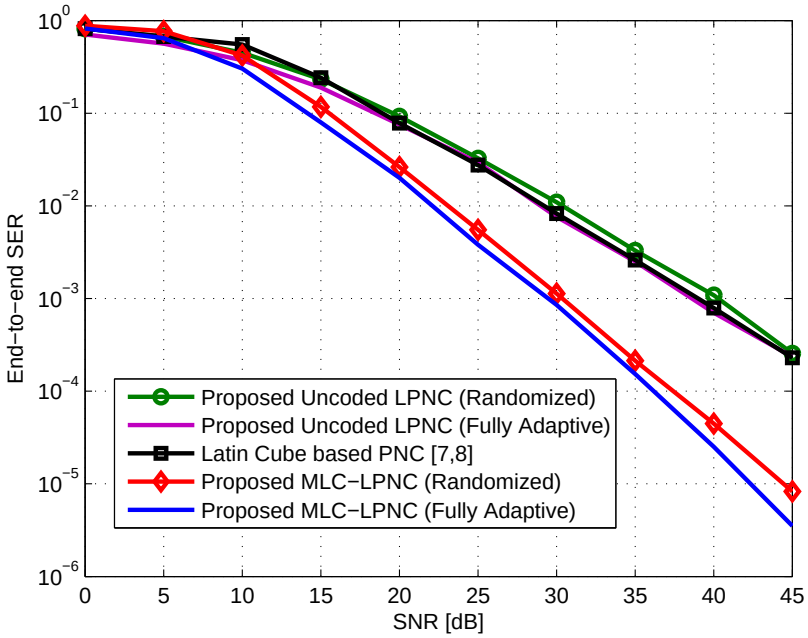

Figure 7.3: FER comparison for different strategies

7.9 Summary

In this chapter, we have proposed a novel LPNC over the 3-WRC. The relay maps the superimposed signal into the linear network coded combination (LNCC, regarded as network coded symbol) by multiplying the user data by a properly selected generator matrix.

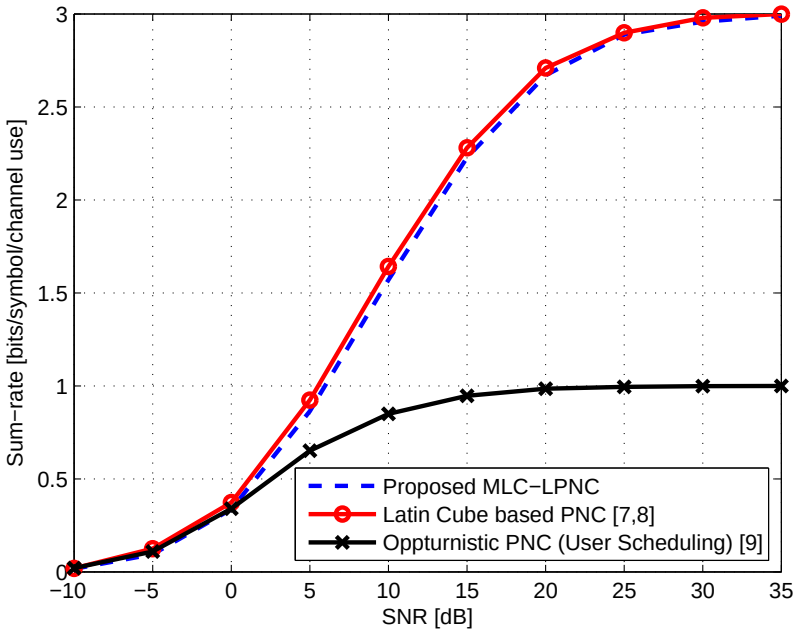

Figure 7.4: Sum-rate comparison for different strategies

A sum-rate based mapping selection scheme is also introduced for generating the optimal LNCC. The unambiguous decoding and minimum cardinality of the proposed LPNC mapping were investigated. The proposed LPNC facilitates the multilevel coding structure using parallel independent coding levels in which each level is a linear function of the user data. This enables the hierarchical decode-and-forward paradigm as in [7]. The simulation results show that: 1) the uncoded LPNC achieves the equal error performance compared with the Latin cube based PNC [56, 57]; 2) the uncoded LPNC provides a superior sum-rate over the opportunistic Scheduling based PNC; and 3) MLC-LPNC shows coding gain over two benchmarks.

Chapter 8

Conclusions and Future Work

Contents

8.1 Summary of Work

In this thesis, we have focused on designing PNC for cooperative wireless networks. To address the challenge of fading in the 2-WRC, we proposed two coded strategies for PNC to compensate the phase shift introduced by the relative fading. Furthermore, a new LPNC over the hybrid ring was also proposed for Rayleigh fading 2-WRC, where all singular fade states can be eliminated by the enlarged NCS alphabet, based on the ring theory. We then redesigned the PNC to accommodate the multi-user scenario such as HWN and M-WRC. For HWN, we have proposed the PNC-JD and ANC-IAML for exploiting the

C-CI. For M-WRC, we have proposed the MLC-LPNC strategy which facilitates the HDF paradigm for multi-user data exchange.

In the following, we summarize the work reported in each chapter of this thesis.

In Chapter 3, RICM and SBC-QF are proposed for coded PNC in the fading 2-WRC. The RICM and SBC-QF eliminate the fading effect at relay and destination, respectively. The RICM exploits the nature of the phase shift which is introduced by the relative fading factor of the 2-WRC such that the rotated coding levels have been shown to mitigate the ambiguous decoding due to the phase shift. In contrast to RICM, SBC combats the fading in the MAC phase at the user side. In such a strategy, the relay maps the received superimposed signal into the network coded soft-bit rather than decodes it. Then the network coded soft-bit is quantized and broadcasted to users. We prove that the designed quantizer is robust in the fading 2-WRC. The fading effect is removed by the soft-bit level XOR operation.

In Chapter 4, we have proposed a novel multilevel coded LPNC-EM for Rayleigh fading 2-WRC. The relay node adaptively selects the linear generator matrix and directly maps the superimposed signal of the two users into the linear network coded combination over the hybrid Galois Field ($\mathrm{GF}(2^2)$ or $\mathrm{GF}(2^3)$). The selection criterion ensures unambiguous decoding and maximizes the individual rate of each user. The LPNC-EM scheme forms two or three independent coding levels which facilitate the use of multilevel coding. This enables the hierarchical decode-and-forward strategy. The numerical results show that uncoded LPNC-EM outperforms the original PNC in [1] and can achieve a error performance as good as that of the 5QAM-DNF in [8]. Furthermore, the multilevel coded LPNC-EM also provides a superior error performance compared with the coded original PNC.

In Chapter 5, HFR-LPNC is proposed for dealing with the singular fading. The superimposed signal of the two users maps the LNCC in different finite rings. The optimal linear coefficients of LNCC are selected based on: 1) maximizing the sum-rate in MAC phase; and 2) ensuring the criterion of unambiguous decoding. The properly designed source coding is used for compressing the LNCC alphabet over hybrid Galois field into the unifying 4-ary alphabet. The end-to-end sum-rates of HGF-LPNC and the 5QAM-

DNF [8] are derived for comparison. It can be confirmed by the analytical results and simulation that 1) HFR-LPNC has a superior ability to mitigate the singular fading compared with 5QAM-DNF; and 2) HGF-LPNC is superior to 5QAM-DNF over a wide range of SNRs.

In Chapter 6, PNC are redesigned to accommodate in the multiuser HWN. To exploit the C-CI, a joint decoding approach is proposed such that the useful and interference symbols can be jointly decoded. For comparison, we also redesign the ANC for HWN, in which interference-aware ML (IAML) detection is used to mitigate the C-CI. Furthermore, the constellation constrained sum-rates for PNC with JD, ANC with IAML and TDMA based PNC are derived. The analytical and simulation result demonstrate the substantial performance enhancement provided by the proposed strategies over the ANC-IMAL AND TDMA-PNC in HWN.

Finally, in chapter 7, a novel linear physical-layer network coding (LPNC) over 3-way relay channels (3-WRC) is proposed. The relay maps the superimposed signal into the linear network coded combination (LNCC, regarded as network coded symbol) by multiplying the user data by a properly selected generator matrix. A sum-rate based mapping selection scheme is also introduced for generating the optimal LNCC. The unambiguous decoding and minimum cardinality of the proposed LPNC mapping are investigated. The proposed LPNC facilitates the multilevel coding structure using the parallel independent coding levels, in which each level is a linear function of user data. This enables the hierarchical decode-and-forward paradigm [7] for multiuser data exchange. The simulation results show that: 1) the un-encoded LPNC achieves the equal error performance compared with the latin cube based PNC [56,57]; 2) the un-encoded LPNC provides a superior sum-rate over the opportunistic Scheduling based PNC; and 3) MLC-LPNC shows the coding gain over two benchmarks.

8.2 Future Work

Future avenues of relevant research are listed as follows:

- The linear code based CPF for multiuser network will be further investigated. In particular, the error correction capability of linear codes will be used to solve the the multiple access interference. Due to the singular fade states, the cardinality of code alphabet should be extended to compensate the error introduced by channels.

- PNC constructed from linear codes will be explored, where the NCSs, generated at the relays, is a valid codeword of the linear block code such that the destination can collect all NCSs and decode them as a codeword. This overcomes the deep fading and errors in the BC phase.

- Lattice network coding will be considered to accommodate the common communication system design over finite field $\mathrm{GF}(2^{\mathrm{m}})$ where m is an integer.

Appendix A: Proof of Theorem 2 in Chapter 4

Proof. Assume that the MAC phase is free from errors. Then the mapping procedure for $s_{\mathcal{L}}^{(q)}$ at the relay can be regarded as discrete memoryless source encoding in which the 4-bit binary tuple $s_{AB} \triangleq (s_A, s_B)$ is the input symbol; and $s_{\mathcal{L}}^{(q)}$ is output symbol. Due to the exclusive law, each s_{AB} corresponds to an unique $s_{\mathcal{L}}^{(q)}$.

The sequence of q-ary symbols $s_{\mathcal{L}}^{(q)}$ is denoted as $\mathbf{s}_{\mathcal{L}}^{(q)}$, where the length of $\mathbf{s}_{\mathcal{L}}^{(q)}$ is N and we assume $N \to \infty$. Let $\mathbf{b}_{\mathcal{L}}^{(q)}$ denote the binary representation of $\mathbf{s}_{\mathcal{L}}^{(q)}$, where the average length of $\mathbf{b}_{\mathcal{L}}^{(q)}$ is $\bar{K} = H\left(s_{\mathcal{L}}^{(q)}\right) \times N$ (the length of $\mathbf{b}_{\mathcal{L}}^{(q)}$ varies from frame to frame). For simplicity of notation, we omit the index of elements in $\mathbf{b}_{\mathcal{L}}^{(q)}$ and similarly hereafter. The element of $\mathbf{b}_{\mathcal{L}}^{(q)}$ is denoted as $B_{\mathcal{L}}^{(q)}$. Clearly, $B_{\mathcal{L}}^{(q)}$ is not uniformly distributed since $s_{\mathcal{L}}^{(q)}$ is not uniformly distributed.

The sequence of 16-ary symbols s_{AB} is denoted as $\mathbf{s}_{AB}$ whose length is also equal to N. We note that s_{AB} is uniformly distributed with probability 1/16 as it is drawn from two QPSK alphabets. Let $\mathbf{b}_{AB}$ denote the binary representation of $\mathbf{s}_{AB}$, where the length of $\mathbf{b}_{AB}$ is $L = \log_2(16) \times N = 4N$. An element of $\mathbf{b}_{AB}$ is denoted as b_{AB}. Clearly, b_{AB} is uniformly distributed since s_{AB} is uniformly distributed. Hence we have $H(b_{AB}) = \log_2(2) = 1$.

We note that the entropy of $s_{\mathcal{L}}^{(q)}$ is constant over during the whole mapping procedure. According to Shannon's variable–length source coding theorem, we have

$$\frac{H\left(B_{\mathcal{L}}^{(q)}\right)}{\log_2(2)} + \varepsilon \geq \frac{\bar{K}}{L} \geq \frac{H\left(B_{\mathcal{L}}^{(q)}\right)}{\log_2(2)}, \tag{1}$$

where $\varepsilon = \frac{1}{L} \to 0$ as $L = 4N \to \infty$. Hence (1) can be further written as

$$\frac{\bar{K}}{L} = \frac{H\left(B_{\mathcal{L}}^{(q)}\right)}{\log_2(2)}. \tag{2}$$

Based on this, we know that when $N \to \infty$ the average code rate of the equivalent source encoder, denoted by $\bar{\mathscr{R}}$, is then given as $\bar{\mathscr{R}} = \frac{H\left(S_{\mathcal{L}}^{(q)}\right)}{4}$.

Now we consider a distorted MAC phase. We note that the relay can receive up to $R_{AB,\max}^{(1)}$ bits per symbol for s_{AB}, where $R_{AB,\max}^{(1)}$ denotes the maximal achievable rate

of s_{AB}. The linear mapper outputs the LNCC $s_{\mathcal{L}}^{(q)}$ with rate up to $I\left(Y_R; S_{\mathcal{L}}^{(q)}\right)$ bits per symbol. The average code (mapping) rate $\bar{\mathscr{R}}$ is constant when $N \to \infty$ since each s_{AB} is corresponding to an unique $s_{\mathcal{L}}^{(q)}$. Based on this, we have

$$\bar{\mathscr{R}} = \frac{H\left(S_{\mathcal{L}}^{(q)}\right)}{4} = \frac{I\left(Y_R; S_{\mathcal{L}}^{(q)}\right)}{R_{AB,\max}^{(1)}}. \tag{3}$$

Based on (13), the input rate with respect to s_{AB}, namely, the sum-rate in the MAC phase, $R_{AB}^{(1)}$, should be bounded by

$$R_{AB}^{(1)} \leq \frac{4}{H\left(S_{\mathcal{L}}^{(q)}\right)} I\left(Y_R; S_{\mathcal{L}}^{(q)}\right). \tag{4}$$

Let $P_{e,i}\{s_{\mathcal{L}}^{(q)} \neq \tilde{s}_{\mathcal{L}}^{(q)}\}$ denote the error rate of the BC phase at user i, where $\tilde{s}_{\mathcal{L}}^{(q)}$denotes the received LNCC. Assuming that the BC is error-free, *A* decodes s_B using successfully received $s_{\mathcal{L}}^{(q)}$ and C-SI s_A. Hence the the end-to-end achievable rate of *B* is equal to the rate of that in the MAC phase, given by

$$R_B^{(1)} = R_B, \quad \text{iff.}\, P_{e,A}(s_{\mathcal{L}}^{(q)} \neq \tilde{s}_{\mathcal{L}}^{(q)}) = 0 \tag{5}$$

and similarly, we have

$$R_A^{(1)} = R_A, \quad \text{iff.}\, P_{e,B}(s_{\mathcal{L}}^{(q)} \neq \tilde{s}_{\mathcal{L}}^{(q)}) = 0. \tag{6}$$

Here $R_i, i \in \{A, B\}$ denotes the end-to-end achievable rate. The results of (5) and (6) can be used to measure the individual achievable rate of each user in the MAC phase.

We understand that if BC phase is error-free, the end-to-end achievable rate of *B* can be calculated as

$$R_B \leq I\left(Y_R; \hat{S}_B | S_A\right), \quad \text{iff.}\, P_{e,A}(s_{\mathcal{L}}^{(q)} \neq \tilde{s}_{\mathcal{L}}^{(q)}) = 0 \tag{7}$$

and similarly, the end-to-end achievable rate of *A* is given by

$$R_A \leq I\left(Y_R; \hat{S}_A | S_B\right), \quad \text{iff.}\, P_{e,B}(s_{\mathcal{L}}^{(q)} \neq \tilde{s}_{\mathcal{L}}^{(q)}) = 0. \tag{8}$$

Then the individual achievable rate of each user in the MAC phase is bounded by

$$\begin{aligned} R_A^{(1)} &\leq I\left(Y_R; \hat{S}_A | S_B\right) \\ R_B^{(1)} &\leq I\left(Y_R; \hat{S}_B | S_A\right). \end{aligned} \tag{9}$$

Based on (4) and (9), we have

$$\begin{aligned} R_A^{(1)} &\leq I\left(Y_R; \hat{S}_A | S_B\right) \\ R_B^{(1)} &\leq I\left(Y_R; \hat{S}_B | S_A\right) \\ R_{AB}^{(1)} &\leq \frac{4}{H\left(S_{\mathcal{L}}^{(q)}\right)} I\left(Y_R; S_{\mathcal{L}}^{(q)}\right). \end{aligned} \tag{10}$$

This completes the proof of **Theorem 2**. □

Appendix B: Proof of Theorem 2 in Chapter 6

Proof. Assume that the MAC phase is free from errors. Then the mapping procedure for $s_{\mathcal{L}}^{(q)}$ at R can be regarded as discrete memoryless source encoding in which the 6-bit binary tuple $\boldsymbol{s}_{ABC}$ is the input symbol; and 4-bit binary tuple $\boldsymbol{s}_{\mathcal{L}}$ is output symbol. Due to the exclusive law, each $\boldsymbol{s}_{ABC}$ corresponds to an unique $\boldsymbol{s}_{\mathcal{L}}$.

We understand that $\boldsymbol{s}_{ABC}$ is uniformly distributed over GF(2^6) as it is drawn from 3 QPSK alphabets. Therefore, in an error-free MAC phase, the rate of $\boldsymbol{s}_{ABC}$, namely, the sum-rate in the MAC stage, is then equal to $H\left(\boldsymbol{s}_{ABC}\right) = \log_2\left(2^6\right) = 6$ bits/symbol. Let L denote the length of the binary sequence of $\boldsymbol{s}_{ABC}$.

As the MAC stage is free from errors, the LNCC $\boldsymbol{s}_{\mathcal{L}}$ after LPNC decoding is then error-free. Due to the uniformity of each source data and linearity of mapping function in (7.7), the resulting $\boldsymbol{s}_{\mathcal{L}}$ tends to be uniformly distributed over GF(2^4). As such, the computation rate of $\boldsymbol{s}_{\mathcal{L}}$, is equal to $H\left(\boldsymbol{S}_{\mathcal{L}}\right) = \log_2\left(2^4\right) = 4$ bits/symbol. Let K denote the length of the binary sequence of $\boldsymbol{s}_{\mathcal{L}}$.

We note that the entropy of $\boldsymbol{s}_{\mathcal{L}}$ is constant over during the whole mapping procedure. According to Shannon's source coding theorem, we have

$$\frac{K}{L} = \frac{H\left(\boldsymbol{S}_{\mathcal{L}}\right)}{H\left(\boldsymbol{S}_{ABC}\right)} \tag{11}$$

such that the average code rate of the equivalent source encoder is then $\bar{\mathcal{R}} = \frac{K}{L} = \frac{H(\boldsymbol{s}_{\mathcal{L}})}{H(\boldsymbol{s}_{ABC})} = \frac{4}{6}$.

Now we consider a distorted MAC phase. We note that the relay R can receive up to $R_{ABC,\max}^{(1)}$ bits per symbol for $\boldsymbol{s}_{ABC}$, where $R_{ABC,\max}^{(1)}$denotes the maximal achievable rate of $\boldsymbol{s}_{ABC}$. The linear mapper outputs the LNCC $\boldsymbol{s}_{\mathcal{L}}$ with rate up to $I\left(Y_R; \boldsymbol{S}_{\mathcal{L}}\right)$ bits per symbol. The average code (mapping) rate $\bar{\mathcal{R}} = \frac{4}{6}$ is constant since each $\boldsymbol{s}_{ABC}$ corresponds to an unique $\boldsymbol{s}_{\mathcal{L}}$. Based on this, we have

$$\bar{\mathcal{R}} = \frac{4}{6} = \frac{I\left(Y_R; \boldsymbol{S}_{\mathcal{L}}\right)}{R_{ABC,\max}^{(1)}}. \tag{12}$$

Based on (1), the input rate with respect to $\boldsymbol{s}_{ABC}$, namely, the sum-rate in the MAC phase, $R_{ABC}^{(1)}$, should be bounded by

$$R_{ABC}^{(1)} \leq \frac{6}{4} I\left(Y_R; \boldsymbol{S}_{\mathcal{L}}\right), \tag{13}$$

which completes the proof of **Theorem 2**. □

Glossary

2-WRC	**T**wo-**w**ay **R**elay **C**hannel
3-WRC	**T**hree-**w**ay **R**elay **C**hannel
AWGN	**A**dditive **W**hite-**G**aussian-**N**oise
BC	**B**roadcast **C**hannel
BER	**B**it **E**rror **R**ate
CPF	**C**om**p**ute-and-**F**orward
CSI	**C**hannel **S**tate **I**nformation
DNF	**D**enoise-and-**F**orward
EM	**E**lectromagnetic
FEC	**F**orward **E**rror **C**orrection
FER	**F**rame **E**rror **R**ate
i.i.d.	**i**ndependent and **i**dentically **d**istributed
LLR	**L**og-**L**iklihood **R**atio
LNCC	**L**inear **N**etwork **C**oded **C**ombination
LPNC	**L**inear **P**hysical-layer **N**etwork **C**oding
MAC	**M**uliple *Acess Channel*
MAP	**M**aximum *A Posteriori*
ML	**M**aximum-**L**ikelihood
MLC	**M**uli-**l**evel Coding
M-WRC	**M**uli-**w**ay **R**elay **C**hannel
NCS	**N**etwork **C**oded **S**ymbol
NCC	**N**etwork **C**oded **C**ombination
PDF	**P**robability **d**ensity **f**unction
PNC	**P**hysical-layer **N**etwrok **C**oding
SBC	**S**oft **B**it **C**orrection
SER	**S**symbol **E**rror **R**ate
SIC	**S**uccessive **I**nterference **C**ancelation
SINR	**S**ignal-to-**I**nterference-plus-**N**oise **R**atio
SNR	**S**ignal-to-**N**oise-**R**atio
RICM	**R**otationally **I**nvariant **C**oded **M**odulation

HFR-LPNC **L**inear **P**hysical-layer **N**etwork **C**oding over the **H**ybrid **F**inite **R**ing

Bibliography

[1] S. Zhang, S. C. Liew, and P. K. Lam, "Hot Topic: Physical-Layer Network Coding," *in Proc. Annual Int. Conf. on Mobile Computing and Networking (MobiCom)*, LA, USA, Sept. 2006.

[2] J. Sykora and A. Burr, "Hierarchical alphabet and parametric channel constrained capacity regions for HDF strategy in parametric wireless 2-WRC," *in Proc. IEEE Wireless Commun. Network. Conf. (WCNC)*, Sydney, Australia, April 2010.

[3] T. Koike-Akino, P. Popovski, and V. Tarokh, "Denoising maps and constellations for wireless network coding in two-way relaying systems," *in Proc. IEEE Global Telecommun. Conf. (GlobeCom)*, USA, 2008.

[4] T. Koike-Akino, P. Popovski, and V. Tarokh, "Denoising strategy for convolutionally-coded bidirectional relaying," *in Proc. IEEE Int. Conf. Comm. (ICC)*, Dresden, Germany, June 2009.

[5] P. Popovski and H. Yomo, "Physical network coding in two-way wireless relay channels," *in Proc. IEEE Int. Conf. Commun. (ICC)*, Glasgow, Scotland, Jun. 2007

[6] S. Katti, S. Gollakota, and D. Katabi, "Embracing wireless interference: Analog network coding," *in Proceeding of ACM SIGCOMM*, Kyoto, Japan, pp. 397-408, Aug. 2007.

[7] J. Sykora and A. G. Burr, "Layered design of hierarchical exclusive codebook and its capacity regions for HDF strategy in parametric wireless 2-WRC," *IEEE Trans. Veh. Technol.*, vol. 60, no.7, pp.3241-3252, Sep. 2011.

[8] T. Koike-Akino, P. Popovski, and V. Tarokh, "Optimized constellations for two-way wireless relaying with physical network coding," *IEEE J. Sel. Areas Commun.*, vol. 27, no. 5, pp. 77-787, Jun. 2009.

[9] C. E. Shannon, "Two-way communication channels," *in Proc. 4th Berkeley Symp. Math. Stat. Probab.*, vol. I, 1961, pp. 611644.

[10] E. C. van der Meulen, "Three-terminal communication channels," *Adv. Appl. Probab.*, vol. 3, no. 1, pp. 120154, 1971.

[11] T. Cover and A. El Gamal, "Capacity theorems for the relay channel," *IEEE Trans. Inform. Theory*, vol. 25, no. 5, pp. 572584, Sep. 1979.

[12] S. Shukla and B. Sundar Rajan, "Wireless network-coded three-way relaying using Latin Cubes", *in Proc. IEEE International Symp. on Pers. Indoor and Mobi. Radio Comm. (PIMRC)*, Syndeny, Austrilia, Oct. 2012.

[13] S. Shukla, V. T. Muralidharan, and B. Sundar Rajan, "Wireless Network-Coded Three-Way Relaying Using Latin Cubes", available online at arXiv:1112.1584 [cs.IT], Dec. 2011

[14] Y. Jeon, Y. T. Kim, M. Park, and I. Lee, "Opportunistic Scheduling for Three-way Relay Systems with Physical Layer Network Coding", *in Proc. IEEE Vehi. Tech. Conf. (VTC-Spring)*, Budapest, Hungary, May 2011.

[15] J. Liu, M. Tao and Y. Xu, "Pseudo Exclusive-OR for LDPC coded two-way relay block fading channels," *in Proc. IEEE Int. Conf. Comm. (ICC)*, Kyoto, Japan, June 2011.

[16] G. Zeitler, R. Koetter, G. Bauch, and J.Widmer,"On Quantizer Design for Soft Values in the Multiple-Access Relay Channel," *in Proc. IEEE Int. Conf. Comm. (ICC)*, Dresden, Germany, June 2009

[17] A. Winkelbauer and G. Matz, "Soft-Information-Based Joint Network-Channel Coding for the Two-Way Relay Channel," *in Proc. IEEE Int. Symp. on Network Coding (NetCod)*, Beijing, China, July 2011.

[18] S. Lloyd, "Least squares quantization in PCM," *IEEE Trans. Inform.Theory*, vol. IT-28, pp. 129-137, 1982.

[19] J. Max, "Quantizing for minimum distortion," *IEEE Trans. Inform.Theory*, vol. IT-6, pp. 7-12, 1960.

[20] D. Zwillinger and S. Kokoska, *Standard probability and Statistics tables and Formulae*, Chapman and Hall/CRC, 2000

[21] J. Hagenauer, "The EXIT chart - Introduction to extrinsic information transferin iterative processing," *in Proc. Eur. Signal Process. Conf.*, Vienna, Austria, 2004

[22] M. Tuchler, S. ten Brink, and J. Hagenauer, "Measures for tracing convergence of iterative decoding algorithms," *in Proc. 4th IEEE/ITG Conf. on Source and Channel Coding*, Berlin, Germany, Jan 2002.

[23] K. Zeger and A. Gersho, "Pseudo-gray coding," *IEEE Trans. Comm.*, vol. 38, no. 12, pp. 2147-2158, Dec. 1990.

[24] J. Liu, M. Tao and Y. Xu, "Pairwise Check Decoding for LDPC Coded Two-Way Relay Block Fading Channels," *IEEE Trans. Commun.*, vol. 60, no. 8, pp. 2065-2076, Aug. 2012

[25] B. Nazer and M. Gastpar,"Compute-and-Forward: Harnessing Interference through Structured Codes," *IEEE Trans. Inform. Theory*, vol. 57, no. pp.6463-6486, Oct. 2011.

[26] B. Nazer and M. Gastpar, "Reliable physical layer network coding," *Proceeding of IEEE*, vol. 99, no. 3, pp. 438-460, Mar. 2011.

[27] U. Niesen and P. Whiting, "The degrees-of-freedom of compute-and-forward," *IEEE Trans. Inf. Theory*, vol. 58, no. 8, Aug. 2012

[28] V. T. Muralidharan and B. S. Rajan, "Distributed Space Time Coding for Wireless Two-way Relaying," *IEEE Trans. Signal Processing*, vol. 61, pp. 980-991, Feb. 2013.

[29] L. Lu and S. C. Liew, "Asynchronous Physical-Layer Network Coding," *IEEE Trans. Wireless Commun.*, vol.12, pp.819-831, Feb. 2012.

[30] U. Bhat and T. M. Duman, "Decoding strategies for physical-layer network coding over frequency selective channels," *in Proc. of IEEE Wireless Commun. and Networking Conf. (WCNC)*, Paris, France, pp.12-18, Apr. 2012.

[31] N. Wang, Z. Ding, X. Dai and A. V. Vasilakos, "On Generalized MIMO Y Channels: Precoding Design, Mapping and Diversity Gain," *IEEE Trans. on Wireless Commun.*, vol.60, no.7, pp.3525-3532, Sep. 2011.

[32] Z. Ding, I. Krikidis, J. Thompson, and K. Leung, "Physical layer network coding and precoding for the two-way relay channel in cellular systems," *IEEE Trans. Signal Process.*, vol. 59, no. 2, pp. 696–712, Feb. 2011.

[33] T. Yang, I. Land, T. Huang, J. Yuan, Z.Chen, "Distance Spectrum and Performance of Channel-Coded Physical-Layer Network Coding for Binary-Input Gaussian Two-Way Relay Channels," *IEEE Trans. Commun.*, vol. 60, no. 6, pp. 1499-1510, Jun. 2012

[34] T. Yang, X. Yuan, P. Li, I. B. Collings, and J. Yuan, "Eigen-direction alignment based physical-layer network coding for MIMO two-way relay channels," *submitted on IEEE Trans. Inf. Theory,*, available on arXiv: http://arxiv.org/abs/1201.2471.

[35] K. Lu, S. Fu, Y. Qian, and H.-W. Chen, "SER performance analysis for physical layer network coding over AWGN channels," *in Proceeding of IEEE Global Commun. Conf. (GlobeCom)*, Hawii, USA, Dec. 2009.

[36] M. Park, I. Choi, and I. Lee, "Exact BER analysis of physical layer network coding for two-way relay channels," *in Proceeding of IEEE Veh. Technol. Conf. (VTC)*, Budapest, Hungary, May 2011.

[37] Y. Huang, Q. Song, S. Wang, and A. Jamalipour, "Symbol error rate analysis for M-QAM modulated physical-layer network coding with phase errors." *in Proceeding of IEEE Int. Sym. on on Personal, Indoor and Mobile Radio Commun. (PIMRC)*, Sydney, Austrilia, Sep. 2012.

[38] R. Ahlswede, N. Cai, S. Y. R. Li, and R. W. Yeung, "Network information flow," *IEEE Trans. Inform. Theory*, vol. 46, no. 4, pp. 1204–1216, Jul. 2000.

[39] S. Y. R. Li, R. W. Yeung, and N. Cai, "Linear network coding," *IEEE Trans. Inform. Theory*, vol. 49, no. 2, pp. 371–381, Feb. 2003

[40] T. Yang and I. B. Collings, "Asymptotically optimal error-rate performance of linear physical-layer network coding in Rayleigh fading two-way relay channels," *IEEE Commun. Letters*, vol. 16, no. 7, pp. 1068–1071, Jul. 2012.

[41] D. S. Dummit and R. M. Foote, Abstract Algebra, 3rd ed. John Wiley & Sons, Inc., 2004.

[42] W. E. Ryan and S. Lin, *Channel Codes: Classical and Modern*, Cambridge University Press, 2009.

[43] M. Valenti, D. Torrieri, and T. Ferrett, "Noncoherent physical-layer network coding using binary cpfsk modulation," *in Proceeding of IEEE Mil. Commun. Conf. (MilCom)*, pp. 1-7, Oct. 2009.

[44] T. Cui F. Gao and C. Tellambura, "Physical layer differential network coding for two-way relay channels," *in Proceeding of IEEE Global Commun. Conf. (GlobeCom)*, New Orleans, CA, 2008.

[45] Z. Yi, M. Ju, and I.-M. Kim, "Outage probability and optimum power allocation for analog network coding," *IEEE Trans. Wireless Commun.*, vol. 10, no. 2, pp. 407-412, Feb. 2011.

[46] G. Wang, W. Xiang, and J. Yuan, "Outage Performance for Compute-and-Forward in Generalized Multi-Way Relay Channels," *IEEE Commun. Letters*, vol. 16, no. 12, pp. 2099–2102, Dec. 2012.

[47] Z. Ding, T. Ratnarajah, and K. Leung, "On the study of network coded AF transmission protocol for wireless multiple access channels," *IEEE Trans. Wireless Commun.*, vol. 7, no. 11, pp. 4568–4574, Nov. 2008.

[48] K. Jitvanichphaibool, R. Zhang, and Y. C. Liang, "Optimal resource allocation for two-way relay-assisted OFDMA," *IEEE Trans. Veh. Technol.*, vol. 58, no. 7, pp. 3311–3321, Sep., 2009.

[49] A. Papadogiannis and A. G. Burr, "Multi-beam assisted MIMO:a novel approach to fixed beamforming," *in Proceeding of Fut. Netw. and Mobile Summit (FUNEMS)*, pp. 1–8, 2011.

[50] Y. Li, R. Louie, and B. Vucetic, "Relay selection with network coding in two-way relay channels," *IEEE Trans. Veh. Technol.*, vol. 59, no. 9, pp. 4489–4499, Nov. 2010.

[51] I. Krikidis, “Relay selection for two-way relay channels with MABC DF: A diversity perspective,” *IEEE Trans. Veh. Technol.*, vol. 59, no. 9, pp. 4620–4628, Nov. 2010.

[52] A. Bletsas, A. Khisti, D. P. Reed, and A. Lippman, “A simple cooperative diversity method based on network path selection,” *IEEE J. Sel. Areas Commun.*, vol. 24, no. 3, pp. 659–672, Mar., 2006.

[53] E. Beres and R. Adve, “Selection cooperation in multi-source cooperative networks,” *IEEE Trans. Wireless Commun.*, vol. 7, no. 1, pp. 118–127, Jan., 2008.

[54] A. Goldsmith, Wireless Communications, Cambridge Univ. Press, NY, USA, 2005.

[55] Z. Faraji-Dana and P. Mitran, ”On non-binary constellations for channel-coded physical-layer Network Coding,” IEEE Trans. Wireless Comms., vol. 12, pp. 312 - 319, Feb. 2003.

[56] S. Shukla and B. Sundar Rajan, “Wireless network-coded three-way relaying using Latin Cubes”, in Proc. IEEE International Symp. on Pers.Indoor and Mobi. Radio Comm. (PIMRC), Syndeny, Austrilia, Oct. 2012.

[57] S. Shukla, V. T. Muralidharan, and B. Sundar Rajan, “Wireless Network-Coded Three-Way Relaying Using Latin Cubes”, available online at arXiv:1112.1584 [cs.IT], Dec. 2011

[58] C. Feng, D. Silva, and F. R. Kschischang, ”An Algebraic Approach to Physical-Layer Network Coding,” in Proc. IEEE Int. Symp. Information Theory (ISIT), pp. 1017-1021, Austin, TX, June, 2010,